2020

Fire performance assessment of concrete with fly ash as the supplemental cementitious material

Fan, Kunjie

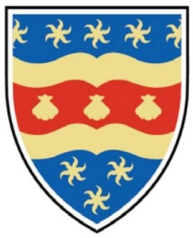

UNIVERSITY OF
PLYMOUTH

Fire performance assessment of concrete with fly ash as the supplemental cementitious material

by

Kunjie Fan

A thesis submitted to the University of Plymouth

in partial fulfilment for the degree of

DOCTOR OF PHILOSOPHY

School of Engineering

September 2020

Acknowledgements

First of all, I would like to express my sincerest gratitude to my director of studies Prof. Long-yuan Li who has given me the opportunity to study in University of Plymouth. As an excellent scholar and great mentor, he has provided a great deal of support with respect to the research and directed me into the academic field with his continuous encouragement. I would also like to thank my second supervisor, Prof. Dawang Li for his supervision and support of my study. I would also like to thank Mr. Terry Richards, the senior technician of materials and structures. He offered substantive help for my experimental programmes.

I would like to sincerely acknowledge the financial support provided by the School of Engineering, University of Plymouth, and the China Scholarship Council for my PhD study in University of Plymouth.

Immense appreciation attributes to my close friends, Junbo Zhao and Jinhua Zhang, for their companionship during the past four years. Above all, I am deeply grateful to my parents, Yunming Fan and Zhengpin Du, who brought me into this wonderful world, loved me from the very beginning and always supported me. Without their love and support, I would not have been able to go this far.

Author's Declaration

At no time during the registration for the degree of Doctor of Philosophy has the author been registered for any other University award without prior agreement of the Doctoral College Quality Sub-Committee.

Work submitted for this research degree at the University of Plymouth has not formed part of any other degree either at the University of Plymouth or at another establishment.

This PhD study was financed with the aid of School of Engineering, University of Plymouth and China Scholarship Council for the UK PhD scholarship.

Word count of the thesis: 33580

Signed: _____

Date: _____

Fire performance assessment of concrete with fly ash as the supplemental cementitious material

Kunjie Fan

Abstract

Material properties of concrete at elevated temperatures are imperative to structural fire safety assessment. However, fire performance of concrete at high temperature is extremely complex since concrete is a heterogeneous material with considerable variations. When it is subjected to thermal exposure, such as fire, concrete undergoes a series of significant physicochemical changes. Its mechanical behaviour is not only temperature dependent, but also loading history dependent, during the heating process. Therefore, the characterization of concrete properties at elevated temperatures is very challenging and the development of reliable and accurate constitutive models remains an unaccomplished task.

The main aim of this thesis can be divided into two scopes: 1) to examine the effect of using fly ash (FA) as the supplemental cementitious material (SCM) on the fire performance of concrete; 2) to investigate the mechanical behaviour of concrete under different thermomechanical conditions and obtain a better understanding of the mechanism of how the pre-fire load affects the fire performance of concrete. Finally, an advanced thermo-mechanical constitutive model for concrete under uniaxial

compression at elevated temperatures is expected to be established, for applications in structural fire engineering. The model has to capture the behaviour of structural concrete with different heating-loading sequences accurately and consider the effect of using FA as SCM on the variation of the properties of concrete during thermal exposure.

An apparatus is specially designed for testing "hot" mechanical properties of concrete materials with different heating-loading regimes. Through the experimental research, the mechanical properties, including compressive strength, peak strain, elastic modulus, complete stress-strain relationship and transient thermal creep (TTC) of concrete under uniaxial compression at elevated temperatures have been investigated. In the experimental programme, both conventional ordinary Portland cement (Karakurt & Topçu) based concrete and FA concrete specimens were tested to examine the difference. In addition, a novel numerical method was proposed, to quantify the effect of temperature gradient on TTC of stressed concrete in transient state tests, so that an explicit TTC model could be formulated.

Through the experimental research and numerical analysis presented in this thesis, the fire performance of FA concrete was examined. It was found that 25% replacement of OPC with FA in the concrete, mitigated the deterioration of the compressive strength, the development of TTC, and the nonlinearity of stress-strain response at elevated temperatures, but hardly influenced the value of the elastic modulus and the peak strain. The applicability of Eurocode EN1992-1-2 to normal strength concrete with

25% replacement of FA as SCM has been verified to be safe. In addition, the effect of loading history during thermal exposure, on the mechanical properties of concrete at the thermal steady state, has been investigated too. This thesis contributes to a better understanding on the mechanism of how loading-heating sequences influence the fire performance of concrete materials.

Finally, an advanced constitutive model for concrete at high temperature has been proposed and verified. Compared with previous models, it has the following advantages of: 1) incorporating a parameter n to consider the variation of the nonlinearity of stress-strain curves with temperature, 2) formulating the elastic modulus separately from the stress-strain curve, 3) distinguishing the stress-strain response of the stressed condition from the unstressed condition and 4) calculating TTC in a completely explicit way, by quantifying the interference caused by the thermal gradient in transient state tests. The relevant parameters in the model have been particularly calibrated for FA concrete as a recommendation for practical engineering.

Contents

List of Figures

List of Tables

List of Abbreviations

CH	calcium hydroxide
CSH	calcium-silicate-hydrate
FA	fly ash
HSC	high strength concrete
HSFC	high strength fly ash concrete
ITZ	interfacial transition zone
LITS	load induced thermal strain
LWC	low weight concrete
NSC	normal strength concrete
NSFC	normal strength fly ash concrete
NWC	normal weight concrete
OPC	ordinary Portland cement
SCM	supplemental cementitious material
TTC	transient thermal creep

List of Parameters

c	specific heat
e	resultant emissivity of the exposure surface
E	elastic modulus
E_{20}	elastic modulus at room temperature
$E(T)$	elastic modulus at temperature T
$E(L,T)$	elastic modulus of stressed concrete with load level L at temperature T
E_{ENV}	initial tangent modulus at temperature T, deduced from ENV
$E_{EC2}^{implicit}$	initial tangent modulus at temperature T, deduced from EC2
f_c	compressive strength
$f_{c,20}$	compressive strength at room temperature
$f_c(T)$	compressive strength at temperature T
$f_c(L,T)$	compressive strength of stressed concrete with load level L at temperature T
f_y	yield strength
f_r	unloading stress in the transient state test
h	convection coefficient

L	pre-fire load level
n	nonlinearity parameter of the stress-strain relationship
n_{20}	nonlinearity parameter at room temperature
$n(T)$	nonlinearity parameter at temperature T
r	yield ratio
$r(L,T)$	yield ratio of stressed concrete with load level L at temperature T
R	radius of concrete cylinder
t	time
T	temperature
T_0	room temperature
$T_{\max}(L)$	failure temperature of stressed concrete with load level L
T_s	surface temperature of concrete specimen
T_e	environment gas temperature
w	moisture content
S	Stefan-Boltzmann constant
ρ	density
ρ_{20}	density at room temperature
α	coefficient of thermal expansion

λ	thermal conductivity
$\lambda_f(L,T)$	compressive strength ratio of stressed concrete with load level L to unstressed concrete, at temperature T
$\lambda_\varepsilon(L,T)$	peak strain ratio of stressed concrete with load level L to unstressed concrete, at temperature T
$\lambda_e(L,T)$	elastic modulus ratio of stressed concrete with a pre-fire load level L to unstressed concrete, at temperature T
Δp	peak plastic strain of concrete at compressive strength
σ	stress
ε	strain
ε_{fts}	free thermal strain
ε_c	peak strain
$\varepsilon_{c,20}$	peak strain at room temperature
$\varepsilon_c(T)$	peak strain at temperature T
$\varepsilon_c(L,T)$	peak strain with e load level L at temperature T
$\varepsilon_{c,\min}$	minimum peak strain at temperature T
$\varepsilon_{\sigma,20}$	initial mechanical strain caused by the pre-fire load at room temperature
$\varepsilon_{\sigma,T}$	mechanical strain in the transient state test
$\varepsilon'_{\sigma,T}$	the sum of mechanical strain and TTC

$\varepsilon_{s,\exp}$	the sum of free thermal strain and mechanical strain
ε_e	elastic mechanical strain
$\varepsilon_{e,T}$	elastic strain at temperature T
$\varepsilon_{ela,T}$	elastic strain caused by the increase of temperature
ε_p	plastic mechanical strain
$\varepsilon_{p,T}$	plastic strain at temperature T
$\varepsilon_{pla,T}$	plastic strain caused by the increase of temperature
$\varepsilon_{r,T}$	accumulated residual strain caused by thermal gradient
$\varepsilon_{pla,tg}$	plastic strain caused by thermal gradient
ε_{tot}	total strain in the transient state test
$\varepsilon_{c,T,EC2}$	value of peak strain at temperature T recommended in EN1992-1-2
ε_{lits}	load induced thermal strain
ε_{ttc}	transient thermal creep
ε'_{ttc}	transient thermal creep derived from semi-implicit model 3
ε''_{ttc}	transient thermal creep derived from semi-implicit model 2

Chapter 1 - Introduction

1.1 Background

Fire represents the most severe situation among all the environmental conditions which structures may be subjected to. Generally, there are two types of thermal exposure for structural concrete: intended exposure and unintentional exposure. The former usually connects with constructions under its service conditions, while the latter is always related to accidental conditions (catastrophes). Service conditions normally involve long-term exposure to temperatures in the range 20°C-200°C and moisture state of unsealed or sealed concrete (RILEM, 2007). Accidental conditions normally involve short-term exposure to temperatures in the range 20°C-750°C or above and transient moisture states, i.e. the concrete is allowed to dry during heating (RILEM, 2007). Quite a lot of differences exist between them, however, no matter what kind of thermal exposure it is, the structural member should be designed to fulfil its aimed functions, without failure, for the specified time in a given thermomechanical scenario, termed as fire resistance of the structure.

Currently, performance-based design is gaining acceptance in structural fire engineering. Performance-based design is about specifying performance requirements and then developing solutions based on sound understanding of the underlying scientific and engineering principles (Wang *et al.*, 2012). Performance based fire resistance design is generally achieved by performing numerical simulations.

Subjected to a defined thermal exposure, temperature distribution can be predicted in the construction member by heat-transfer analysis. The results can then be applied into thermal-mechanical analysis, where a general static numerical method can be applied to assess the fire resistance performance of a structural member. In this way, specific problems can be investigated and even some structural conditions that are very difficult for fire tests, like collapse, can be simulated. Compared with standard fire tests or prescriptive methods, the numerical simulation is more flexible, economical, time-effective and environmentally friendly. To use numerical simulations to assess the fire safety of a structure is a concept with respect to its structural members, instead of its structural materials. However, the accuracy of the simulation is heavily dependent on the constitutive equations at elevated temperatures employed for the materials.

Structural concrete is widely used in civil engineering due to its many advantages. It generally possesses the best properties for fire resistance over most other building materials (Purkiss & Li, 2013; Wang *et al.*, 2012). Its constituent materials (cement and aggregates) are essentially non-combustible. The lower thermal conductivity, higher specific heat, and less strength deterioration with temperature, mean a slower rate of heat transfer and strength loss, which enables concrete to act effectively protecting itself and the whole structure, from fire damage. The use of structural concrete is thus common in applications where the fire resistance is an issue or in applications where elevated temperatures can arise, such as in nuclear reactor vessels

(Schneider, Diederichs & Ehm, 1982). Clearly, the mechanical properties of concrete at elevated temperatures play a key role in structural fire engineering. For the elastic analysis used in practice, the variations of compressive strength and elastic modulus with temperature are the basic required parameters, while in a more advanced analysis, the variation of the plastic strain in compression should also be properly defined (Gao *et al.*, 2013; Ožbolt *et al.*, 2014; Wang *et al.*, 2018a; Wang *et al.*, 2018b; Yin, Zha & Li, 2006).

However, the properties and behaviour of concrete at high temperatures is extremely complex, since it is a heterogeneous composite material with considerable variations. In compression, concrete exhibits inelastic volumetric expansion. Its mechanical behaviour is highly nonlinear and influenced by micro-cracking. When concrete is subjected to sufficient heat, such as fire, it undergoes a series of significant physicochemical changes, resulting in specific phenomena such as transient thermal creep (TTC) (Khoury, 1983). These changes cause the properties to deteriorate at elevated temperatures. Many of these deteriorations are not only temperature dependent but also loading history dependent, which adds another dimension of complexity to its high temperature behaviour.

For all these reasons, the characterization of concrete properties at elevated temperatures is very challenging and has been the subject of much research for many decades. The development of a reliable and accurate constitutive model, remains an unaccomplished task.

1.2 Problems

The failure mode of structural concrete in fire varies according to the nature of the fire (e.g. rate of temperature increase and maximum temperature); the loading system; and the type of structure exposed to the fire (Khoury, 2000). Failure could occur due to: the failure of reinforcement as the tensile strength of the steel is reduced on heating (bending failure); the reduction of bond strength between the steel and concrete with the increase in temperature (bond failure); loss of shear or torsional strength (shear-torsion failure); loss of compressive strength (compressive failure); spalling. Reinforced concrete members under compression (e.g. columns) usually fail in fire due to concrete failure in the compression zone as its strength diminishes with heating (Khoury, 2000), therefore, it is important to formulate a constitutive model for concrete at high temperature.

Due to the needs of practical engineering, the effect of fire on the compressive mechanical properties of concrete has been studied since early 1922 (Lea & Stradling, 1922). Later in the 1970s and 1980s, the development of nuclear reactor systems added another impetus for research in this field (Bažant, 1972; Bazant, 1983; Gross, 1975; Harada et al., 1972; Schneider, Diederichs & Ehm, 1982; Thelandersson, 1983). Until now considerable research has been performed to assess the fire performance of concrete materials, however, further investigations are still needed for some issues.

1.2.1 Stress-strain relationships of unstressed concrete

The structural concrete heated without applied load except for its self-weight is called unstressed concrete. The mechanical properties of unstressed concrete at elevated temperatures have been studied extensively in previous research. However, there are two problems with the existing uniaxial compressive constitutive models. To begin with, the elastic modulus is generally defined as the initial tangent modulus or the secant modulus of the stress-strain curve (Anderberg & Thelandersson, 1976; EN1992-1-2, 2004), which is not reasonable due to the development of thermal cracks at elevated temperatures. Additional strain would be caused by compressing the thermal cracks when unstressed concrete is tested at elevated temperatures. This additional strain should be included in the stress-strain curve since it is part of the plastic deformation, but it should be excluded from the elastic modulus because it is irrecoverable. Therefore, the elastic modulus for unstressed concrete at elevated temperatures should be formulated individually instead of being defined from the stress-strain curve directly. In addition, at present, the available uniaxial compressive constitutive models for unstressed concrete at the thermal steady state, assume the nonlinearities of the stress-strain relationships remain unchanged when the temperature increases, which is in contradiction to practical experimental observations.

1.2.2 Stress-strain relationships of stressed concrete at high temperature

Concrete structures are generally mechanically loaded prior to any temperature attack, indicating that the structural concrete exposed to thermal exposure, is always heated under applied load in practical engineering situations. Meanwhile, previous studies have demonstrated that the behaviour of concrete loaded thermomechanically, relies on the sequences in which the heating and loading are applied (Gernay, Millard & Franssen, 2013; Torelli *et al.*, 2017; Torelli *et al.*, 2018). Therefore, it is desirable to simulate the stressed concrete at high temperature experimentally and determine the corresponding stress-strain relationships of the stressed concrete specimens. However, there are only a few experimental studies in which the concrete was loaded during heating and then tested under the thermal steady state.

In some previous experiments, it was found that both the compressive strength and the elastic modulus of specimens that were loaded when they were heated were higher than those of unstressed specimens, while the peak strain at compressive strength was reduced by the applied stress during the heating process. One assumption for the increase in compressive strength and the decrease in peak strain of stressed specimens proposed by some authors, is that the cement paste is densified by the applied stress (Khoury, 1983; Naus, 2006; Pimienta, McNamee & Mindeguia, 2018). On the contrary, there are some experimental results that differ from the above observations (Petkovski, 2010; Sullivan & Sharshar, 1992), in which the applied stress during the heating process has little impact on the mechanical properties of the concrete under

uniaxial compression. Until now, the essential mechanism of how the sustained load during the heating process affects the mechanical behaviour of concrete is still not clear and there is lack of a comprehensive constitutive model considering this effect.

1.2.3 Explicit TTC model

Under thermal exposure, the mechanical properties of concrete subjected to repeated cycles of heating-cooling and loading-unloading is very complicated. The main challenge in analysing this kind of problem is how to accurately simulate TTC caused by the pre-fire load on the virgin heating.

Existing research shows that the thermal strain of concrete is significantly reduced when a constant compressive load is applied while heating (Torelli *et al.*, 2016). Such a reduction has been commonly seen as an additional thermal strain component due to the presence of a constant stress occurring in the loaded direction, termed as transient thermal creep (Schneider, Schneider & Franssen, 2008; Thienel & Rostásy, 1996; Vlahinić *et al.*, 2012), which is a key property unique to concrete among structural materials. It has been demonstrated that any mechanical analysis of stressed and heated concrete structures, which ignores TTC, would bring erroneous results (Alogla & Kodur, 2018; Kodur & Alogla, 2017; Lu *et al.*, 2015; Sadaoui & Khennane, 2009; Wei *et al.*, 2017). Therefore, how to precisely simulate TTC is significant for the assessment of a heated and stressed concrete structure.

To measure TTC in experiments and to evaluate the behaviour of concrete at high

temperatures, two types of uniaxial testing methods are often used, namely the thermal-steady state test and the transient state test. The specimen in the steady state test is heated uniformly to a pre-defined temperature before it is mechanically loaded, which is a traditional experimental method for obtaining the stress-strain relationships of concrete at a high temperature. For the transient state test the specimen is mechanically loaded before it is heated. Although these two methods have the same terminal state of external mechanical load and temperature, their yielded strains are different due to the different historical heating-loading paths. This difference is generally known as TTC.

As the definition, TTC is the difference between the strain measured in a transient state test and the strain measured in a corresponding steady state test. Thus, it is calculated from experimental results instead of being measured directly. However, it is believed that part of this difference is the mechanical strain caused by the interaction between the temperature gradient and the pre-fire load during transient state tests. This mechanical strain could be substantial for concrete with a fast heating rate, but is always neglected in the calculation. The previous TTC models, formulated without excluding this potential interference, are termed as semi-implicit models. One purpose of this thesis is to develop a numerical method to calculate the additional mechanical strain caused by the temperature gradient in the transient state test and to develop an explicit TTC model.

1.2.4 Fire performance of concrete with fly ash (FA) as the supplemental cementitious material (SCM)

FA is fine waste particles generated from the combustion of pulverized coal in electricity power generation plants. It has been widely used as a SCM in concrete for several decades (Elahi *et al.*, 2010; Juenger & Siddique, 2015; Khatri, Sirivivatnanon & Gross, 1995; Lothenbach, Scrivener & Hooton, 2011; Malhotra, 1993). As an industrial byproduct, FA is available in many countries and its recycling brings significant economic and environmental benefits. These advantages have resulted in the increased use of FA in concrete, especially in the ready-mixed concrete industry. Nonetheless, there is some concern on whether or not FA would affect the fire safety of concrete material.

Due to the difficulty in apparatus, available studies on hot tests are much more limited than residual tests and only a few have managed measuring the complete stress-strain relationships of both stressed and unstressed concrete specimens. In addition, the most widely cited hot tests (Anderberg & Thelandersson, 1976; Anderberg & Thelandersson, 1978; Gross, 1975; Harada *et al.*, 1972; Schneider, 1988) were performed from 1960s to 1990s and the corresponding constitutive models and/or provisions were also established in that period. After that, it seems that the impetus to perform hot tests on concrete has been decreased. However, many of the early studies used primarily ordinary Portland cement (OPC) as binders, indicating the results probably do not apply to FA concrete. Therefore, the effect of using FA as a SCM in

concrete on the TTC and stress-strain relationships of concrete at high temperatures needs to be investigated.

1.3 Outline

Chapter 1 presents a general introduction into the research background and existing problems in fire performance assessment of concrete materials. In addition, the objectives of this thesis are listed in this Chapter.

Chapter 2 gives a literature review relevant to the research, including experimental methods to assess the mechanical properties of concrete at elevated temperatures, physicochemical changes of concrete at elevated temperatures, thermal properties of concrete at elevated temperatures, mechanical properties of unstressed concrete at elevated temperatures, mechanical properties of stressed concrete at elevated temperatures, and the effect of using FA as SCM on concrete properties at elevated temperatures. Based on the literature review, the knowledge gap of existing work is identified and summarized.

Chapter 3 presents the experimental programme carried out to investigate the mechanical behaviour of OPC concrete and FA concrete under different fire-loading scenarios, as an effective way to formulate the advanced constitutive model. Full details of the materials, test procedures and different phases for the conditioning and testing of the concrete specimens are described, including the test rig designed for the compressive tests at elevated temperatures.

Chapter 4 presents the results obtained from a series of tests (series A), in which a series of thermal steady state tests of OPC concrete and FA concrete were designed and performed. Also presented is the comparison between the experimental results and Eurocode EN1992-1-2 to examine the applicability of the current code to FA concrete. Based on the experimental results obtained, an advanced stress-strain model for FA concrete was proposed. Compared with existing models, the proposed model has the advantages of considering the variation of the nonlinearities of stress-strain relationships with increasing temperature and distinguishing elastic modulus from the secant modulus of the stress-strain curve.

Chapter 5 presents the results obtained from a series of tests (series B), in which specimens were heated with sustained load (10%，30%，50%，70% of reference strength). After completion of the 1 hour holding period at test temperatures the specimens were quickly unloaded and immediately tested to failure. The compressive strength, peak strain, elastic modulus and stress-strain shape of stressed specimens at different pre-fire load levels from 400 °C to 900 °C are reported, to investigate the effect of the loading history during the heating process on the stress-strain behaviour of concrete at high temperatures. Finally, a uniaxial compressive constitutive model for stressed concrete under the thermal steady state as a function of loading history during the heating process was proposed and verified.

Chapter 6 proposes a novel numerical method to calculate the effect of temperature gradient on TTC of stressed concrete during the heating process. Ideally, the specimen

in a transient state test should have a uniformly distributed temperature increase. However, this is never achieved in practice. On the other hand, the specimen in a steady state test has normally had a uniformly distributed temperature before it is mechanically loaded. Therefore, except for the mechanical strain estimated by the steady state test directly, there is an extra mechanical strain component caused by the temperature gradient developed in the transient state test.

Chapter 7 reports the results of another series of tests (series C), in which the specimens were heated with sustained load (10%，30%，50%，70% of reference strength) until failure. The results including the temperature distribution of the concrete specimens and deformation-temperature relationships are presented and the results have been analysed via the numerical method proposed in Chapter 6 to exclude the effect of thermal gradient on TTC. Finally, the explicit TTC of OPC concrete and FA concrete have been formulated and compared, to investigate the effect of using FA as SCM in concrete on the development of TTC.

Chapter 8 summarizes the main contributions of the thesis. Findings and the proposed constitutive model are listed. In addition, several suggestions are given for further studies.

Chapter 2 - Literature review

2.1 Experimental methods to assess mechanical properties of concrete at elevated temperatures

There are a large number of experiments on assessing the fire performance of concrete materials, but the specific testing methods adopted by various authors are different. In general, they can be distinguished according to testing at high temperature or after cooling down from thermal exposure (Ma *et al.*, 2015; Schneider, 1988; Youssef & Moftah, 2007). The former is usually termed as the "hot" test, while the latter is referred to as the "residual" test, aimed at assessing the post-fire behaviour. It should be mentioned that, in the cooling phase after thermal attack, there will be a further loss of compressive strength as a consequence of the continuing disintegration, which makes it hard to reach general conclusions, since the storage of concrete specimens in the cooling phase varies in different hydrothermal conditions (Arioz, 2007; Cheng, Kodur & Wang, 2004; Lie, 1992; Sivakumaran & Dilger, 1984; Xu *et al.*, 2001). Therefore, hot tests are necessary to evaluate the high temperature behaviour of concrete.

Meanwhile, it has been demonstrated that the performance of concrete under thermomechanical conditions depends on the sequences in which heating and mechanical loading are applied, because the applied stress during heating, influences the mechanical properties of concrete (Schneider & Schneider, 2009; Schneider,

Schneider & Franssen, 2008). Therefore, the test performed on the specimens heated without load (defined as "unstressed" test), cannot accurately simulate the most usual fire scenarios in structural engineering, where concrete is generally loaded prior to thermal exposure. In contrast, the test performed on the specimens loaded during the heating process, is defined as the "stressed" test, which is necessary for precisely reproducing the practical conditions of concrete structures under mechanical load and thermal load at the same time.

In addition, no matter it is under stressed condition or unstressed condition, hot tests can be further categorized as the "thermal-steady state test" and the "thermal transient state test". The concrete specimens in the steady state test were generally heated to achieve a uniform temperature first and then they were tested (Khoury GA, 1998; Lie & Kodur, 1996). The thermal steady state test for stressed concrete means the specimen is loaded during heating. When the stressed specimen is heated to the target temperature, it will be unloaded and then immediately reloaded to failure. This is mainly used to obtain the stress-strain relationships of concrete at different temperature levels (Khaliq & Kodur, 2011). In contrast, in the thermal transient state test, the specimen is tested during the transient heating process, to measure the deformation-temperature relationship under different thermal-mechanical loading scenarios (Khoury, 2006; Phan & Carino, 2002). The specimen would not, therefore, achieve a uniform temperature field through its cross section when it is tested (Huismann *et al.*, 2011). These two tests are typical representations of the

thermomechanical conditions possible in concrete.

2.2 Physicochemical changes to concrete at elevated temperatures

With elevated temperatures, significant changes to the microstructure and chemical composition of the concrete would develop gradually and continuously over a temperature range, from ambient to over 1000 °C, resulting in progressive variations of mechanical properties of concrete (Bažant, Cusatis & Cedolin, 2004; Bažant & Yunping, 1994; Hossain, 2006; Kalifa, Chéné & Gallé, 2001; Kalifa, Menneteau & Quenard, 2000; Kallel *et al.*, 2017; Kallel *et al.*, 2018; Naus, 2006).

At low temperatures the main reactions are dehydration and water expulsion (Hager, 2013). Prior to thermal exposure, about 30% to 60% of the volume of saturated cement paste and about 2% to 10% of the volume of saturated structural concrete are occupied by evaporable water (Naus, 2006). With increasing temperature, evaporable water starts to escape until about 105 °C, when almost all the evaporable water will have been lost as long as there is sufficient exposure time. Above 105 °C, chemically combined water will be gradually lost from dehydration of the cement paste until the temperature reaches to 850 °C when the dehydration is completed (Zhang & Ye, 2012).

From 30 °C to 300 °C, in addition to evaporation, the dehydration of cement paste happens at the same time. The maximum dehydration rate occurs at around 180 °C (Naus, 2006). Dehydration of the calcium hydroxide (CH) generally develops in the

temperature range of 460 °C to 540 °C, and will be completed at about 600 °C (Zhang & Ye, 2012). A further process of significant physicochemical change in cement paste takes the form as the decomposition of the calcium-silicate-hydrate phases (CSH) with formation of β-C_2S, which occurs in the temperature range of 600 °C to 700 °C (Zhang, Ye & Koenders, 2013).

Apart from the physicochemical reactions taking place in cement pastes during thermal exposure, many variations also develop in aggregates. As aggregates occupy normally 65% to 75% of the concrete volume, the fire performance of concrete is significantly affected by the type of aggregate used (Peng & Huang, 2008). Common aggregates are generally stable up to 300–350 °C. Siliceous aggregates may undergo crystal transformations resulting in significant increases in volume [e.g., crystalline transformation of α-quartz (trigonal) to β-quartz (hexagonal) between 500 °C and 650 °C with an accompanying increase in volume of ~5.7%] (Naus, 2006). At higher temperatures, between 600 °C and 900 °C, calcareous aggregates (calcite – $CaCO_3$), magnesite ($MgCO_3$), and dolomite ($MgCO_3$/ $CaCO_3$) will dissociate into an oxide and CO_2 (Zhang & Ye, 2013). When the temperature is increased up to 1300 °C, concrete melts. Tab.2.1 below, summarized by Hager (Hager, 2013), lists the general physicochemical reactions discussed above.

Tab.2.1 Physicochemical changes to concrete at elevated temperatures (Hager, 2013)

Temperature range	Changes
20 °C - 200 °C	Loss of capillary water and physically bound water; 80 °C - 150 °C: dehydration of ettringite; Dehydration of C-S-H phase;
300 °C - 400 °C	350 °C: break up of some siliceous aggregates (flint);
400 °C - 600 °C	460 °C - 540 °C: decomposition of portlandite $Ca(OH)_2 \rightarrow CaO + H_2O$; 573 °C: quartz phase change α - β in aggregates and sands;
600 °C - 800 °C	Second phase of the C-S-H decomposition, formation of β-C_2S;
800 °C - 1000 °C	840 °C dolomite decomposition; 930 °C – 960 °C calcite decomposition $CaCO_3 \rightarrow CaO+CO_2$; Ceramic binding initiation which replaces hydraulic bonds;
1300 °C	Total decomposition of concrete, melting.

2.3 Thermal properties of concrete at elevated temperature

Compared with mechanical properties, the thermal properties of concrete at elevated temperatures have been well studied and they are not the main obstruction in structural fire engineering. Therefore, this section mainly presents the fundamental characteristics of thermal properties of concrete at elevated temperatures and the calculation model recommended in EN-1992-1-2 (EN1992-1-2, 2004).

2.3.1 Thermal conductivity

The variation of thermal conductivity with rise of temperature depends on the amount of moisture content in concrete, the mix proportions and the type of aggregate. Determination of thermal conductivity is based on experimental data and empirical relationships in different codes. In EN 1992-1-2, the upper and lower limits of THE thermal conductivity at elevated temperatures for normal-weight concretes (NWC) are provided:

Upper limit:

$$\lambda=2-0.2451\times\frac{T}{100}+0.0107\times\left(\frac{T}{100}\right)^2 \tag{2.1}$$

Lower limit:

$$\lambda=1.36-0.136\times\frac{T}{100}+0.0057\times\left(\frac{T}{100}\right)^2 \tag{2.2}$$

where λ is the thermal conductivity of concrete; T is the temperature.

As illustrated in Fig.2.1, thermal conductivity of concrete decreases gradually with increasing temperature. Generally, the thermal conductivity at room temperature of conventional NWC, ranges between 1.4 and 2 $\mathrm{W/(m\cdot K)}$, will be higher than that of low weight concrete (LWC), ranges around 1 $\mathrm{W/(m\cdot K)}$.

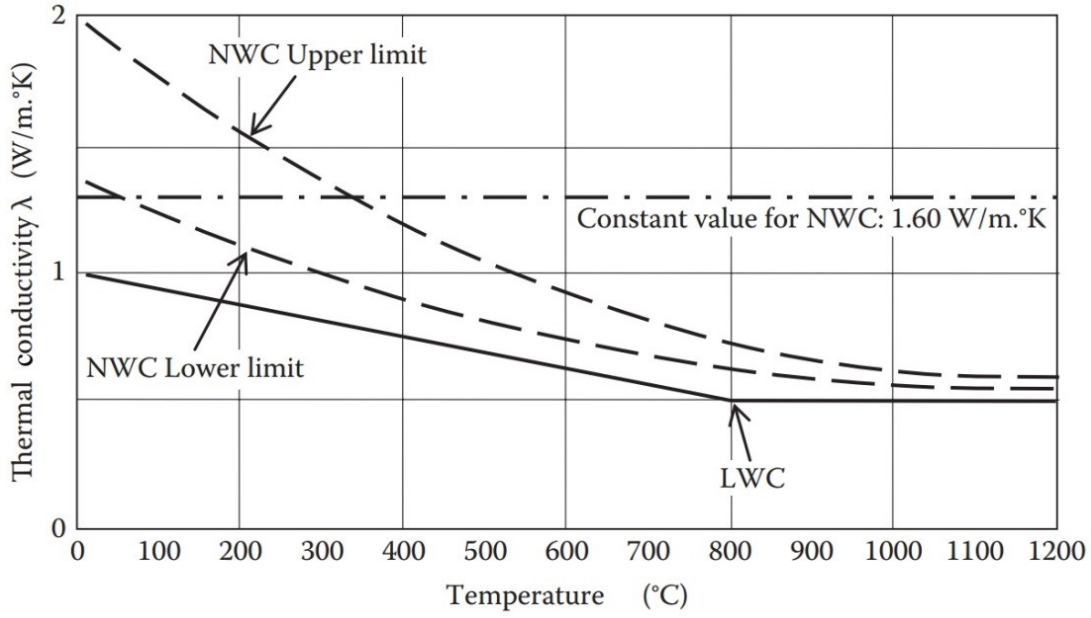

Fig.2.1 Thermal conductivity of NWC and LWC as a function of temperature in EN 1992-1-2 (Wang *et al.*, 2012)

2.3.2 Specific heat capacity

Specific heat of concrete also depends on the moisture content, aggregate type, and density of concrete (Harmathy & Allen, 1973; Phan, 1996), among which aggregate type plays the most significant role. The moisture content is significant at temperatures up to 200 °C because the specific heat of wet concrete is twice that of dry concrete (Wang *et al.*, 2012). In EN 1992-1-2 the specific heat of NWC is formulated simply:

$$c=\begin{cases}900 & 20 \le T \le 100 \\ 800+T & 100 < T \le 200 \\ 900+0.5T & 200 < T \le 400 \\ 1100 & 400 < T \le 1200\end{cases} \tag{2.3}$$

where c is the specific heat of concrete and the unit of temperature T is °C.

As illustrated in Fig.2.2, for NWC, the specific heat of concrete at ambient temperature is around 900 J/(kg·K) for different aggregate types and it remains almost constant up to 100 °C, followed by gently increasing up to about 400 °C and then remains constant. For LWC, a single conservative value of 840 J/(kg·K) is used.

It should be noted that, between 100 °C and 200 °C, if the influence of evaporation of free water needs to be considered, a spike could be added. For a case of 3% water content in concrete, the value at the spike is taken as 2020 J/(kg.K), while for a case of 10% water content in the concrete, the value is taken as 5600 J/(kg.K). If simplification for specific heat is needed in some situations, a constant value of 1000 J/(kg.K) is permitted.

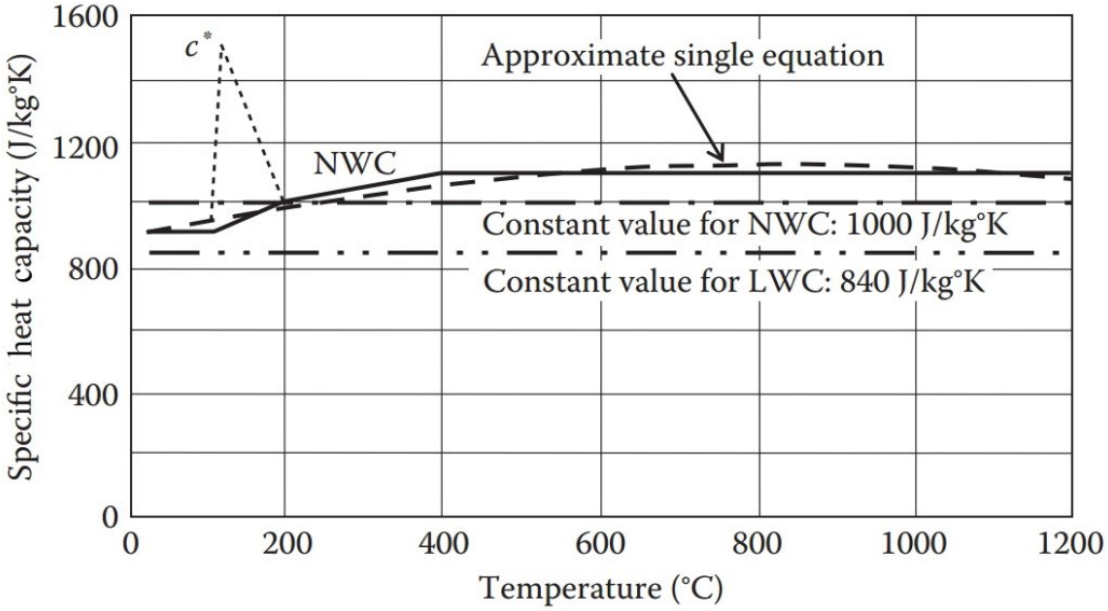

Fig.2.2 Specific heat capacity of NWC and LWC as a function of temperature in EN 1992-1-2 (Wang *et al.*, 2012)

2.3.3 Density

Density of concrete usually decreases with increasing temperature, due to loss of moisture, but the variation is generally not substantial (Lie & Kodur, 1996). There is very slightly difference between carbonate and siliceous aggregate concretes up to about 600 °C. However, beyond 600 °C, the density of siliceous aggregate concrete will not change a lot, while carbonate aggregate concrete will experience a larger percentage of density loss, due to the dissociation of aggregate (Kodur & Harmathy, 2008). In EN 1992-1-2, this difference has been ignored and the simplified formulation is given as:

$$\rho=\begin{cases}\rho_{20} & 20\le T\le 115\\ \rho_{20}\times\left(1-\dfrac{0.02(T-115)}{85}\right) & 115<T\le 200\\ \rho_{20}\times\left(0.98-\dfrac{0.03(T-200)}{200}\right) & 200<T\le 400\\ \rho_{20}\times\left(0.95-\dfrac{0.07(T-400)}{800}\right) & 400<T\le 1200\end{cases} \tag{2.4}$$

where ρ is the density of concrete; ρ_{20} is the density of concrete at room temperature and the unit of temperature T is °C.

2.3.4 Free thermal strain

Free thermal strain, is the strain developed in unrestrained concrete during heating. Although shrinkage develops in pure cement paste with increasing temperature, free thermal strain of concrete generally shows as expansion since its major constituent by volume, aggregate, expands with increasing temperatures. Therefore, the type of aggregate has a great impact on the development of free thermal strain in concrete. For siliceous aggregates, the free thermal strains are strongly influenced by the volume expansion, resulting from the α-β phase transition of quartz, which occurs at 573 °C (Wang *et al.*, 2012). For calcareous aggregates, the thermal strains are mainly concerned with the decomposition of calcium carbonate. Above differences have been distinguished in EN 1992-1-2 (see Fig.2.3).

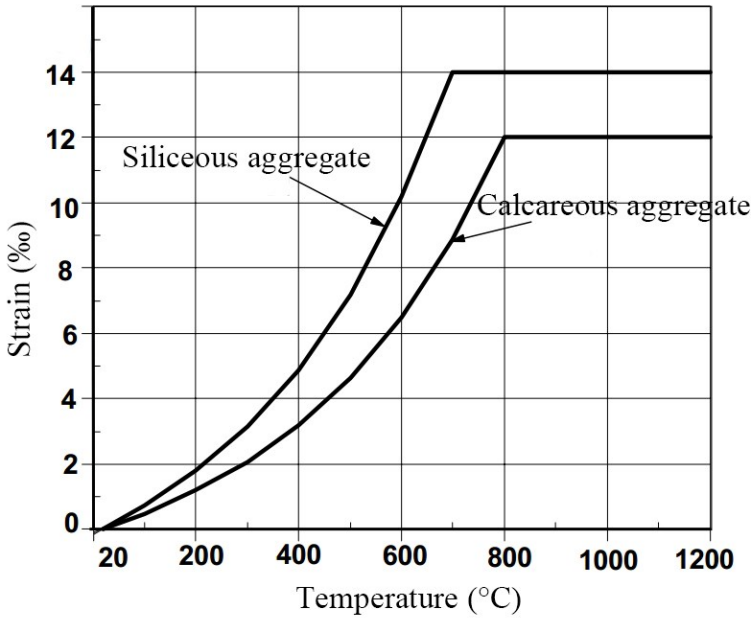

Fig.2.3 Free thermal strain of siliceous aggregates concrete and calcareous aggregates concrete as a function of temperature in EN 1992-1-2

Curve for siliceous aggregates concrete:

$$\varepsilon_{fts}=\begin{cases}-1.8\times10^{-4}+9\times10^{-6}T+2.3\times10^{-11}T^{3} & 20\le T\le 700\\ -14\times10^{-3} & 700<T\le 1200\end{cases} \tag{2.5}$$

Curve for calcareous aggregates concrete:

$$\varepsilon_{fts}=\begin{cases}-1.2\times10^{-4}+6\times10^{-6}T+1.4\times10^{-11}T^{3} & 20\le T\le 805\\ -12\times10^{-3} & 805<T\le 1200\end{cases} \tag{2.6}$$

where ε_{fts} is the free thermal strain of concrete and the unit of temperature T is °C.

2.4 Mechanical properties of unstressed concrete at elevated temperatures

As introduced in Section 2.1, the mechanical properties of concrete at elevated temperatures can be tested under stressed and unstressed conditions. For unstressed

conditions, the mechanical properties of concrete at elevated temperatures have been studied extensively in previous research and there is not much disagreement on the basic conclusions. Therefore, this section mainly presents the fundamental characteristics of mechanical properties of concrete at elevated temperatures and the calculation model recommended in EN-1992-1-2.

2.4.1 Compressive strength

Frequently, the 'hot' compressive strength loss of unstressed concrete occurs slowly at an early stage. There is less than 20% loss up to around 200-400 °C, then followed by an obvious rapid descending phase ranging from 400 °C to 600 °C, which can be partly attributed to the decomposition of CH and the quartz phase change of aggregates and sands, at around 573 °C, resulting in a disintegration of the microstructure in interfacial transition zone. Above 600 °C, concrete will lose most of its load-bearing capacity. The rate of decrease in compressive strength during the whole process depends on the water-cement ratio, cement paste-aggregate interfacial transition zone, type of aggregates and admixture, and SCMs (such as silica fume, FA, and slag). In EN 1992-1-2, the degradation of compressive strength in unstressed concrete is distinguished according to aggregate types: NWC siliceous, NWC calcareous and LWC, as illustrated in Fig.2.4.

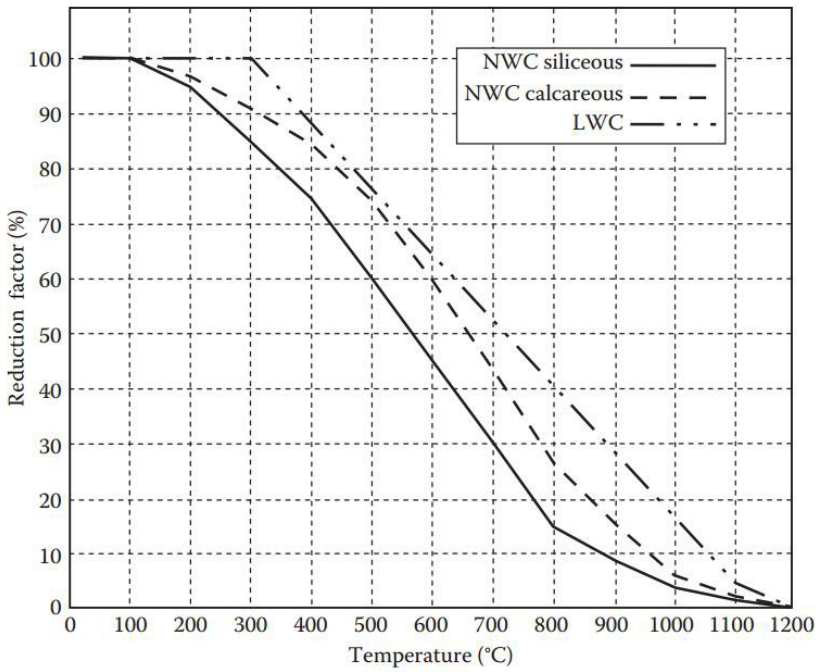

Fig.2.4 Reduction factors for uniaxial compressive strength of NWC and LWC at high temperatures in EN 1992-1-2 (Wang *et al.*, 2012)

2.4.2 Tensile strength

It is well known that the tensile strength of concrete is generally a few percent of its compressive strength so that tensile strength of concrete is conventionally ignored even for ambient temperature conditions. At elevated temperatures, tensile strength of concrete would be reduced furthermore. Therefore, there is little reason to consider it in simple fire resistance design, given the fact that there must be some uncertainties which exist in evaluating its exact value since the required experiments to measure tensile strength of concrete at elevated temperatures is very difficult. However, for some specific conditions, in which the tensile strength of concrete at elevated temperatures is necessary, EN 1992-1-2 provides a simple reduction factor $k_{c,t}$ as a function of temperature for estimating the tensile strength of concrete at elevated

temperatures, as illustrated in Fig.2.5.

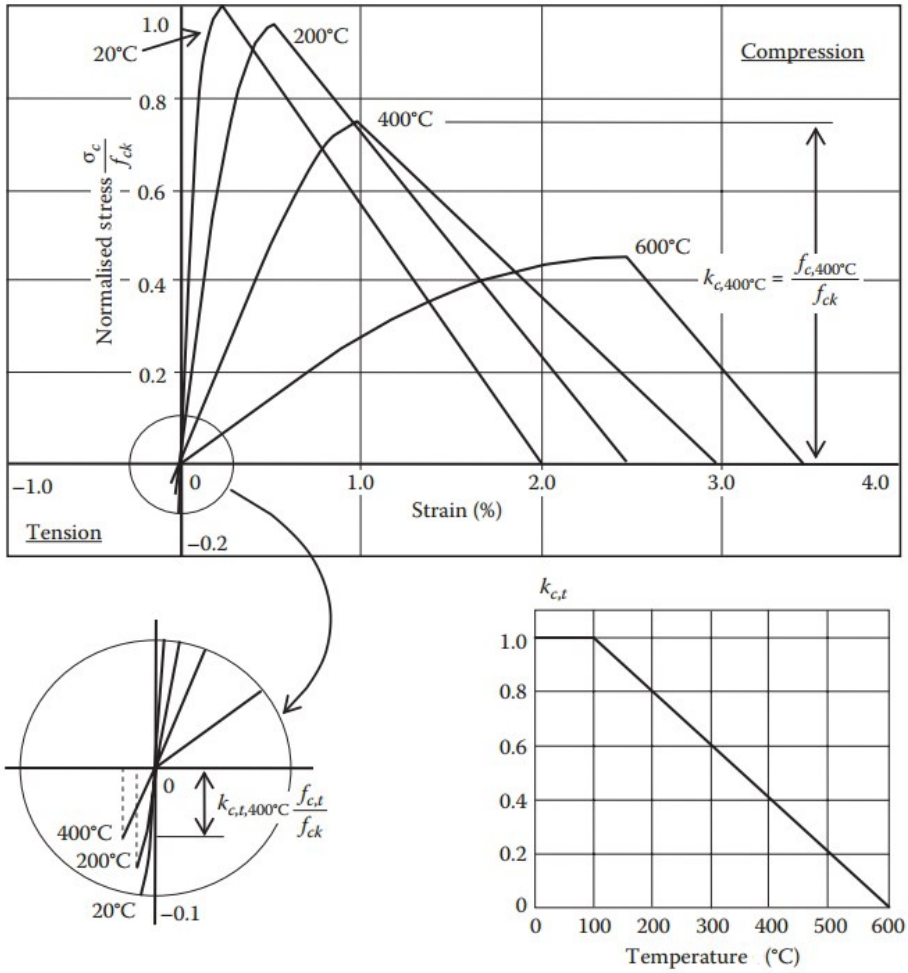

Fig.2.5 Uniaxial tensile strength of concrete at elevated temperatures in EN 1992-1-2 (Wang *et al.*, 2012)

2.4.3 Peak strain

The strain measured at compressive strength is named as peak strain in this thesis. There are very few studies that have specially investigated the variation of uniaxial compressive peak strain of concrete at the thermal steady state with temperature, while it is generally discussed together with the complete stress-strain response. The development of peak strain in concrete at elevated temperatures is proved to be nearly

independent of the aggregate type and heavily influenced by the applied stress during heating. In EN-1992-1-2, a single curve is proposed to evaluate the peak strain of concrete at high temperature, as illustrated in Fig.2.6. It should be noted that this curve has implicitly included the TTC, indicating it is very conservative.

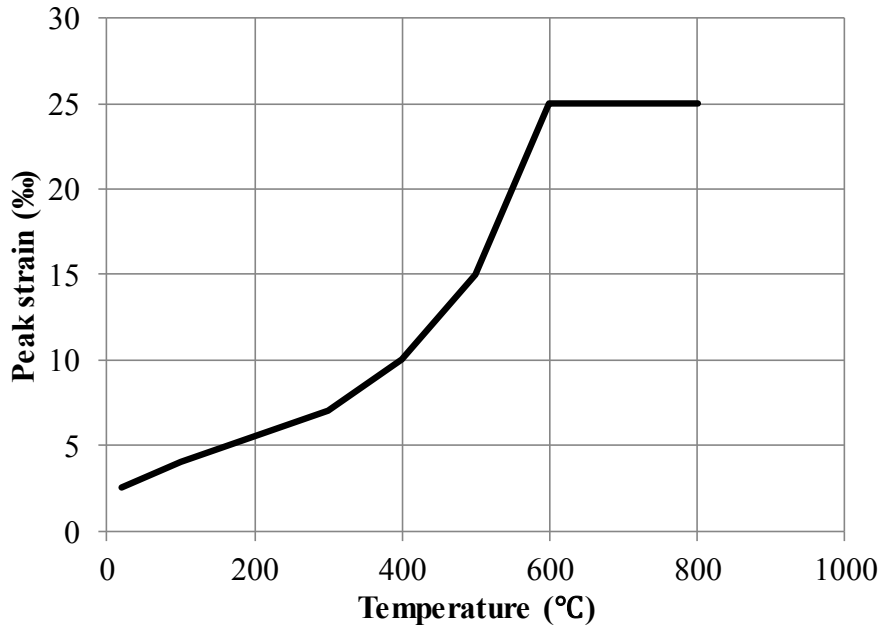

Fig.2.6 Uniaxial compressive peak strain of concrete at elevated temperatures in EN 1992-1-2 (EN1992-1-2, 2004)

2.4.4 Elastic modulus

Results in literature suggest that the primary factor influencing the elastic modulus of unstressed concrete at elevated temperatures is the type of aggregate. However, because the stress-strain curve of concrete is nonlinear, the elastic modulus can be determined by different methods. In EN 1992-1-2, it is defined as the initial tangent modulus, while in other studies it is defined as the secant modulus or tangent modulus at any point (Anderberg & Thelandersson, 1976; Cruz, 1962; Maréchal, 1970; Philleo,

1958; Schneider, 1976). It can be concluded that the determination method of the elastic modulus is not unified at present, resulting in obvious divergence in results of different studies, as illustrated in Fig.2.7. In addition, thermal cracks would develop in unstressed concrete during thermal exposure. The strain caused by compression in these cracks should be included in the tangent and secant modulus of the stress-strain curve since it is part of the plastic deformation. On the other side, it should be excluded from elastic modulus because it is irrecoverable. Therefore, evaluating elastic modulus from the stress-strain curve might be not reasonable for concrete at elevated temperatures. Until now, this has not been investigated.

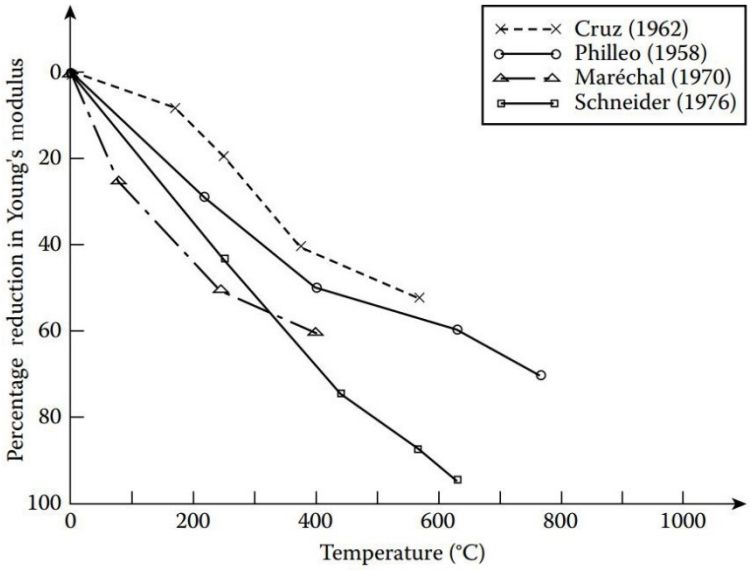

Fig.2.7 Variation in Young's modulus of concrete with temperature (Purkiss & Li, 2013)

2.4.5 Stress-strain relationships

The uniaxial compressive stress-strain relationship for unstressed concrete at the thermal steady state has been formulated in previous research. Three most widely accepted models are listed below:

Model proposed by Furumura:

$$\frac{\sigma}{f_c}=\frac{\varepsilon}{\varepsilon_c}e^{1-\frac{\varepsilon}{\varepsilon_c}} \tag{2.7}$$

Model proposed by Anderberg:

$$\frac{\sigma}{f_c}=1-\left(1-\frac{\varepsilon}{\varepsilon_c}\right)^2 \tag{2.8}$$

Model in EN1992-1-2:

$$\frac{\sigma}{f_c}=\frac{\varepsilon}{\varepsilon_c}\frac{3}{2+\left(\frac{\varepsilon}{\varepsilon_c}\right)^3} \tag{2.9}$$

where σ, ε are the instantaneous stress and strain, respectively; f_c is the compressive strength; ε_c is the peak strain at compressive strength.

The main problem for these three models is that all of them assume the nonlinearities of the stress-strain relationships stay unchanged when the temperature increases. Fig.2.8 shows the comparison of the stress-strain relationships at different temperatures after they have been normalized by the corresponding peak values. In Fig.2.8, the dash lines are taken from the experimental studies of Anderberg (Anderberg & Thelandersson, 1976) and the solid lines are calculated by Eqs.(2.7)-(2.9). It is evident from Fig.2.8 that the nonlinearities of experimentally obtained stress-strain relationships vary with temperature; whereas the theoretical models

cannot capture this phenomenon because they use a constant nonlinearity. This is an important characteristic but has been frequently ignored in previous studies.

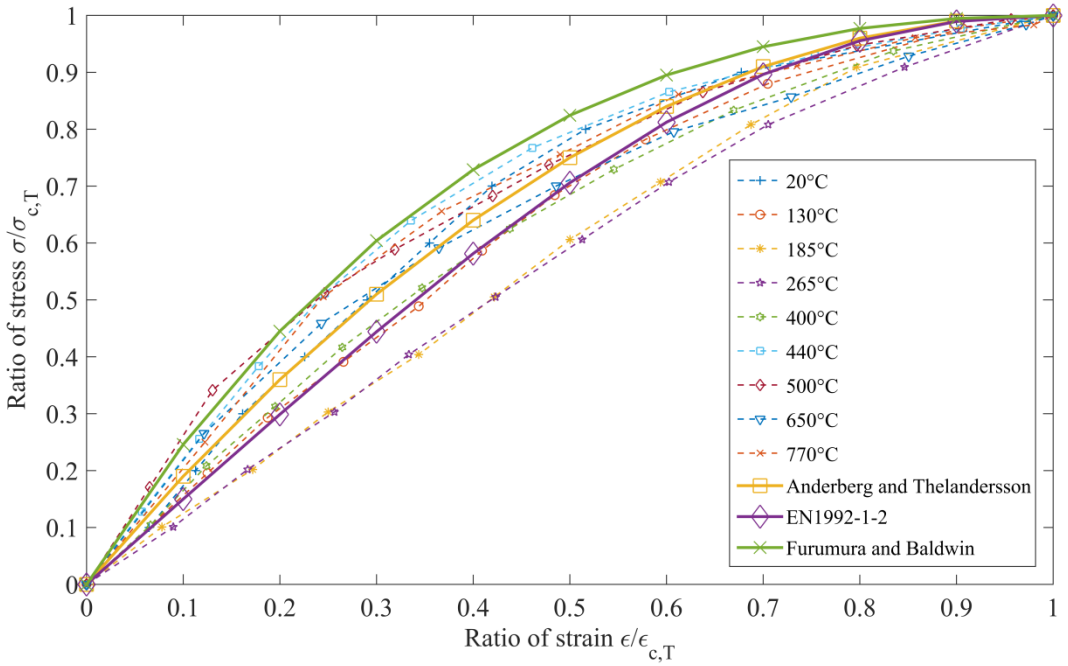

Fig.2.8. Normalized stress-strain relationships from different resources

(Anderberg & Thelandersson, 1976; EN1992-1-2, 2004; Furumura, Abe & Shinohara, 1995)

2.5 Mechanical properties of stressed concrete at elevated temperatures

Under practical conditions, concrete structures subjected to thermal exposure are always heated with applied loads, indicating concrete is generally heated under stressed condition. However, there are only few experimental studies in which the concrete was stressed when it is heated and then tested at the thermal steady state. Even in the limited research that focused on stressed concrete at elevated temperatures, the main aim was generally to investigate the development of load induced thermal strain (LITS) / TTC during the transient heating process, instead of the mechanical performance at the thermal steady state. Therefore, until now, the

mechanical properties of stressed concrete at the thermal steady state has not been distinguished from those of unstressed concrete in many numerical analyses and there is no complete constitutive model applicable to stressed concrete at the thermal steady state yet. In addition, for existing TTC models, the effect of the temperature gradient during the transient state test has not been excluded, resulting in overestimation. The research status and problems for stressed concrete at elevated temperatures will be discussed and presented in this section.

2.5.1 Stress-strain response at the thermal steady state

In 1956, Malhotra first performed hot tests on stressed concrete at the thermal steady state (Malhotra, 1956). It was reported that the hot compressive strength of the concrete specimens that were compressively loaded under a sustained stress level of approximately 0.2 of the reference strength (uniaxial compressive strength at ambient temperature) during the heating process was higher than that of specimens heated without any load. The enhancement increased with elevated temperatures, from 4% at 200 °C to 21% at 500 °C.

In 1971, the experimental research of Abrams (Abrams, 1971) confirmed the findings in Malhotra's research, in which the concrete specimens with different mix proportions were loaded under uniaxial compressive stress levels of 0.25, 0.40 and 0.55 of the reference strength during the heating process to 204 °C, 482 °C and 704 °C. Compared with the specimens heated without any load, 5%–25% higher hot strength in stressed

concrete specimens was reported, regardless of constituents, mix proportions, initial compressive strength, testing temperature or load level during heating.

In 1988, the results presented by Schneider (Schneider, 1988) showed that for temperature ranging from 150 °C to 750 °C, the elastic modulus increased obviously when the stress level applied on specimens increased from 0 to 0.3 of the reference strength, but little change was observed when the stress level increased from 0.3 to 0.5 of the reference strength.

In 1998, residual tests on stressed high strength concrete (HSC) specimens were performed by Khoury et al. (Khoury GA, 1998), in which HSC specimens were firstly heated up to 700 °C under sustained compressive stress of 0.2 of the reference strength, after achieving the thermal steady state at the target temperature they were cooled them down and tested at room temperature. It is reported that the residual compressive strength, elastic modulus of the stressed specimens were significantly higher than those of the unstressed specimens. On the other hand, the peak strain of the stressed specimens was obviously lower, particularly for temperatures ranging from around 400 °C to 700 °C, as illustrated in Fig.2.9. However, for temperatures lower than 400 °C, the above phenomenon was not obvious. The authors proposed some assumptions, like “densification of the cement paste” and “reduction of tensile stresses during cooling”, to explain the enhancement in strength.

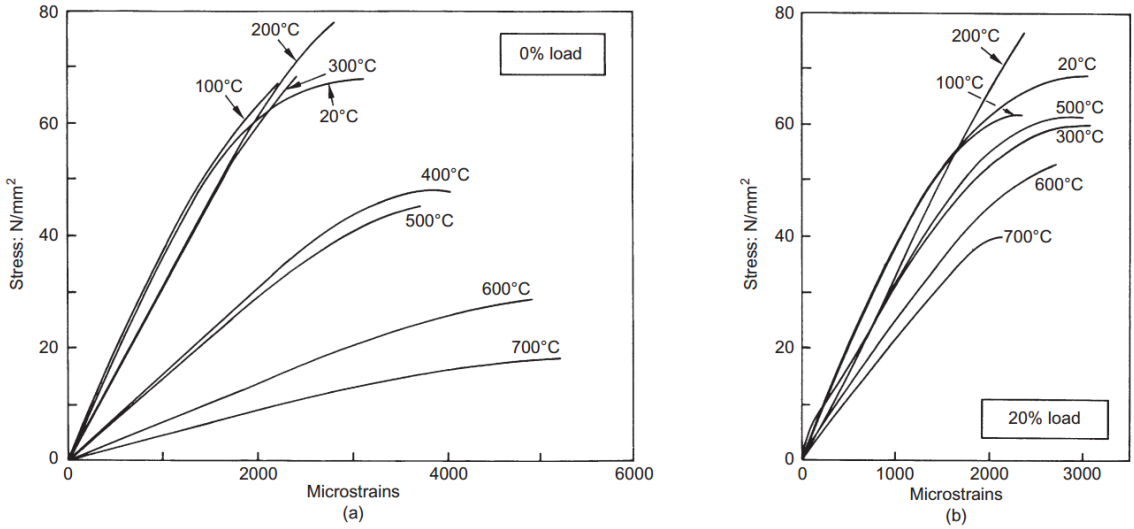

Fig.2.9 Influence of loading during heating on the residual stress–strain relationships of C70 concrete (Khoury GA, 1998)

Until now, there are only very limited studies in relevant fields, particularly for those performed with the hot experiment method. The main characteristics of the effect of applied stress during the heating process on the mechanical properties of stressed concrete at the thermal steady state have been confirmed, but the mechanism underlying it is still not understood. Furthermore, at present, there is no available constitutive model applicable to stressed concrete at the thermal steady state.

2.5.2 TTC

2.5.2.1 Introduction

In 1966 Hansen and Eriksson (Hansen & Eriksson, 1966) discovered that the mechanical strain developed in cement and mortar specimens that were heated under load was more than that of specimens that were firstly heated and then loaded. This relatively large extra strain component is named as TTC. TTC is the reason why

concrete does not break up when heated above 100 °C, where the thermal incompatibility of the aggregates and cement paste is far too large to be accommodated by their elastic strains (Bažant & Chern, 1987). It develops during first heating under load and is unique to concrete among structural materials.

Over the last several decades, numerous experimental studies have confirmed the existence and the main features of TTC (Anderberg & Thelandersson, 1976; Arthanari & Yu, 1967; Hassen & Colina, 2006; Illston & Sanders, 1974; Khoury, 1995; Mindeguia *et al.*, 2013; Pan, Sanjayan & Collins, 2014; Petkovski & Crouch, 2008; Rickard, Gluth & Pistol, 2016; Schneider, 1976). These experimental research focused on the deformation-temperature relationships and the relevant factors. However, despite a large number of experimental studies published on TTC, there are very few studies on developing physical models, which can describe its underlying mechanism. Most of the existing models were developed based on the experimental data by using regression methods. Its mechanism and calculation method are still ambiguous and need to be further elucidated.

2.5.2.2 Effect of TTC

For restrained structural members, TTC is generally beneficial during the virgin heating since it develops in the loaded direction, thus mitigating the additional compressive stresses due to restraints (Khoury, Grainger & Sullivan, 1985a; Schneider, 1988) and produces a stress-redistribution preventing local compressive

stresses. In addition, compressive stresses produce an overall reduction of tensile cracks resulting from the thermal incompatibility between cement paste and aggregates in the direction of the load. By contrast, for structural members subjected to heating-cooling cycles, the existence of TTC could be harmful. Since TTC is mainly irrecoverable, thermal incompatibilities between the aggregates and cement paste may cause severe damage at a material level during the cooling phase. In addition, when the degrading hot compressive strength of concrete is approaching the applied stress level, substantial damage may develop (Kordina, Ehm & Schneider, 1986). Therefore, TTC plays a significant role in the performance of concrete structures subject to heating-cooling cycles under mechanical loads. Accurate understanding and modelling of this phenomenon is crucial for a reliable assessment of the effects of thermal loads on concrete structures.

2.5.2.3 Characteristics of TTC

a. Temperature-, load- and constituents-dependent

TTC gradually increases with the rise of temperature, but exhibits highly nonlinear features and is reasonably proportional to the applied stress level (Gernay, 2012). The value of TTC is 2–3 times higher when measured in cement paste than in concrete with aggregates (Khoury, Grainger & Sullivan, 1985b) and it increases with the decrease of water-cement ratio (Colina, Moreau & Cintra, 2004; Colina & Sercombe, 2004). This might be attributed to the high pore pressure as a result of the low

permeability (Kalifa, Menneteau & Quenard, 2000). Moreover, unlike free thermal strain, the type of aggregates has little impact on TTC up to about 400 °C, while it becomes more important for higher temperatures. Therefore, it could be concluded that TTC occurs in hardened cement paste (Anderberg & Thelandersson, 1976; Khoury, Grainger & Sullivan, 1986; Mindeguia *et al.*, 2013) and somehow is restrained by the aggregates.

b. Time- and initial moisture content- independent

Development of TTC is commonly treated as a quasi-instantaneous process, i.e. as a time-independent phenomenon (Anderberg & Thelandersson, 1978). This assumption is based on the fact that it mostly occurs during the transient heating process, and the time needed for it to fully develop after the temperature has been stabilized is generally little when compared to the usual duration of basic creep (Bažant & Chern, 1987; Illston & Sanders, 1973; Sabeur & Colina, 2014). For unsealed conditions, the initial moisture content has been demonstrated to have little effects on TTC above 250 ◦C, while it has been found to significantly influence TTC at lower temperatures (Mindeguia *et al.*, 2013; Petkovski & Crouch, 2008; Torelli *et al.*, 2016).

c. Irrecoverable

TTC only developed on the virgin heating, and is mostly irrecoverable on unloading and cooling. If stressed concrete specimens are reheated after cooling down from a thermal exposure, no appreciable extra TTC develops until the temperature is higher

than the maximum value reached in the first heating process (Hassen & Colina, 2006; Illston & Sanders, 1973; Illston & Sanders, 1974; Noumowe *et al.*, 1996; Sadaoui & Khennane, 2009), which means that it could be eliminated by preheating cycles performed under unstressed conditions.

2.5.2.4 Method to quantify TTC

The underlying mechanism of TTC is very complicated and still not clear, therefore all available models are formulated by using experimental data regression. However, there is one important factor that is always neglected in these experimental researches, which is the effect of temperature gradient in the transient state test on mechanical strain.

To measure TTC in experiments and to evaluate the behaviour of concrete at high temperatures, two types of uniaxial testing methods are generally used: the thermal-steady state test and the thermal transient state test, as shown in Fig.2.10. The specimen in the steady state test is heated uniformly to a pre-defined temperature before it is mechanically loaded, which is a traditional experimental method for obtaining the stress-strain relationships of concrete at a high temperature. For the transient state test the specimen is mechanically loaded before it is heated. In simple terms, the steady state test is characterized by heating first followed by the loading; whereas the transient state test is characterized by loading first followed by heating. Although these two methods have the same terminal state of external mechanical load

and temperature, their yielded strains are different due to the different historical heating-loading paths. This difference is generally defined as TTC (Castillo, 1987; Rickard, Gluth & Pistol, 2016; Schneider, 1976). However, it is believed that part of this difference is the mechanical strain caused by the interaction between the temperature gradient and the pre-fire load during transient state tests. This mechanical strain could be substantial for concrete with fast heating rate and could be calculated by using the coupled thermal and stress analysis method. Part of the present study is to develop a calculation method for this kind of mechanical strain and to examine its influence on the experimentally obtained TTC.

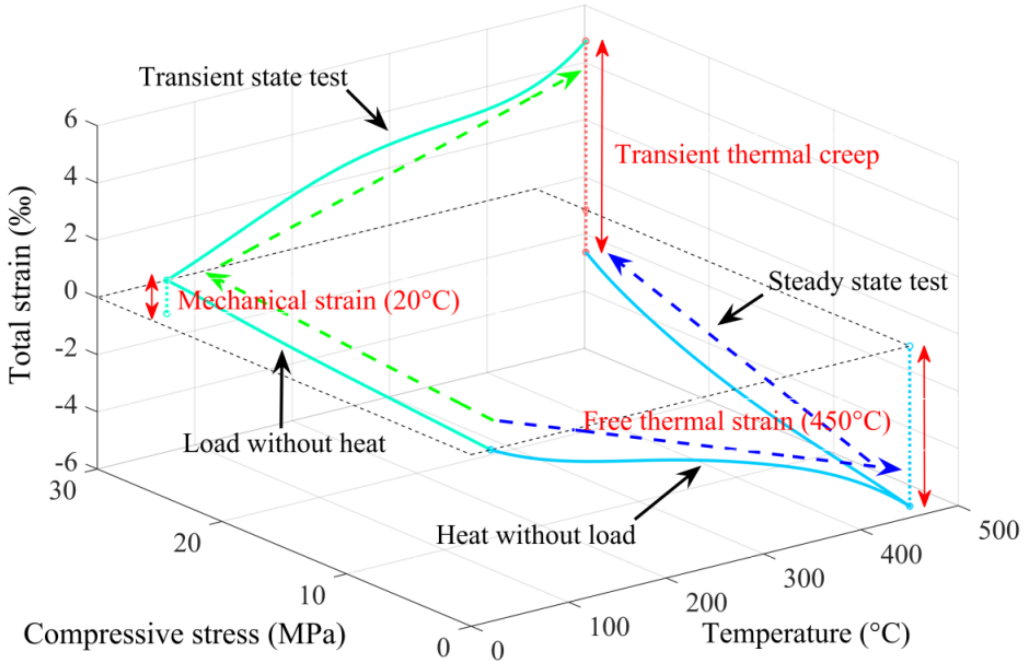

Fig.2.10 Definition of TTC and different test methods

As the definition, TTC is the difference between the strain measured in a transient state test and the strain measured in a corresponding steady state test. Thus, it is calculated from experimental results instead of being measured directly. Note that the

result obtained in a transient state test is the strain-temperature relationship at a constant stress level; whereas the result obtained in the steady state test is the stress-strain relationship at a constant temperature, which means that a pair of tests can give an estimation of TTC at one single point of the given constant temperature and constant stress. However, since TTC is a function of both temperature and mechanical stress, one has to perform a series of transient state tests with different pre-fire load levels and a series of steady state tests at different temperatures in order to obtain this function.

2.5.2.5 Problems for previous TTC models

In addition to the complexity of experiments, another difficulty is how to extract TTC accurately from other strain components. The free thermal strain can be measured by a reference transient test with 0% load level and the normal creep at high temperature could be ignored due to the short time of the transient state test. There is no disagreement on the analysis of these two components. The main argument is the mechanical strain in the transient state test. The mechanical strain can be divided into elastic and plastic parts, both of which vary with temperature and can be formulated by using the results obtained from the corresponding steady state tests. The calculation of the elastic strain is relatively simple, since it is only related to the mechanical stress and the temperature-dependent elastic modulus. In contrast, the calculation of the plastic strain is debatable. In some studies the plastic strain was assumed to be part of TTC (Gernay, 2012; Gernay & Franssen, 2012; Khoury, 1983; Pan, Sanjayan &

Collins, 2014); while in others it was separated from TTC (Schneider & Schneider, 2009; Schneider, Schneider & Franssen, 2008; Thelandersson, 1987), but its calculation did not take into account the effect of temperature gradient.

Ideally, the specimen in a transient state test should have a uniformly distributed temperature increase. However, this is never achieved in practice. According to an experiment by Anderberg and Thelandersson (Anderberg & Thelandersson, 1976), even a small cylinder specimen with only 75 mm diameter and 150 mm height, under a relatively low heating rate of 5 °C/min, the largest temperature difference between its centre and exposed surface in the transient state test could be more than 100 °C. On the other hand, the specimen in a steady state test has normally had a uniformly distributed temperature before it is mechanically loaded. Therefore, except for the mechanical strain estimated by the steady state test directly, there is an extra mechanical strain component caused by the temperature gradient in the transient state test. Based on the explanation mentioned above, it can be concluded that there are three strain components in concrete when it is under the action of thermal-mechanical load:

1) Free thermal strain ε_{fts} - that includes the thermal expansion strain due to increasing temperature and shrinkage strain caused by loss of water.

2) Mechanical strain $\varepsilon_{\sigma,T}$ in the transient state test - an instantaneous stress-related strain, which can be calculated by using the steady state constitutive model as follows,

$$\varepsilon_{\sigma,T} = \varepsilon_{\sigma,20} + \varepsilon_{ela,T} + \varepsilon_{pla,T} + \varepsilon_{pla,tg} \tag{2.10}$$

where $\varepsilon_{\sigma,20}$ is the initial mechanical strain caused by the pre-fire load at ambient temperature, $\varepsilon_{ela,T}$ and $\varepsilon_{pla,T}$ are the additional elastic and plastic strains caused by the increase of temperature calculated from the steady state constitutive model, respectively, $\varepsilon_{pla,tg}$ is the mechanical strain caused by temperature gradient in the transient state test.

3) TTC ε_{ttc} - an extra strain component in addition to ε_{fts} and $\varepsilon_{\sigma,T}$, which only happens in the virgin heating process of pre-loaded concrete and represents the effect of the specific historical loading and heating path.

Considering the short duration of the transient state test, the normal creep can normally be ignored. Thus, the decomposition of the total strain in a transient state test can be expressed as follows,

$$\varepsilon_{tot} = \varepsilon_{fts} + \varepsilon_{\sigma,20} + \varepsilon_{ela,T} + \varepsilon_{pla,T} + \varepsilon_{pla,tg} + \varepsilon_{ttc} \tag{2.11}$$

Due to the difficulty of performing fire experiments, not many models have been established since 1970s. Tab.2.2 gives a summary of these models (Anderberg & Thelandersson, 1976; EN1992-1-2, 2004; Gernay & Franssen, 2012; Nielsen, Pearce & Bićanić, 2004; Philleo, 1958; Schneider, 1976; Terro, 1998). The term implicit used in Tab2.2 refers to the manner in which the mechanical strain is formulated together with TTC and is calculated as the difference between the total strain developed in the transient state test and the free thermal strain. A typical example for this is the stress-strain relationship given in EN1992-1-2,

$$\frac{\sigma}{f_c(T)} = \frac{\varepsilon'_{\sigma,T}}{\varepsilon_{c,T,EC2}} \frac{3}{2+\left(\frac{\varepsilon'_{\sigma,T}}{\varepsilon_{c,T,EC2}}\right)^3} \tag{2.12}$$

where σ is the applied stress, $\varepsilon'_{\sigma,T}$ is the stress-related strain defined as the sum of mechanical strain and TTC, $f_c(T)$ is the compressive strength at temperature T, and $\varepsilon_{c,T,EC2}$ is the value of peak strain at temperature T recommended in EN1992-1-2.

Tab.2.2 Existing TTC models

Category	Model	Authors
Implicit	$\varepsilon_{tot}=\varepsilon'_{\sigma,T}+\varepsilon_{fts}$ $\varepsilon'_{\sigma,T}=\varepsilon_{tot}-\varepsilon_{fts}=\varepsilon_{\sigma,T}+\varepsilon_{ttc}$	Eurocode (EN1992-1-2, 2004)
Semi-implicit 1 (LITS)	$\varepsilon_{tot}=\varepsilon_{lits}+\varepsilon_{\sigma,20}+\varepsilon_{fts}$ $\varepsilon_{lits}=\varepsilon'_{\sigma,T}-\varepsilon_{\sigma,20}=\varepsilon_{ela,T}+\varepsilon_{pla,T}+\varepsilon_{pla,tg}+\varepsilon_{ttc}$	Nielsen et al. (Nielsen, Pearce & Bićanić, 2004), Diederichs (Philleo, 1958), Khoury and Terro (Khoury, 1983; Terro, 1998)
Semi-implicit 2	$\varepsilon_{tot}=\varepsilon''_{ttc}+\varepsilon_{ela,T}+\varepsilon_{\sigma,20}+\varepsilon_{fts}$ $\varepsilon''_{ttc}=\varepsilon_{lits}-\varepsilon_{ela,T}=\varepsilon_{pla,T}+\varepsilon_{pla,tg}+\varepsilon_{ttc}$	Gernay and Franssen (Gernay & Franssen, 2012)
Semi-implicit 3	$\varepsilon_{tot}=\varepsilon'_{ttc}+\varepsilon_{pla,T}+\varepsilon_{ela,T}+\varepsilon_{\sigma,20}+\varepsilon_{fts}$ $\varepsilon'_{ttc}=\varepsilon''_{ttc}-\varepsilon_{pla,T}=\varepsilon_{pla,tg}+\varepsilon_{ttc}$	Schneider (Schneider, 1976), Anderberg and Thelandersson (Anderberg & Thelandersson, 1976)

In contrast to the implicit models, the mechanical strain and TTC are formulated separately in explicit models, which represent the real physical meaning of TTC. However, many existing models are neither implicit nor completely explicit, but are semi-implicit. These semi-implicit models can be divided into three types (see Tab2.2). The first type does not separate TTC from the variation of mechanical strain with temperature and it defines the sum of them as load induced thermal strain (LITS). For example, Nielsen et al. (Nielsen, Pearce & Bićanić, 2004) proposed a linear model for

the development of LITS. Diederichs (Diederichs, Jumppanen & Penttala, 1988) presented a nonlinear model for the calculation of LITS as follows,

$$\varepsilon_{lits} = L\left(4.12\times10^{-5}(T-T_0) - 1.72\times10^{-7}(T-T_0)^2 + 3.3\times10^{-10}(T-T_0)^3\right) \quad (2.13)$$

where T_0 is the ambient temperature, L is the pre-fire load level. A similar model named master LITS curve, was developed by Khoury and Terro (Khoury, 1983; Terro, 1998) as follows,

$$\varepsilon_{lits} = -4.39\times10^{-5} + 2.73\times10^{-6}T + 6.35\times10^{-8}T^2 - 2.19\times10^{-10}T^3 + 2.77\times10^{-13}T^4 \quad (2.14)$$

The second type can be considered as an improvement on the first one by separating the variation of elastic strain with temperature. For example, Gernay and Franssen (Gernay & Franssen, 2012) formulated TTC individually on the basis of EC2 (EN1992-1-2, 2004) and ENV (ENV1992-1-2, 1995),

$$\varepsilon''_{ttc} = \frac{\sigma}{E^{implicit}_{EC2}} - \frac{\sigma}{E_{ENV}} = \frac{2}{3}\frac{\varepsilon_{c,T,EC2} - \varepsilon_{c,\min}}{f_c(T)/f_{c,20}}\frac{\sigma}{f_{c,20}} \quad (2.15)$$

where $E^{implicit}_{EC2}$ and E_{ENV} are the initial tangent modulus of the stress-strain curve at temperature T deduced from EC2 and ENV respectively, $f_{c,20}$ is the compressive strength of concrete at room temperature and $\varepsilon_{c,\min}$ is the minimum peak strain at temperature T.

The third type includes the models proposed by Schneider and Anderberg and Thelandersson. In the studies of Schneider (Schneider, 1976), $\varepsilon_{pla,T}$ was formulated explicitly away from ε'_{ttc} when the pre-fire load level was over 0.5. According to the empirical boundary limit imposed by Schneider, TTC is calculated based on the stress

ratio as follows,

when $\sigma / \sigma_{c,20} \le 0.3$:

$$\varepsilon'_{ttc} = \frac{\sigma}{E(T)}\left(\frac{\sigma \times (T-20)}{100\sigma_{c,20} + \sigma \times (T-20)} + C_1 \tanh\left[\frac{(0.3w+2.2)(T-20)}{1000}\right] + C_2 \tanh\left[\gamma_0 \times (T - T_g)\right] + C_3\right) \quad (2.16)$$

when $\sigma / \sigma_{c,20} > 0.3$:

$$\varepsilon'_{ttc} = \frac{\sigma}{E(T)}\left(\frac{T-20}{T-313.3} + C_1 \tanh\left[\frac{(0.3w+2.2)(T-20)}{1000}\right] + C_2 \tanh\left[\gamma_0 \times (T - T_g)\right] + C_3\right) \quad (2.17)$$

where $E(T)$ is the elastic modulus at temperature T, w is the moisture content in %, C_1, C_2, C_3, γ_0, T_g are the parameters for calibration. In the study of Anderberg (Anderberg & Thelandersson, 1976), TTC is expressed as the function of free thermal strain and applied stress directly as follows,

$$\begin{cases} \varepsilon'_{ttc} = k\dfrac{\sigma}{f_{c,20}}\varepsilon_{fts} & ,\ 20 \le T \le 550 \\ \dfrac{\partial \varepsilon'_{ttc}}{\partial T} = 0.0001\dfrac{\sigma}{f_{c,20}} & ,\ 550 \le T \le 800 \end{cases} \quad (2.18)$$

where $k = 2.35$ is a material parameter used for experimental data fitting. This formula is simple and clear but it cannot take into account the effect of plastic strain caused by temperature gradient, which means that it is not completely explicit too.

According to the analysis described above, the differences among the existing models is the way in which the strain components are split, while their common problem is that part of the mechanical strain, at least the $\varepsilon_{pla,tg}$ caused by the temperature gradient, is implicitly included in TTC. Note that no matter how TTC is defined and what method is adopted for calculating it, the final target is the same, which is to

formulate the extra strain caused by different historical loading and heating paths, while the implicit or semi-implicit inclusions of mechanical strain in existing TTC models makes it incapable of capturing this difference precisely. It should be emphasised here that the incomplete separation between mechanical strain and TTC does not affect the calculation of total strain developed in transient state tests since it is only the difference of division methods for constituents. However, the separation of mechanical strain from TTC could help our understanding of the evolution of concrete transient strain and the development of stress-stain-temperature constitutive equations for concrete materials at elevated temperatures.

2.6 Effect of using FA as SCM on concrete properties at elevated temperatures

FA has been widely used as SCM in concrete for several decades. Nonetheless, there is some concern on whether the FA would affect the fire safety of concrete materials. FA itself has little cementitious value, but if it is used together with OPC in making concrete the reactive silica in it will chemically react with CH to form CSH possessing cementitious properties. When concrete is heated above 100 °C and in the presence of moisture, this process would be amplified, which could beneficially reduce the amount of CH and increase the mass of the solid skeleton of CSH, resulting in a stronger and less permeable material (Khoury *et al.*, 2002). In this way, the FA concrete, besides having an increased structural performance at ambient temperature, might also show a different performance at elevated temperatures. However, dehydration from the CSH also becomes significant above about 100 °C. The release of water would contribute to

the evaporation of moisture. With lower porosity and permeability in FA concrete, the vapour migration rate might be slower than the evaporation rate of pore water, which could lead the development of pore pressure (Khoury, 2000; Kodur, 2014; Naus, 2006). The built-up of pore pressure, together with the reduction in strength due to the thermal decomposition of cement hydration products and the increase in the internal stresses caused by thermal gradient can cause severe damage in concrete. Therefore, the mechanical behaviour of FA concrete at high temperature is complicated and difficult to predict.

Until now, only in the study of Diederichs (Diederichs, 1987), were FA concrete specimens tested under thermal steady state tests. However, Diederichs' work was aimed at investigating the mechanical properties of high-strength concrete (HSC) at elevated temperatures, rather than on the effect of FA. The compressive strength of the FA concrete samples in his study was higher than 100 MPa and the corresponding water-binder ratio was as low as 0.27. Generally, HSC suffers from pronounced higher rates of strength loss than does normal strength concrete (NSC) due to its denser structure and lower permeability (Cheng, Kodur & Wang, 2004) which limit the ability of vapour in the concrete to escape and thus cause more destruction in cement matrix. The results of his experiment showed that the strength loss of high-strength fly ash concrete (HSFC) differs a lot from NSC made with OPC and is closer to conventional HSC without FA. This indicates that the effect of FA might be hidden and/or taken over by the low water-binder ratio in HSFC. Although FA itself could also yield a

similar pore pressure effect as described above, it might bring benefits as a result of the accelerated and further activated chemical reactions. Therefore, it is necessary to perform tests on normal-strength fly ash concrete (NSFC) to avoid the overshadowing caused by HSC itself. After excluding the potential interference due to the low water-binder ratio, the effect of FA on the mechanical properties of concrete at high temperature would be clearer.

On the other side, research presented by Khoury et.al in 1985 (Khoury, Grainger & Sullivan, 1985b) compared the LITS of FA concrete and OPC concrete during thermal exposure. However, the stress-strain relationships of concrete under the thermal steady state had not been tested in his research and the aggregate types in the FA concrete specimens and reference OPC specimens are different, therefore, the mechanical strain included in the LITS cannot be quantified and the effect of FA on the development of TTC is still unclear.

The above study shows that the experimental research on the mechanical behaviour of FA concrete at elevated temperatures, including the stress-strain response at the thermal steady state and TTC developed during the heating process for stressed conditions, is incomplete. Meanwhile, the utilization of FA is still insufficient at present. There is still a large amount of FA disposed in landfill every year (Abdulkareem *et al.*, 2014; Nadeem, Memon & Lo, 2014; Ryu *et al.*, 2013), which has a negative impact on the environment. A more comprehensive verification of the compressive behaviour of FA concrete during thermal exposure could help broadening

its potential application in engineering.

2.7 Knowledge gaps

Fire performance of concrete at elevated temperatures still attracts significant attention from researchers and there has been substantial work and publications in the relevant field, however, some issues need further investigation, especially in the following aspects:

1) Until now, there is no complete uniaxial compressive constitutive model for concrete at the thermal steady state, which can distinguish the stressed condition from unstressed condition. This review shows that most of the hot tests aiming at assessing the fire performance of concrete were performed on heated but unstressed specimens. The results obtained from these experiments cannot accurately reproduce practical fire scenarios in which concrete structures are always loaded (stressed) during heating. The study presented in this Chapter has addressed the lack of experimental data on the effect of applied stress during the heating process on the subsequent stress–strain relationship of concrete under uniaxial compression.

2) For unstressed concrete at the thermal steady state, elastic modulus is generally defined as the initial tangent modulus or the secant modulus of the stress-strain curve, which is not reasonable due to the development of thermal cracks. Additional strain would be caused by compressing the thermal crack openings when unstressed concrete is tested at elevated temperatures. This additional strain should be included in the

stress-strain curve since it is part of the plastic deformation, but it should be excluded from elastic modulus because it is irrecoverable. Therefore, elastic modulus for unstressed concrete at elevated temperatures should be formulated individually instead of being defined from the stress-strain curve directly.

3) At present, the available uniaxial compressive constitutive models for unstressed concrete at the thermal steady state assume the nonlinearities of the stress-strain relationship remains unchanged when the temperature increases, which is in contradiction to practical experimental observations.

4) One of the differences among the existing TTC models is the way in which the strain components are split in transient state tests, while their common problem is that part of the mechanical strain, at least the one caused by temperature gradient, is implicitly included in TTC. The implicit or semi-implicit inclusion of mechanical strain in existing TTC models makes the numerical analysis incapable of capturing precisely the extra strain caused by different historical loading and heating paths, due to the overestimation of TTC at high temperatures.

5) The experimental research on assessing fire performance of concrete with FA as SCM is incomplete. Experimental studies carried out in the last several decades focused mainly on the residual test of unstressed concrete after thermal exposure to different temperature levels. Most available data or models of the hot mechanical properties were formulated for concrete mixes used in the 1970–1980s, which were

generally conventional OPC concrete, indicating that they probably do not apply to concrete with SCM. As FA is the most widely used SCM, the effect of adding FA in concrete on its mechanical behaviour at elevated temperatures should be examined and the corresponding parameters, like compressive strength, peak strain, elastic modulus and TTC, should be calibrated using extensive experimental data.

2.8 Objectives

The main aim of this thesis is to develop an advanced thermomechanical constitutive model for concrete under uniaxial compression at elevated temperatures, for applications in structural fire engineering. The model has to capture the behaviour of structural concrete with different heating-loading sequences accurately and consider the effect of using FA as a SCM on the variation of concrete properties during thermal exposure. Specific objectives can be summarized as:

1) To investigate the variation in the nonlinearities of uniaxial compressive stress-strain curves with elevated temperatures and the difference between the elastic modulus and the secant modulus of unstressed concrete at elevated temperatures.

2) To explore the mechanism of how the applied stress during thermal exposure affects the fire performance of concrete by comparing the stress-strain responses of the concrete tested under different heating-loading sequences, and thus formulating a constitutive model that has distinguished stressed and unstressed conditions.

3) To develop a numerical method to analyse the stress fluctuation and mechanical strain caused by the temperature gradient in transient state tests, and thus to formulate an explicit TTC model and compare it with previous models to quantify the overestimation of TTC in previous research.

4) To examine the effect of partly replacing OPC with FA in concrete, on the mechanical properties of concrete at elevated temperatures. The parameters include compressive strength, peak strain, elastic modulus, nonlinearity of stress-strain curves and TTC.

Chapter 3 - Experimental details

3.1 General

This chapter presents the experimental programmes carried out to investigate the mechanical behaviour of OPC concrete and FA concrete under different fire-loading scenarios, as an effective way of formulating an advanced constitutive model. The target temperatures range from 200 °C up to 900 °C with the intervals of 100 °C ± 50 °C. Full details of the materials, test procedures and different phases of the conditioning and testing of the concrete specimens are described below, including the test rig designed for compressive tests carried out at elevated temperatures. (Pan *et al.*, 2015)

3.2 Materials

All tests in the presented experimental programme were carried out on two types of normal strength structural concrete, conventional OPC concrete and FA concrete. The only difference between them is that in FA concrete, 25% of cement content is replaced with FA. All samples were made from BS EN 197-1 CEM I type OPC. FA used in the investigation conforms to the requirements of dry BS EN 450-1 Type F (low calcium). The detailed chemical compositions of the cementitious materials are provided by the suppliers (Hanson UK and ScotAsh), as listed in Tab.3.1. The coarse aggregate was crushed granite quarried from the Hingston Down quarry. The fine aggregate was natural river sand.

Tab.3.1 Chemical composition of the binders

Binders	Composition (%)												
	SiO_2	Al_2O_3	Fe_2O_3	CaO	MgO	SO_3	TiO_2	K_2O	Na_2O	Cl	Loss on Ignition	Free CaO	Insoluble Residue
Cement	20.81	5.22	2.50	63.95	2.10	3.41	-	0.57	0.33	0.06	2.48	1.3	0.63
FA	62.81	21.02	11.63	4.25	1.70	-	1.35	2.06	2.23	-	2.11	-	-

3.3 Specimen preparation

The dimensions of the specimens were the cylinders of 50 mm diameter and 150 mm height, which gives a length/diameter ratio (slenderness) equal to 3. According to RILEM TC 200-HTC (RILEM, 2007) such dimensions could avoid the end effect during the heating process and the relatively small diameter used for the specimens was to minimize the inevitable structural effect during heating. In addition, RILEM TC 200-HTC has specified that the maximum aggregate size should not be less than 8 mm, while the specimen diameter should be at least five times the aggregate size for cast specimens. Therefore, the size of coarse aggregate was selected as 10 mm.

All specimens were cast as described in RILEM TC 200-HTC and cured under polyethylene sheets in a laboratory environment for 24 hrs. The specimens were then demoulded and moved into a tank of water for curing, which was used to provide 100% RH and 20 °C for 90 days. Before tests, the samples were oven dried at 30 °C for another 10 days, and the two end surfaces were polished to ensure that they are parallel and both perpendicular to the axis of the cylinder. In steady state tests, three parameters (compressive strength, peak strain, elastic modulus) and complete stress-

strain relationship were investigated. In transient state tests, transient thermal creep (TTC) of concrete under uniaxial compression at elevated temperatures was investigated. A minimum of two "replicate" specimens were tested for any unique combination of test and material parameters. If the test results differed by more than 20%, a third or more specimens were tested. If the result of a single specimen differed by more than 20% from the mean value of all other specimens, that specimen was excluded from the evaluation. Tab.3.2 and Tab.3.3 give the mix proportions and properties of the concrete samples used in the present study respectively.

Tab.3.2 Concrete mix proportions

Material	Mass (kg/m^3)	
	OPC concrete	FA concrete
Cement type-I 52.5	468	351
FA (Class F)	-	117
Coarse aggregate, crushed granite (10mm)	710	710
Fine aggregate	910	910
Water	235	235
Plasticizer (BASF MasterPolyheed 410)	6.5	6.5
Water/cement ratio	0.5	0.67
Water/binder ratio	0.5	0.5

Tab.3.3 Concrete properties

	OPC concrete	FA concrete
Compressive strength at 28 days, N/mm^2	43.28	36.72
Compressive strength at 90 days, N/mm^2	48.85	45
Density, kg/m^3	2368	2399

3.4 Equipment

All tests were carried out on an instron-5582 testing machine as illustrated in Fig.3.1. Thermal exposure of concrete samples (50 mm diameter × 150 mm length) was performed by using a split tube furnace with a chamber (60 mm diameter × 300 mm length). The compressive strain of the specimen was measured via a ceramic load extending placed outside of the furnace. The measurement was calibrated by a group of reference tests, in which the same load and heat as used in the tests were performed on the bottom loading rod without a concrete specimen on it and the corresponding temperature and displacement were measured. The results were then used to calculate the interference from the equipment.

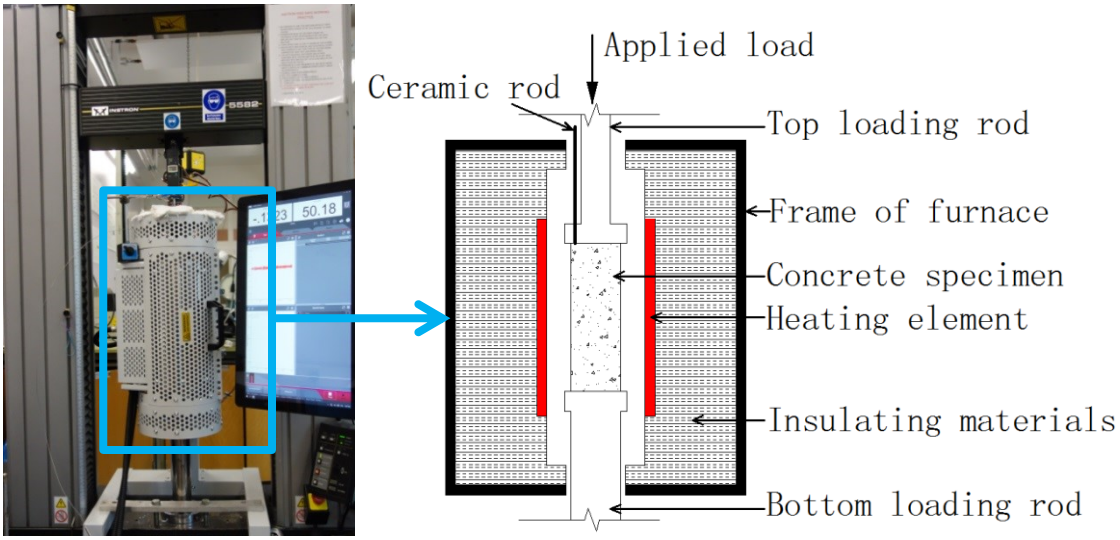

Fig.3.1. Experiment setup

The heating rate of the furnace was controllable, and the temperature distributions within the samples were monitored by thermocouples attached on the surface and at

the centre of the specimens. Three points on the surface were set to ensure heating of the concrete specimen was axially uniform, as shown in Fig. 3.2. According to RILEM TC 200-HTC, maximum differences between any of the three surface temperature readings shall not exceed 1 °C at 20 °C, 5 °C at 100 °C and 20 °C at 750 °C. For intermediate values, the maximum axial temperature differences permitted were calculated by linear interpolation between the two adjacent points. The representative surface temperature is the average temperature of the three measurements taken on the surface of the specimen.

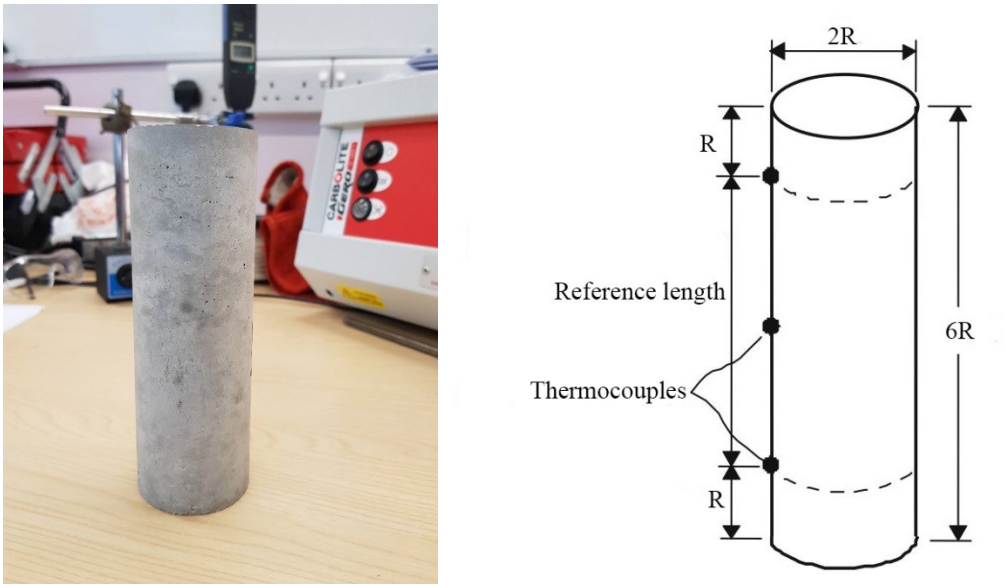

Fig.3.2 The actual specimen and arrangement of thermocouples on the surface

Prior to testing, a small compressive stress, not exceeding 0.05 MPa, was applied in the direction of the specimen's central axis. Then the specimen was subjected to a load cycle between the 5% and 15% of the reference strength. The loading and unloading were performed at a rate of 0.5 MPa/s and the hold time was 60 s (see Fig.3.3). The

ceramic rod was then placed at a location symmetrical to the former location and the above loading cycle repeated. The changes in length of the two loading cycles should not exceed 20% of the mean value. Otherwise, the following was checked: strain measuring device; centring of the specimen; flatness and orthogonality of the flat ends of the specimen. Appropriate adjustments were made and the load cycle was repeated until the 20% criterion was met.

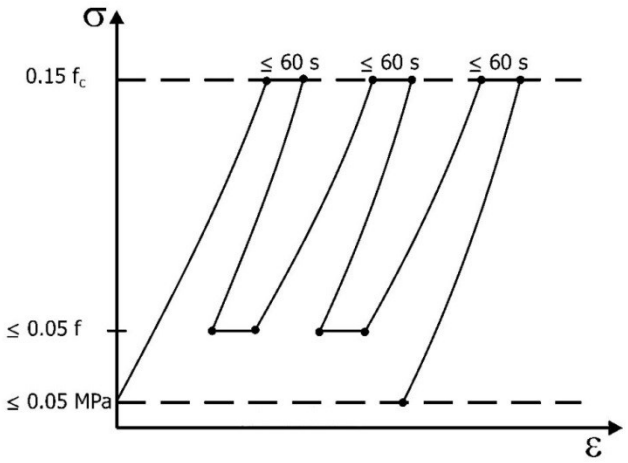

Fig.3.3 Schematic illustration of specimen cycling during installation at ambient temperature

(RILEM, 2007)

3.5 Test programme

The experimental programme was designed to investigate: (1) Effect of using FA as SCM on the mechanical properties of concrete at elevated temperatures, including compressive strength, peak strain, elastic modulus, complete stress-strain response and TTC; (2) Effect of loading history during the heating process on the hot stress-strain behaviour of concrete and development of LITS.

The aim of the test programme is to develop a thermo-mechanical constitutive model for concrete at material level, therefore, ideally, the specimen in the test programme should have a uniformly distributed temperature increase. However, this cannot be achieved in practice considering the time restriction and the development of basic creep during the long term heating process. On the other hand, if the heating rate is too high, significant temperature gradient and related thermal stress will develop, which will interfere the results. Therefore, according to the limitation of maximum heating rate recommended in RILEM TC 200-HTC, 5 °C/min is selected as the heating rate in the experimental programme.

According to the different purposes, all the tests were categorized into three series.

Series A: Unstressed specimen at the thermal steady state (heating without load and holding at constant temperature)

The specimens were heated using the heating rate of 5 °C/min to corresponding target temperatures, as shown in Fig.3.4. During the heating and holding process, moisture in the tested specimen was allowed to escape freely and a small load of 0.05 MPa was applied on the specimen to ensure the measurement of free thermal strain. The influence of the small pre-load on the deformational behaviour of the specimen during heating was negligible. In the whole process, temperatures, applied forces and uniaxial displacements of the sample were recorded simultaneously.

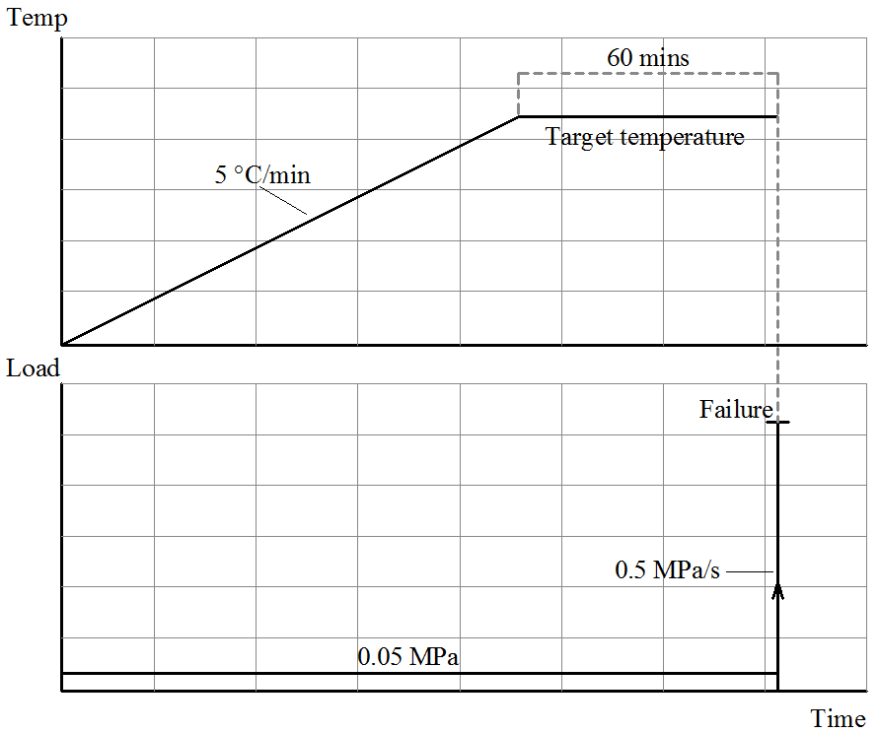

Fig.3.4 Loading-heating regime for the tests of Series A

After a further heating period of 60 mins at the target temperature, which was found to be sufficient to reach a nearly stable state in the specimen (the temperature difference between side surface and centre was less than 2 °C), the testing commenced with a cycling of the specimen according to Fig.3.5. The cycling was performed between stress levels of 5% and 30% of the compressive strength at the target temperature. The compressive strength at the target temperature was predicted according to the recommended value in EN1992-1-2 in the initial test at the target temperature, while in the replicate test it was predicted according to the initial test. If the test results differed by more than 20%, a third or more specimens were tested. The rate of loading and unloading was kept to 0.5 MPa/s and the holding time at the 5% and 30% stress levels was 30 s.

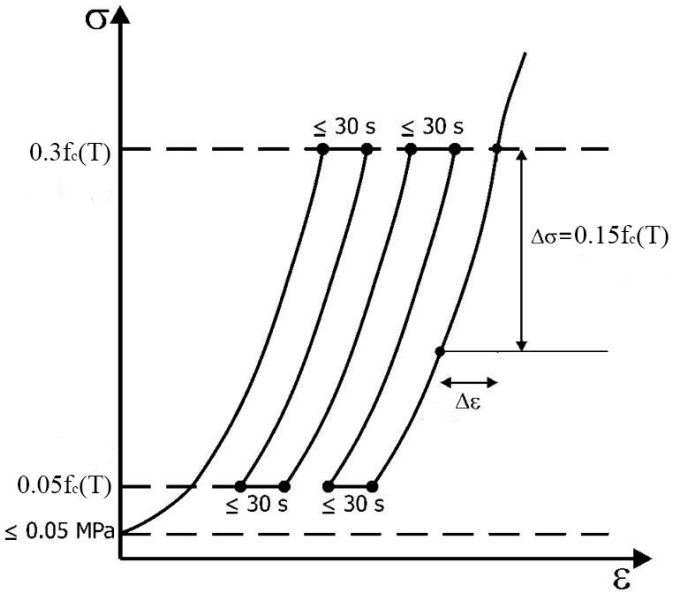

Fig.3.5 Schematic illustration of the test procedure showing how the initial secant modulus and elastic modulus are distinguished and determined (RILEM, 2007)

The specimen was loaded to failure in the third loading cycle, in which the compressive strength, peak strain, elastic modulus and stress-strain shape were determined. It should be noted that two different kinds of modulus were defined in this thesis. For the purpose of formulating the complete stress-strain relationship for unstressed concrete, the secant modulus which is determined by the strain increment in the stress interval from 0.05 to 0.3 of $f_c(T)$ in the first loading cycle is termed as initial secant modulus. In contrast, the elastic modulus here is defined as the secant modulus which is determined by the strain increment in the stress interval from 0.15 to 0.3 of $f_c(T)$ in the third loading cycle:

$$E=\frac{\Delta\sigma}{\Delta\varepsilon} \tag{3.1}$$

For the stress-rate controlled loading regime, the test was ended when the maximum compressive strength was reached. In the whole process, stress-strain response was

recorded continuously and the measured strain at compressive strength was recorded as peak strain, as described in Fig.3.6. A minimum of two "replicate" specimens were tested for any unique combination of test and material parameters. If the test results differed by more than 20%, a third or more specimens were tested. If the result of a single specimen differed by more than 20% from the mean value of all other specimens, that specimen was excluded from the evaluation.

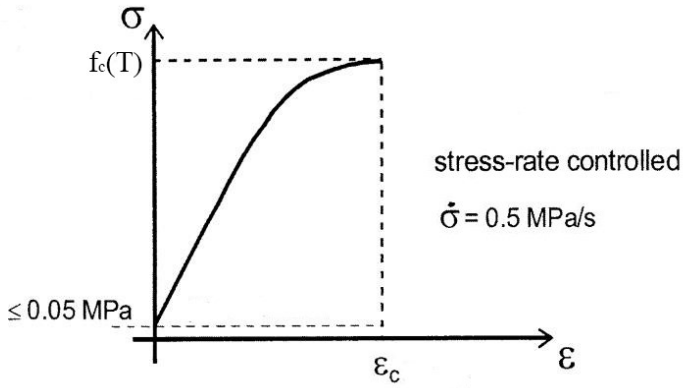

Fig.3.6 The stress–strain relationship of concrete under uniaxial compression determined by stress-rate controlled tests (RILEM, 2007)

Series B: Stressed specimens at the thermal steady state (heating with constant load and holding at constant temperature)

For stressed specimens at the thermal steady state, a uniaxial compressive load was applied in the direction of the central axis of the specimen at a rate of 0.5 MPa/s to the required constant load level at 20°C immediately prior to heating and then kept constant during the heating and holding process, as illustrated in Fig.3.7. According to RILEM TC 200-HTC, recordings of temperature and length change were taken at

intervals of 1 minute during the heating process and 5 minutes at the holding process. After maintaining 60 mins at the target temperature, the pre-fire load of the stressed specimen was reduced to 0.05 MPa and the corresponding variation of strain in the unloading process was recorded. The testing procedure to determine the stress-strain response was exactly as the procedure for unstressed specimens, as described above. The difference between Series A and Series B is with/without a sustained load in the heating process. By comparing the results obtained from Series A and Series B, the effect of the loading history during the heating process on the compressive mechanical properties of concrete at the thermal steady state could be examined. Moreover, by performing the same tests on OPC concrete specimens and FA concrete specimens respectively, the effect of using FA as SCM on the compressive mechanical properties of concrete at the thermal steady state could be investigated.

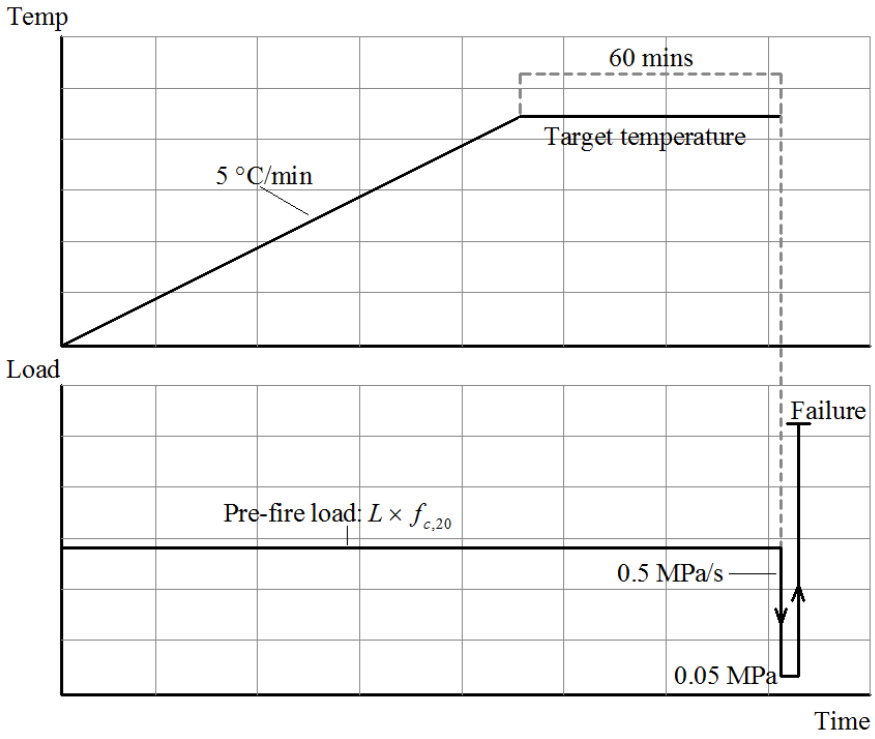

Fig.3.7 Loading-heating regime for the tests of Series B

Series C: Stressed specimen at the thermal transient state (heating with constant load until failure)

The strain-temperature relationships under different load levels can be obtained from Series A and Series B. However, it should be noted that stressed specimens in Series B were loaded to failure under the thermal steady state, indicating that the transient strain-temperature relationship is incomplete. Therefore, Series C was designed to obtain the complete transient strain of stressed concrete. The heating and loading process for Series C was exactly the same as Series B. The only difference was that in Series C, there was no holding process and the stressed specimen was kept heated until failure, as illustrated in Fig.3.8.

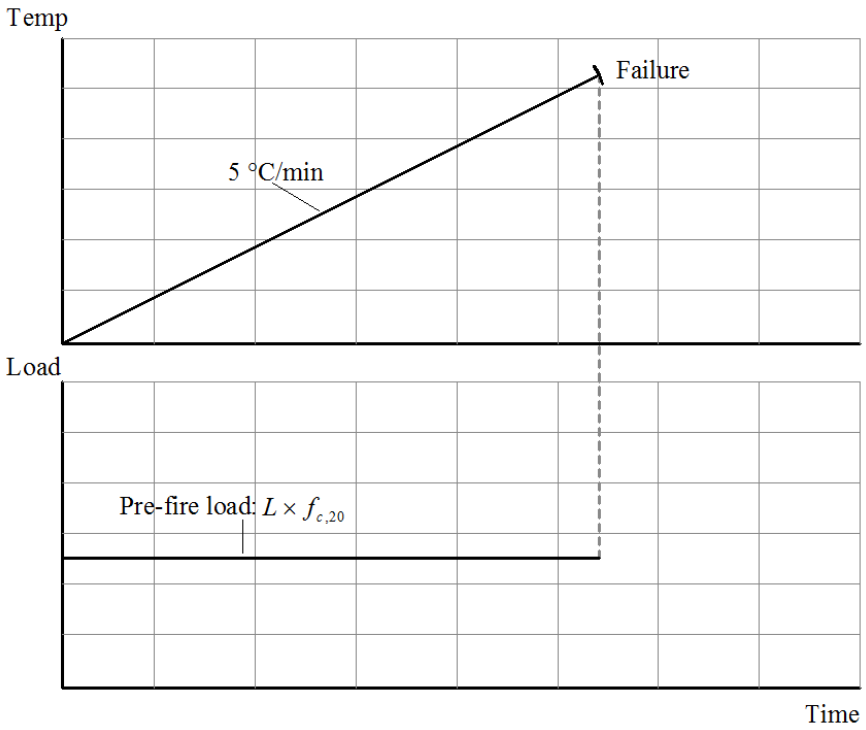

Fig.3.8 Loading-heating regime for the tests of Series C

Chapter 4 - Uniaxial compressive constitutive model for unstressed concrete under the thermal steady state*

4.1 General

This chapter presents the results obtained from tests of Series A, in which a series of thermal steady state tests of OPC concrete and FA concrete were designed and performed (Fan *et al.*, 2019a). Also presented is the comparison between the experimental results and Eurocode EN1992-1-2 to examine the applicability of the current code to FA concrete. Based on the experimental results obtained, an advanced stress-strain model for unstressed concrete was proposed and the parameters for FA concrete were formulated. Compared with existing models, the proposed model has the advantages of both considering the variation of the nonlinearities of stress-strain relationships with increasing temperature and distinguishing elastic modulus from the secant modulus of the stress-strain curve. Finally, microstructures of the samples heated to different temperatures were examined by using SEM to investigate the thermal effect on the organization of the pore microstructure. Relative average deviations of parameters investigated in tests of series A are presented in Appendix.

* Chapter 4 is mainly based on the published work: "K. Fan, D. Li, N. Damrongwiriyanupap, L. Li, Compressive stress-strain relationship for fly ash concrete under thermal steady state, Cement and Concrete Composites. 104 (2019) 103371."

4.2 Mechanical properties of FA concrete at high temperatures

The mechanical properties of conventional OPC concrete (without SCMs) under uniaxial compression at the thermal steady state have been extensively studied and the results obtained by different researchers show a good agreement with each other when the samples used are made from the same aggregate type (calcareous/siliceous) and identical water/cement ratio. However, other parameters, like the dimensions of sample, heating rate or variations of raw materials, seem to have very limited impact on the results, as long as they vary within the practical range for NSC and RILEM TC 200-HTC. Several previous tests are, therefore, selected as a reference group representing the normal-strength OPC concrete. The samples used in our tests are made from the same aggregate type (siliceous) and identical water/binder ratio (0.5) as the reference group for the purpose of comparison. The details are summarized in Tab.4.1. For the purpose of comparison, the results of HSFC provided by Diederichs (Diederichs, Jumppanen & Penttala, 1988) are also listed as a reference group.

Tab.4.1 Reference group for unstressed thermal steady tests

Group	Reference					Experiment	
Concrete type	OPC concrete (without SCMs)				FA concrete		OPC concrete
Parameters to be compared	Strength		Deformation		Strength & deformation		
Resources	Abrams (Abrams, 1971)	Malhotra (Malhotra, 1956)	Schneider (Schneider, 1988)	Furumura (Furumura, Abe & Shinohara, 1995)	Diederichs (Diederichs, Jumppanen & Penttala, 1988)	Series A	
Water/binder	0.5	0.5	-	0.41	0.27	0.5	0.5
Initial strength (MPa)	27	40	-	44	106.9	45	48.85
Cementitious materials	100%OPC	100%OPC	100%OPC	100%OPC	75%OPC 25%FA	75%OPC 25%FA	100%OPC
Aggregate type	Siliceous	Siliceous	Siliceous	Siliceous	Siliceous	Siliceous	Siliceous
Abbreviation	NSC (normal strength concrete)	NSC	NSC	NSC	HSFC (high strength fly ash concrete)	NSFC (normal strength fly ash concrete)	NSC

4.2.1 Compressive strength

The temperature-compressive strength relationships are plotted in Fig.4.1, in which the compressive strength is normalized by the strength of the unheated specimens, respectively. The solid lines represent the results from our tests and each point on it is an average of at least two specimens at each temperature level. As can be seen, NSFC shows a trend similar to NSC without SCMs. Initially, the compressive strength of NSFC remains unchanged to 200 °C and increases to about 105% at 300 °C, which is attributed to the further hydration of FA under hydrothermal conditions. Above that, the compressive strength decreases gradually with elevated temperature due to the dehydration of CSH. The decrease rate reaches the maximum value around 550 °C when the crystalline transformation from α-quartz to β-quartz of aggregates may take place. In the whole range, the drop of compressive strength in NSFC stays lower than that of NSC, which indicated that further hydration of the reactive silica in FA during the heating process does improve the high temperature performance of concrete. Given the replacement percentage of FA is only 25%, the improvement is therefore not prominent, but at least the positive effect of FA during thermal exposure is confirmed. It therefore can be concluded from the results shown in Fig.4.1 that the Eurocode model (ENV1992-1-2, 1995), represented by the dotted line in Fig.4.1, is quite safe when it is applied to FA concrete.

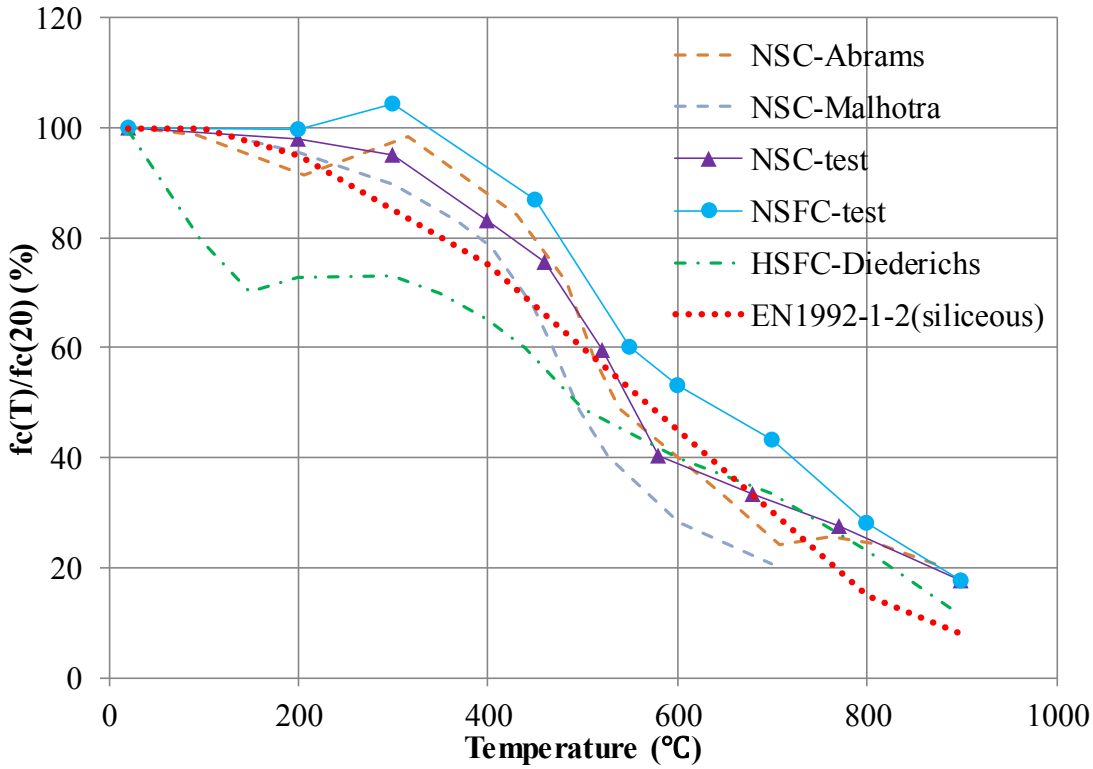

Fig.4.1. Normalized compressive strength of unstressed concrete at different temperatures

According to the comparison between the results from Abrams (Abrams, 1971) and Malhotra (Malhotra, 1956), it can also be concluded that the variation of the initial unheated strength seems to have little impact on the normalized value of the compressive strength at different temperature levels. Nonetheless, the above conclusion only applies to NSC. When it comes to HSC, a very different variation of compressive strength with temperature was observed. As illustrated in Fig.4.1, the chain line of HSFC drops much faster than the solid curve of NSFC at an early stage, which is the consequence of the denser microstructure and corresponding higher pore pressure in HSFC. It could be inferred that there are critical values for the parameters that yield condensation in cement paste, like water/binder ratio or replacement percentage of FA. Beyond the critical values, a highly condensed microstructure may

be produced in concrete which results in destructive pore pressure under thermal exposure. On the other hand, the difference between NSFC and HSFC decreases with the increasing of temperature. When the temperature reaches to 800 °C, they are very close to each other, indicating that the compressive strength at relatively high temperature (beyond 600 °C) is almost independent of pore pressure. The variation in aggregates might be the main contribution in this phase.

4.2.2 Peak strain at compressive strength

The peak strain at compressive strength is a key deformation characteristic in evaluating the plastic strain of concrete, but it is hard to determine at high temperature due to the difficulty in measurement. Thus, there are few available results on it. Fig.4.2 shows that the peak strains at compressive strength of NSC and NSFC, tested by Schneider (Schneider, 1988), Furumura (Abe *et al.*, 1999; Furumura, Abe & Shinohara, 1995) and us, are almost identical to each other before 300 °C and only a slight difference is observed afterwards, which indicates that FA has no significant influence on the peak strain. The thermal incompatibility between aggregate and cement paste might be the main contribution and, in that case the aggregate type should be the decisive factor. From the common trend of these three curves it can be concluded that the peak strain at compressive strength remains approximately unchanged until 200 °C and increases rapidly above that. In contrast, the peak strain of HSFC increases visibly slower than that of NSFC for temperatures between 200 °C and 450 °C, suggesting a more brittle behaviour, which could be attributed to its

denser structure and corresponding higher loss of compressive strength in that temperature range. Another interesting result observed from Fig.4.2 is that the temperature-peak strain relationship in Eurocode is much higher than those of experimental results. This is because the peak strain in Eurocode has implicitly included an extra strain component called TTC which resulted from the pre-fire load (Torelli *et al.*, 2016). This implicit inclusion is safe and conservative in many cases, but it might yield an inaccurate estimation of the deformation in concrete when the pre-fire load varies during the thermal exposure. For an advanced analysis, TTC should be calculated explicitly and Eurocode may not be applicable in that situation (Gernay, 2012; Gernay & Franssen, 2012).

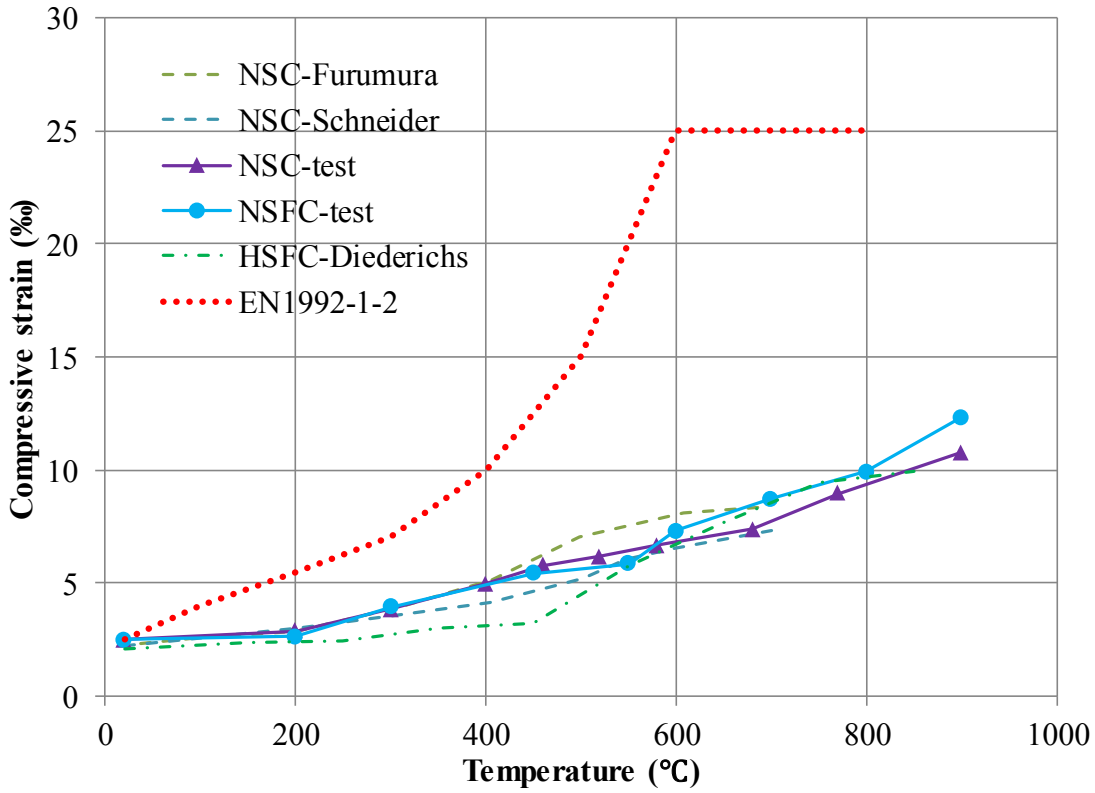

Fig.4.2 Peak strain of unstressed concrete at different temperatures

4.2.3 Elastic modulus

As discussed above, the compressive strength decreases while the peak strain increases with the rise of temperature, which means that the concrete becomes softer under thermal exposure. Therefore, it is important to evaluate the variation of its stiffness, represented by the temperature-dependent elastic modulus. As a deformation characteristic, the temperature-dependent variation of elastic modulus is also controlled by the type of aggregate and hardly influenced by the partly replaced FA, which is similar to the behaviour of the peak strain as discussed above. As illustrated in Fig.4.3, the decrease of the elastic modulus of concrete with increasing temperature generally exceeds the decrease of its strength, and the curves for FA concrete and OPC concrete are in good agreement with each other since they are all made from siliceous aggregates.

As defined in Section 3.4 and shown in Fig.4.3, the secant modulus evaluated according to the first loading cycle was significantly lower than the elastic modulus evaluated from the third loading cycle. This is attributed to the compression of thermal cracks. In the first loading cycle, the thermal cracks developed in the heating process were compressed, resulting in a larger deformation than the third loading cycle under the same load value. Fig.4.3 shows these two types of modulus are very close to each other when concrete is loaded at ambient temperature. The difference between them increases with elevated temperatures and the maximum rate of the variation happens between 400 °C and 600 °C. Above that, the α-β phase transition of quartz in siliceous

aggregate has completed, thus the difference is relatively stable.

The elastic modulus represents the elastic behaviour of unstressed concrete at high temperatures, while the secant modulus of the stress-strain curve represents the real deformation of unstressed concrete at high temperature by including part of the plastic deformation caused by the closure of the thermal cracks. Both of them are necessary to define the real stress-strain behaviour of unstressed concrete at high temperatures. However, in most previous studies these two types of modulus were not clearly distinguished and generally only one of them was assessed.

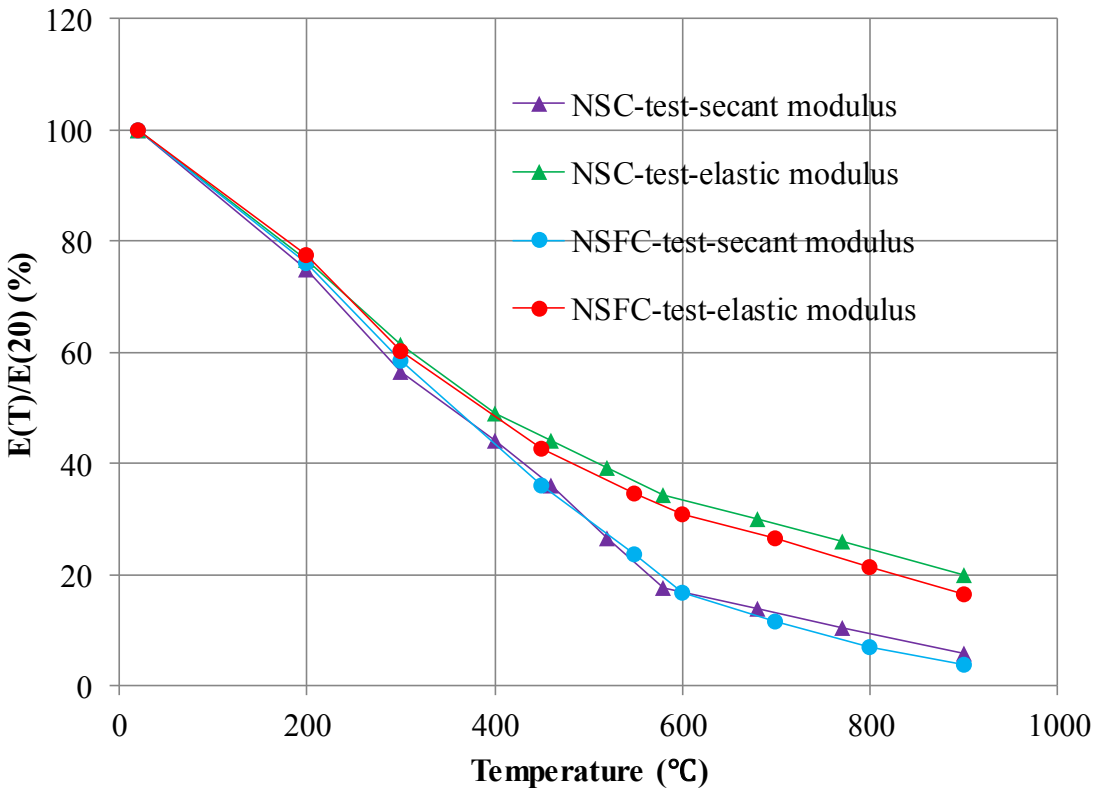

Fig.4.3. Normalized elastic modulus and secant modulus of unstressed concrete at different temperatures

4.3 Development of an advanced stress-strain model

4.3.1 Determination of the basic equation

As introduced in Section 2.4.5, all existing stress-strain models for unstressed concrete assume the nonlinearities of the stress-strain relationships remain unchanged when the temperature increases. As illustrated in Fig.4.4, the dash lines represent the normalized experimental stress-strain relationships of NSFC at different temperatures, while the solid lines are calculated by the models listed in Section.2.4.5.

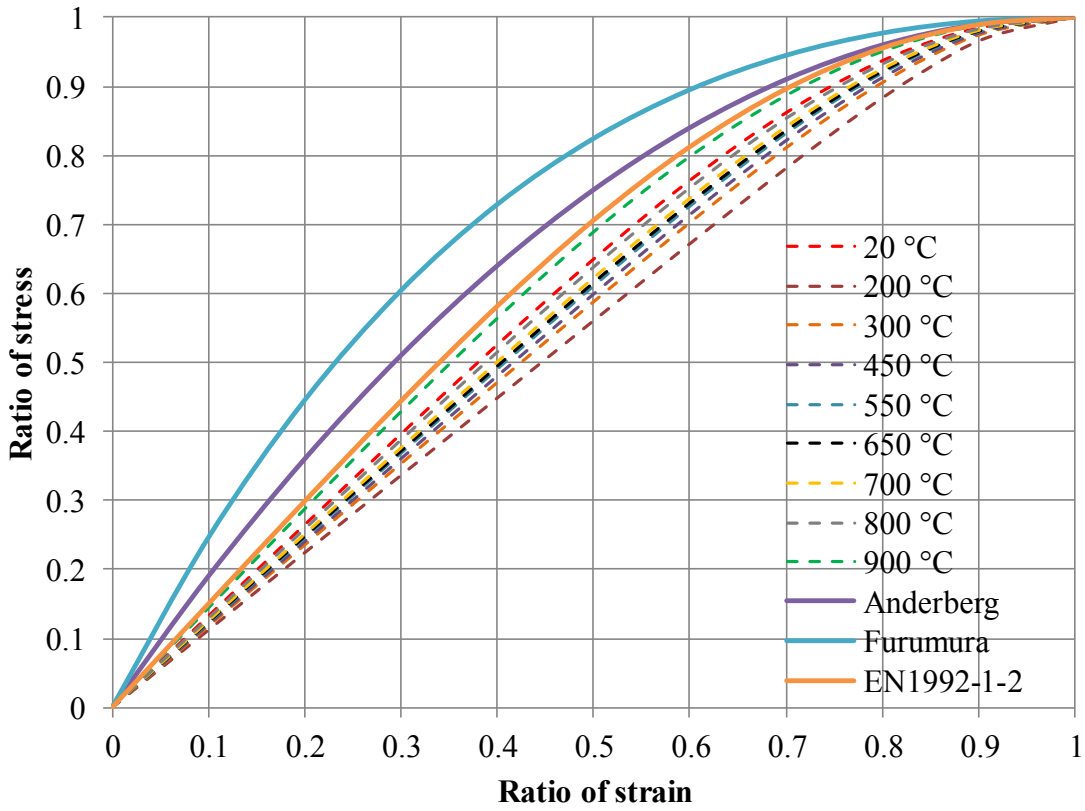

Fig.4.4 Normalized stress-strain relationships of unstressed NSFC at different temperatures

It is evident that the nonlinearities of experimentally obtained stress-strain relationship vary with temperature, while the three theoretical models are incapable of capturing

this phenomenon since their nonlinearities are constant. This is an important characteristic but has been frequently ignored. In the present study, Eq.(4.1) proposed by Popovics (Popovics, 1973) is selected as the basic equation since it has the advantage of incorporating a parameter "n" to control the nonlinearities of the curves.

$$\frac{\sigma}{f_c}=\frac{\varepsilon}{\varepsilon_c}\frac{n}{n-1+\left(\frac{\varepsilon}{\varepsilon_c}\right)^n} \tag{4.1}$$

where σ, ε are the instantaneous stress and strain, respectively; f_c is the compressive strength of unheated concrete; ε_c is the peak strain at compressive strength of unheated concrete; n is a parameter related to the nonlinearity of the stress-strain relationship of concrete at ambient temperature.

4.3.2 Nonlinearity of stress-strain relationships

By applying Eq.(4.1) to the experimental stress-strain data, the parameter "n" at different temperature levels can be determined. Fig.4.5 shows that parameter "n" of NSFC increases to 9 at 200 °C and then drops quickly to 6.6 at around 300 °C. After that, the rate of decrease slows down. When the heating terminates at 900 °C, it drops back to approximately the initial value. The higher value of n means that the stress-strain response is more linear. Fig.4.4 shows that the experimentally obtained curves are more linear than those of the previous OPC concrete models, which indicates that n has a higher value and there is less plastic strain in FA concrete. This is in accordance with the trend of the purple solid line representing the experimental temperature-n relationship of NSC in Fig.4.5, which has a similar trend as NSFC but

with lower values. The characteristic could be ascribed to the increased skeleton of CSH caused by the reaction between FA and CH. The rapid increase of n at an early stage is a consequence of the further reaction of unreacted binders, while the decrease at later stages might be caused by the thermally induced micro-cracks in the cement paste and the decomposition of CSH.

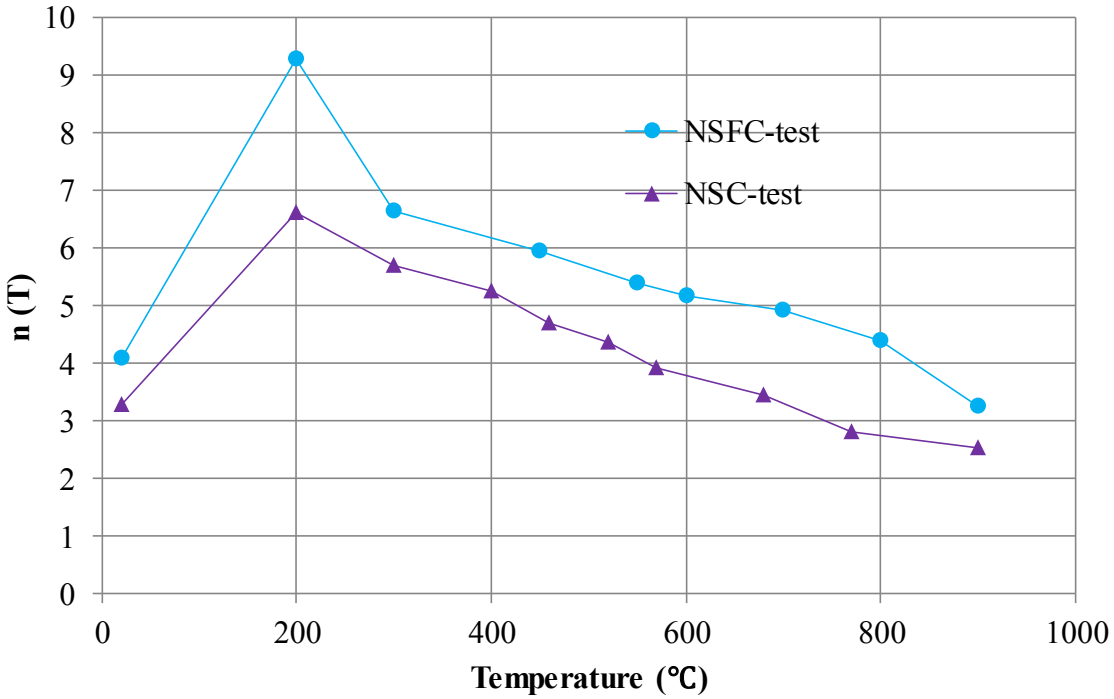

Fig.4.5. Parameter n of unstressed concrete at different temperatures

4.3.3 Advanced stress-strain model

With knowledge of the basic stress-strain equation, and the variation of compressive strength, peak strain and nonlinearity parameter n as mentioned above, a complete temperature-dependent stress-strain model is proposed as follows,

$$\frac{\sigma}{f_c(T)}=\frac{\varepsilon}{\varepsilon_c(T)}\frac{n(T)}{n(T)-1+\left(\frac{\varepsilon}{\varepsilon_c(T)}\right)^{n(T)}} \tag{4.2}$$

where $f_c(T)$ is the compressive strength at temperature T; $\varepsilon_c(T)$ is the peak strain at

temperature T; $n(T)$ is the nonlinearity parameter at temperature T. To simplify the model, the variations of the three temperature-dependent parameters for NSFC are represented by using the linear relationships to best fit the original curves, as demonstrated in Fig.4.6.

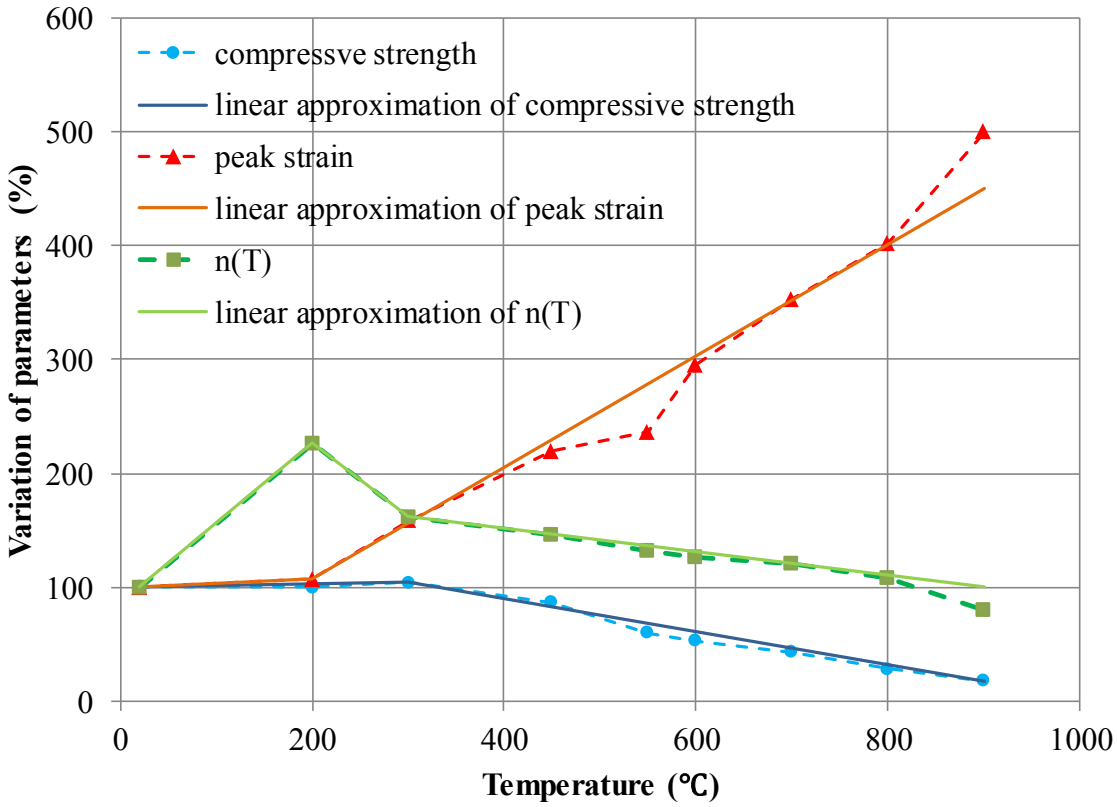

Fig.4.6. Linear approximation used for three decisive parameters (NSFC)

In this way, the complete compressive stress–strain model for FA concrete could be incorporated with Eqs.(4.3)-(4.5) to achieve a simpler solution in analysis.

$$f_c(T)=\begin{cases} f_{c,20}\times\left(1.0+2.0\times10^{-4}\times T\right) & 20\le T\le 300 \\ f_{c,20}\times\left(1.5-1.5\times10^{-3}\times T\right) & 300< T\le 900 \end{cases} \tag{4.3}$$

$$\varepsilon_c(T)=\begin{cases} \varepsilon_{c,20}\times\left(1.0+3.9\times10^{-4}\times T\right) & 20\le T\le 200 \\ \varepsilon_{c,20}\times\left(0.10+4.9\times10^{-3}\times T\right) & 200< T\le 900 \end{cases} \tag{4.4}$$

$$n(T)=\begin{cases} n_{20}\times\left(0.86+7.1\times10^{-3}\times T\right) & 20\le T\le 200 \\ n_{20}\times\left(3.6-6.5\times10^{-3}\times T\right) & 200< T\le 300 \\ n_{20}\times\left(1.9-1.0\times10^{-3}\times T\right) & 300< T\le 900 \end{cases} \tag{4.5}$$

Meanwhile, considering the fact that the secant modulus of the stress-strain curve is unable to represent the real elasticity of concrete at high temperatures, the elastic modulus is additionally formulated as:

$$E(T)=E_{20}\times\left(1.05-1.69\times10^{-3}T+8.00\times10^{-7}\times T^{2}\right) \tag{4.6}$$

4.3.4 Verification of proposed model

Fig.4.7 shows the comparison between the experimentally obtained stress-strain curves of NSFC, represented by the red dot points, and those calculated from the proposed model, in which the black dash lines represent the results calculated by Eq.(4.2) with parameters directly measured from experiments and the light blue solid lines represent the results calculated by using the simplified model Eqs.(4.2)-(4.5). It is obvious from the comparisons that the theoretical model behaves excellently, whereas the simplified model differs marginally from the experimental data but with generally acceptable errors. This indicates that, when the model is adopted, the parameters incorporated can be determined by either way (measured value or simplified relationships), depending on the expected efficiency and accuracy specifically.

Note that the proposed model is also applicable to OPC concrete, but the formulation of the key parameters, should be replaced. There are a lot of available formulations for

the compressive strength and peak strain of OPC concrete at the thermal steady state. In this thesis, these two parameters were not formulated once again. As for the redefined elastic modulus, FA is proven to have no obvious impact on it, as illustrated in Fig.4.3. Thus the redefined elastic modulus formulated for FA concrete is applicable to OPC concrete too. The only parameter which needs to be specially formulated for OPC concrete is parameter n. According to the experimental data presented in Fig.4.5, n for normal strength OPC concrete can be formulated as:

$$n(T)=\begin{cases} n_{20}\times\left(0.89+5.7\times10^{-3}\times T\right) & 20\le T\le 200 \\ n_{20}\times\left(2.31-1.8\times10^{-3}\times T\right) & 200< T\le 900 \end{cases} \tag{4.7}$$

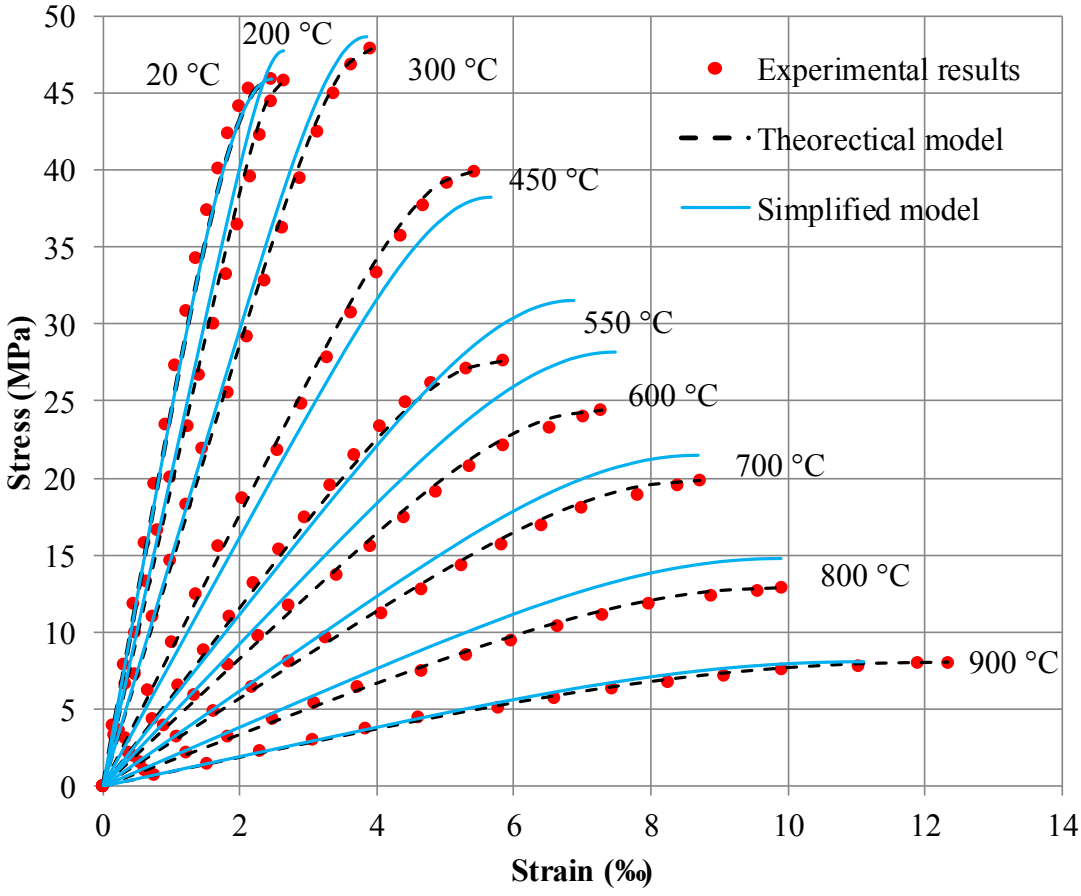

Fig.4.7. Comparison of experimental stress-strain relationships with the proposed model (NSFC)

4.4 Microstructure imaging

The microstructures of crushed powder samples of the NSFC specimens at different temperatures were examined by using SEM techniques to understand the thermal effect on the change of the micro-structure organization of FA concrete. For each temperature case, at least 3 scans have been performed at different locations. Meanwhile, the representative EDS results of chemical compositions of the hydrated cement paste, aggregate and unreacted FA are presented in Tab.4.2. Compared with Tab.3.1, the chemical compositions of FA are almost identical. And the chemical compositions of the hydrated cement paste are similar to the unreacted cement but with higher proportion of O and Si, which should be attributed to the hydration of the cement and FA. On the other hand, it could be noted that the chemical compositions of aggregate are very similar to FA. They could be distinguished from each other by the sizes of them. The particle size of FA generally ranges from 1 um to 100 um which is far less than that of aggregate.

Tab.4.2 Chemical compositions of the hydrated cement paste, aggregate and unreacted fly ash

Composition	Cement paste	Aggregate	Fly ash
		%	
O	37.93	45.90	41.89
Ca	39.60	2.35	3.16
Si	14.02	36.83	30.35
Al	3.81	5.16	11.67
Fe	2.07	2.05	8.58
S	1.05	-	-
K	0.77	3.36	1.31
Mg	0.51	0.68	0.92
Na	0.24	2.82	1.35
Ti	-	0.85	0.77

As illustrated in Fig.4.8.a and Fig.4.8.b, some unreacted FA particles were observed in the unheated specimen and the specimen heated to 200 °C. In contrast, Fig.4.8.c shows that after the specimens were heated to 450 °C, the unreacted particles disappeared due to the reaction between the FA and CH, which is in consistent with what was reported in the literature (Khoury *et al.*, 2002). Moreover, the cement paste is reasonably dense and compact at ambient temperature and 200 °C. However, with increasing temperature, the microstructure of the cement matrix seems to have undergone significant changes. At 450 °C, some discrete pores developed due to vapour migration and increased pore pressure. After the temperature increased to 550 °C, the aggregate begun to expand rapidly as it is approaching the temperature for α-β phase transformation (Hertz, 2005). The sharp increase of expansion of the aggregate at around 550 °C is opposite to the shrinkage of cement paste, resulting in severe damage and cracks at the interface between aggregates and adjacent cement paste, which is the reason for the observed maximum degradation rate of the compressive strength at this temperature in our experiments. At last, when the temperature hits 700 °C, the CSH phase has decomposed and the cement matrix has turned into a loose white material that is very porous and weak. The corresponding deterioration of the mechanical properties of concrete at this temperature is very obvious as illustrated in Fig.4.7.

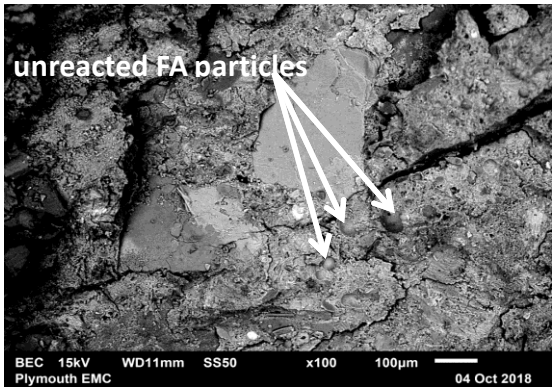

(a) 20 °C

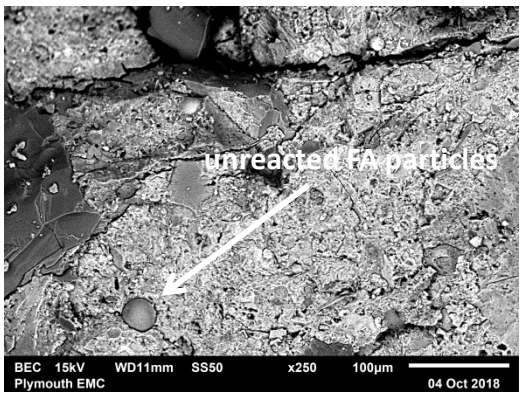

(b) 200 °C

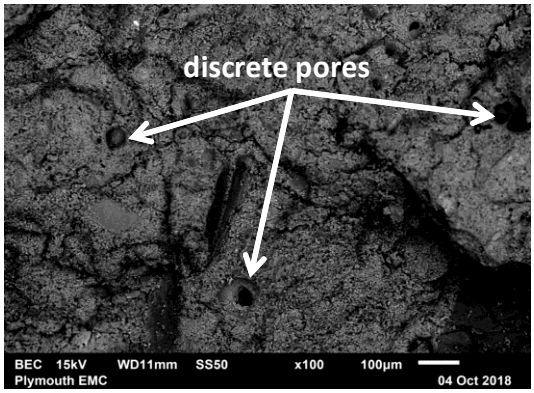

(c) 450 °C

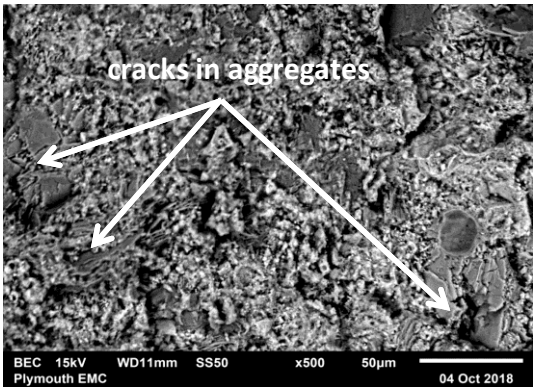

(d) 550 °C

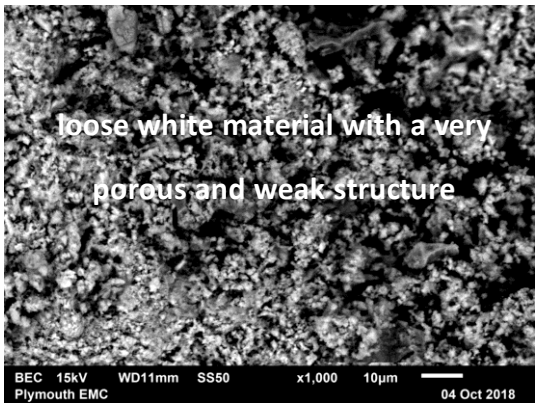

(e) 700 °C

Fig.4.8. Microstructures of crushed unstressed FA concrete specimens at different temperatures

4.5 Conclusions

This chapter has presented an experimental study of the mechanical properties of unstressed specimens (OPC concrete and FA concrete) under the thermal steady state. The results presented include the compressive strength, peak strain at compressive strength, elastic modulus, and stress-strain relationship at temperatures ranging from ambient to 900 °C. From the results presented the following conclusions can be drawn:

1) 25% replacement of cement with FA in concrete hardly influences its deformation characteristics at high temperatures, but the temperature-dependent compressive strength are enhanced due to the further reaction between FA and CH under hydrothermal conditions.

2) Eurocode EN1992-1-2 seems to be safe to be applied to NSC with 25% replacement of FA as SCM. However, the peak strain at compressive strength recommended in EN1992-1-2 has implicitly included the TTC, which should be explicitly calculated using the advanced analysis method.

3) Porosity of cement paste has a significant influence on the mechanical properties of concrete at high temperatures, especially at early stages of thermal exposure (before 500 °C). There might be a critical value for the replacement percentage of FA, which will lead to an increase of the solid skeleton of the cement paste and potential destructive pore pressure during heating. Therefore, the higher replacement percentages of FA in cement should be further verified.

4) Due to the development of thermal cracks, the elastic modulus of concrete at elevated temperatures is higher than the secant modulus of the stress-strain curve which is determined by the strain increment in the stress interval from 0.05 to 0.3 of $f_c(T)$. The difference increases with elevated temperatures and the maximum rate of variation happens between 400 °C and 600 °C. Above that, the α-β phase transition of quartz in siliceous aggregate has completed, thus the difference is relatively stable.

5) The shape of stress-strain relationship, represented by the nonlinearity of the curve, is found to vary with temperature. Adding FA into concrete makes it behave more linearly and reduces its plasticity due to the increased skeleton of CSH caused by the further hydration of FA during heating.

6) An advanced uniaxial compressive constitutive model for unstressed concrete under the thermal steady state was formulated and verified. Compared with previous models, the present model has the advantage of incorporating a parameter $n(T)$ to consider the variation of the nonlinearity and distinguishing elastic modulus from the secant modulus of the stress-strain curve. In addition, the key parameters in the proposed model are calibrated for FA concrete.

Chapter 5 - Uniaxial compressive constitutive model for stressed concrete under the thermal steady state as a function of load history during the heating process

5.1 General

For the tests discussed in Chapter 4 (Series A), the concrete specimens were heated without carrying any load to a target temperature. The target temperature was held for 60 minutes and then the specimens were immediately loaded up to failure. However, concrete structures are generally stressed prior to any thermal exposure, thus it is necessary to formulate a constitutive model for this condition too. This chapter reports on tests of Series B, in which specimens are heated with a sustained load (10%，30%，50%，or 70% of reference strength). After the completion of 60 minutes holding period at the test temperature, the specimens were quickly unloaded and then immediately tested to failure.

The maximum temperature that structural concrete may be subjected to depends on the application of the structure. For example, in the Netherlands, the Ministry of Public Works, the Rijswaterstaat (RWS), and the TNO Centre for Fire Research have established a fire curve on the basis of Dutch experience in tunnel fires (Khoury, 2000). This RWS Dutch fire curve models a most severe hydrocarbon fire, rapidly exceeding 1200 °C after 60 min, which indicates that high temperature needs to be considered in some specific fire scenarios. On the other hand, according to the results

presented in Chapter 4, no matter it is OPC concrete or FA concrete, the corresponding compressive strength at 400 °C is above 80% of the reference strength, which suggests that the deterioration of concrete is minor up to test temperatures of about 400 °C. Therefore, the influence caused by the pre-fire load below 400 °C will not be discussed in this Chapter and the focus is placed on the temperatures above 400 °C.

Considering the fact that the mechanism of how the sustained load during the heating process influences the temperature-dependent stress-strain response is still not understood and there is not any applicable model for these thermomechanical conditions, OPC concrete is selected as the experimental material for the tests in this Chapter, instead of FA concrete, so that the conclusions will be more widely applicable. Finally, some FA concrete specimens were tested under the same conditions to verify the applicability of the proposed model. Relative average deviations of parameters investigated in tests of series B are presented in Appendix.

5.2 Mechanical properties

5.2.1 Compressive strength

Fig.5.1 shows the temperature-normalized compressive strength relationships of OPC concrete under different pre-fire loads. As can be seen, the compressive strength of OPC concrete under different loads show little difference at 400 °C and 460 °C, which indicates that the effect of pre-fire load on the compressive strength before 460 °C is relatively slight. However, above 460 °C, the specimens seem to be strengthened by

applied stress. The compressive strength of the stressed specimens are significantly higher than those of the unstressed specimens. Clearly, the specimens stressed with higher pre-fire load levels undergo less deterioration in compressive strength. The rate of this trend quickly develops from 460 °C to 580 °C, which is likely to be attributed to the decomposition of CH in this temperature range.

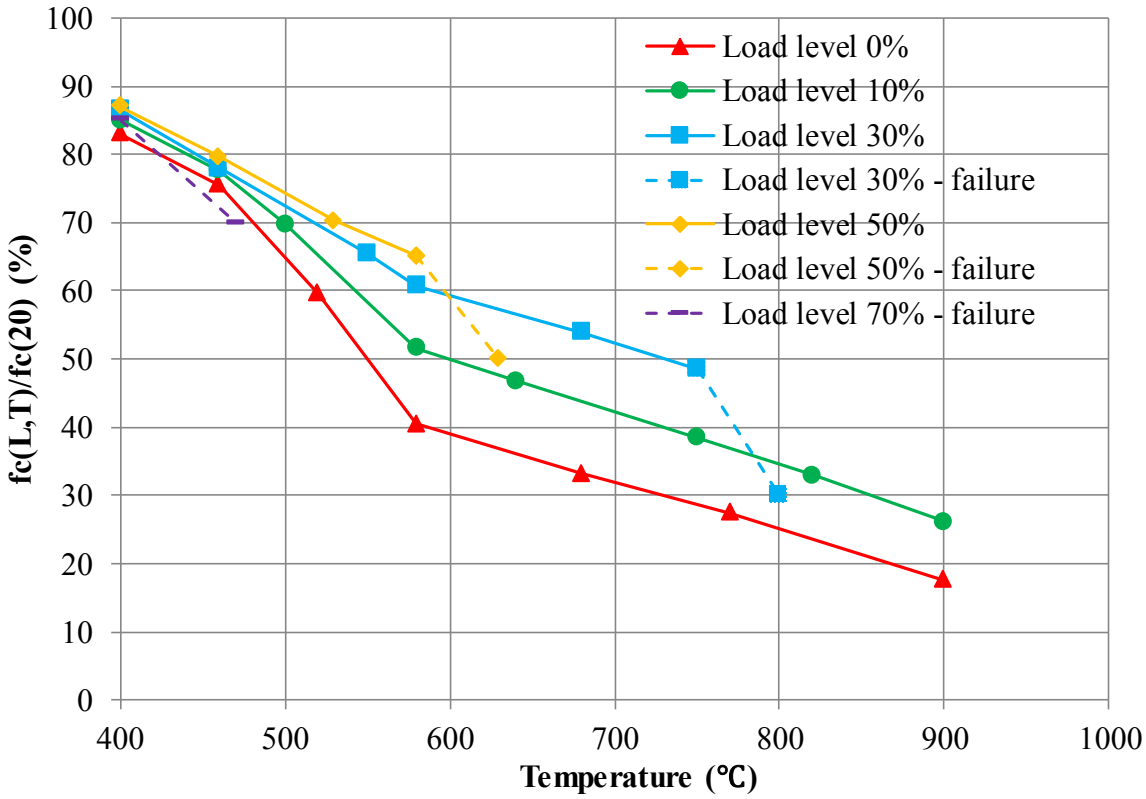

Fig.5.1 Normalized compressive strength-temperature relationships of specimens with different load levels

According to the existing research (Mindess, Young & Darwin, 2003; Monteiro, 2006; Taylor, 1997), CH is an important component in the interfacial transition zone, as shown in Fig.5.2. In general, the weakest link of the chain is considered to be the strength-limiting phase in concrete. Based on the physicochemical changes in concrete

at elevated temperatures summarized in Tab.2.1, CH remains stable up to around 400 °C. When the temperature is higher than 460 °C, CH will decompose, and the chemical bond water will be released and a strong vapour pressure in micro-pores of interfacial transition zone (ITZ) will be developed. The average pore size in ITZ will increase, resulting in the loss of compressive strength (Monteiro, 2006). However, when specimens are heated under pre-fire loads, some micro-cracks are produced and accumulated during the heating process, which lead to a reduction in the build-up of vapour pressure in micro-pores as a result of the decomposition of CH, thus preventing explosive micro-cracks opening in ITZ. Therefore, the damage caused by the applied load is not only compensated, but also benefits the vapour diffusion process. It should be noted that the load level itself has little impact on the results as long as it is larger than 0.3, which means that this value is enough to release the vapour pressure in the temperature range. CH completely decomposes at around 540 °C, therefore it can be seen that the solid lines representing different load levels are almost parallel to each other from 580 °C to the end，which indicates that the enhancement caused by the pre-fire load in this phase is insignificant. The damage of the micro-pore structure in ITZ offers a possible explanation for a mechanism that is compatible with the observations obtained from our tests.

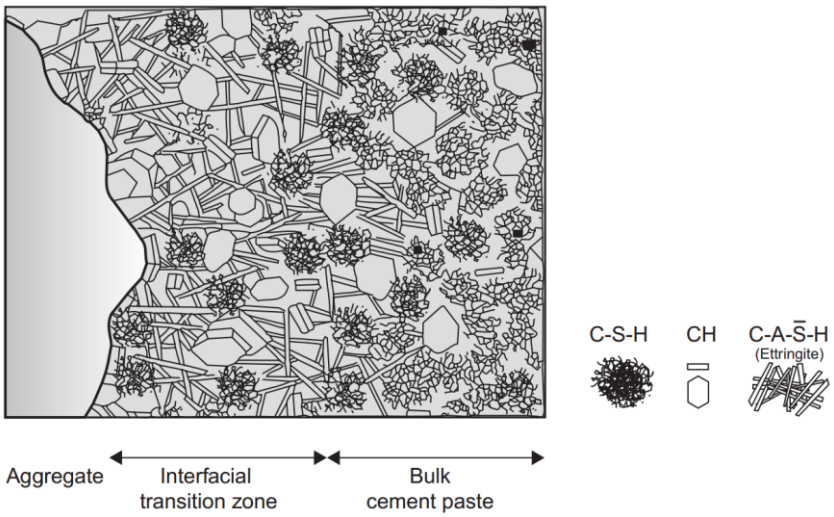

Fig.5.2 Diagrammatic representation of the interfacial transition zone (Monteiro, 2006)

It should be noted that with the increasing temperature, stressed specimens would fail at some point in the transient heating process before it achieves the thermal steady state. This condition is represented by the dash lines shown in Fig.5.1, which shows that the temperature at the fail point of the stressed specimens is always lower than the prediction based on the corresponding solid line. When the unstressed curve is compared with the failure points, the increase in compressive strength caused by the pre-fire load would be significantly underestimated, which might be the reason why the strengthening effect caused by the pre-fire load was not clearly observed in some of the previous research. The sharp decrease in compressive strength and sudden break down are caused by the strong stress fluctuation in the stressed specimens as a result of the temperature gradient during the heating process. More details of the latter aspect will be discussed in Chapter 6.

5.2.2 Peak strain

The temperature-peak strain relationships of concrete under different load levels are

plotted in Fig.5.3. Compared with compressive strength, peak strain is even more sensitive to the pre-fire load. At 400 °C and 460 °C, the compressive strength is little influenced by the pre-fire load, whilst the peak strain is clearly reduced in specimens under the pre-fire load. Unlike the compressive strength, the peak strain in stressed specimens remains almost unchanged in the temperature range where CH decomposes (460 °C - 540 °C). The relative reduction caused by the pre-fire load increases proportionally from 400 °C to 680 °C. The obvious variation occurs above 680 °C, where the peak strain of unstressed specimen increases at a higher rate while the peak strain of stressed specimen significantly decreases. As an observation of the compressive strength, the peak strain reduces with the increase of the pre-fire load when the load level is below 0.3, while there is little change in peak strain with the increase of the pre-fire load when the load level is over 0.3.

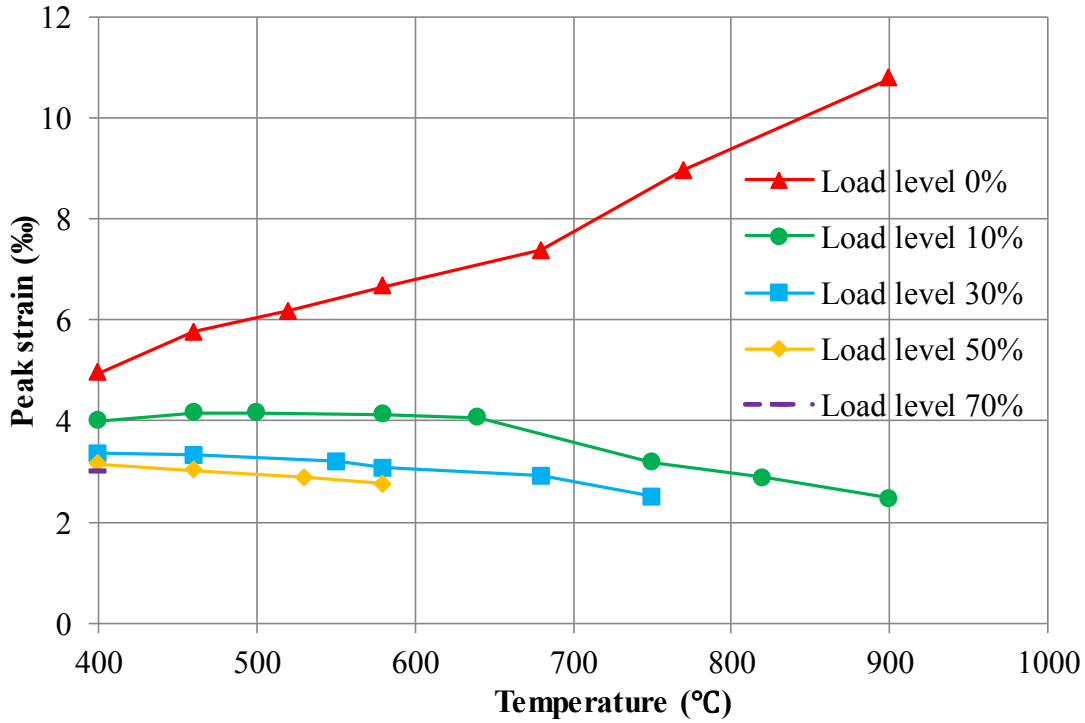

Fig.5.3 Peak strain-temperature relationships of specimens with different load levels

With increasing temperature, a considerable amount of the presumed ductility in concrete has vanished during the heating process, so that the peak strain turned out to be unexpectedly small. There are two possible mechanisms which can explain these observations. To begin with, when concrete is heated, cracks would develop due to thermal expansion, shrinkage and incompatibility between the aggregate and the cement paste. If concrete is loaded during heating, the development of cracks would be constrained. Part of the reduction of peak strain of stressed specimens is attributed to this mechanism, especially for relatively low temperature ranges. Second, the sustained load during heating keeps producing deformation energy at each temperature increment continuously, which means that the ductility has been released during the heating process of the stressed specimen. This kind of deformation process is responsible for the reduction in peak strain and the development of TTC. More details of this aspect will be discussed in Chapter 7, where strain measurements corresponding to such a load and temperature history are presented.

5.2.3 Elastic modulus

In addition to the peak point of stress-strain curves, sustained stresses during heating also affect the elastic behaviour of concrete. As shown in Fig.5.4, the stressed elastic modulus is always higher than unstressed elastic modulus and the stress level itself has great impact within a range of L =0.1 to 0.3. The mechanism of the effect of pre-fire load on elastic modulus should be similar with the compressive strength since elastic modulus is related to ITZ too. The critical phase is 460 °C to 580 °C. The

decomposition of CH and the damage caused by vapour pressure in ITZ, are the main causes of higher stressed elasticity.

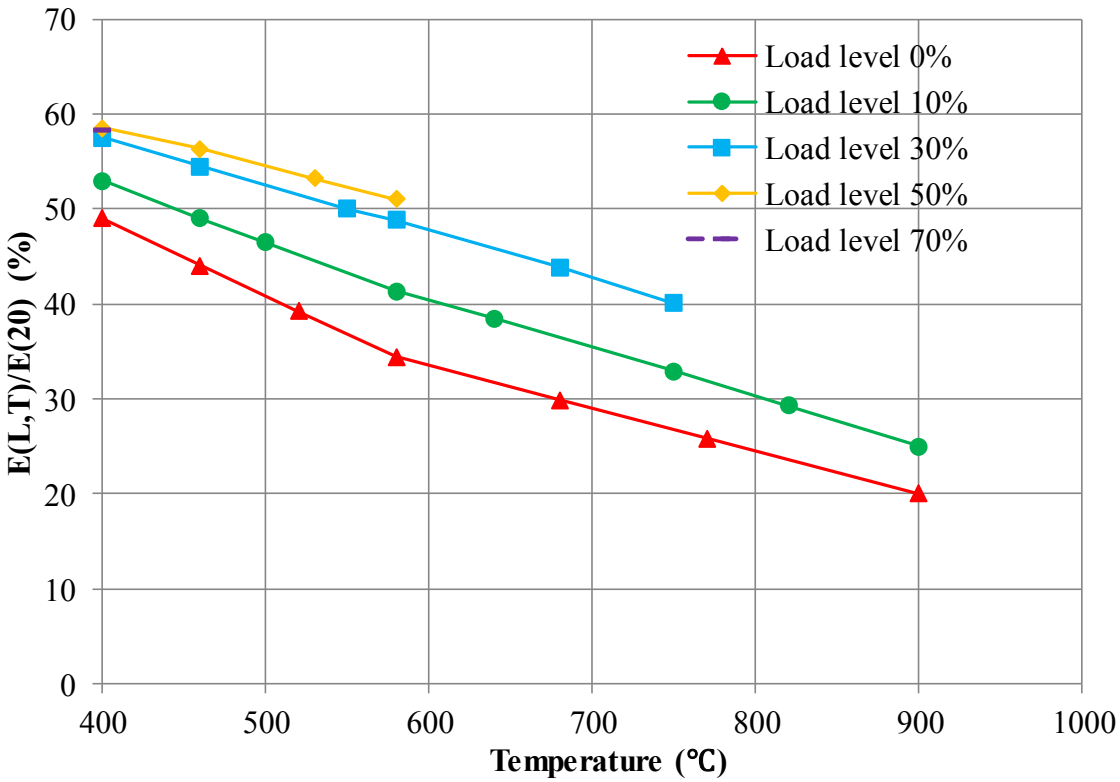

Fig.5.4 Normalized elastic modulus-temperature relationships of specimens with different load levels

5.2.4 Stress-strain shape

As discussed in 5.2.1-5.2.3, specimens under a sustained load during the heating period indicate a significant relative variation of compressive strength, peak strain and modulus of elasticity compared with the specimens which were not loaded during heating, but tested under the same conditions. However, in addition to these three key parameters, sustained stresses during the heating period also influence the shape of the stress-strain relationships at high temperature. This has not been discussed in previous research.

According to the experimental results, the stress-strain shape for a specimen with a pre-fire load level L, at temperature T is plotted in Fig.5.5. It is different from the stress-strain curve shape of unstressed specimens discussed in Chapter 4. Firstly, it is linear to yield strength $r(L,T)\cdot f_c(L,T)$, where $r(L,T)$ and $f_c(L,T)$ are the yield ratio and compressive strength of the specimen with a pre-fire load level L, at temperature T, respectively. The yield strength is not only higher than 0.3 $f_c(L,T)$ but also greater than the pre-fire load $L\cdot f_{c,20}$, which indicates that the stress-strain response of the stressed specimens at a high temperature is more linear than that of the unstressed specimens, and this is not only caused by the unloading process. Then, above the yield strength the remainder of the stress-strain relationship behaves nonlinearly, and the peak plastic strain at compressive strength Δp is lower than that of the unstressed specimens, indicating a more brittle behaviour.

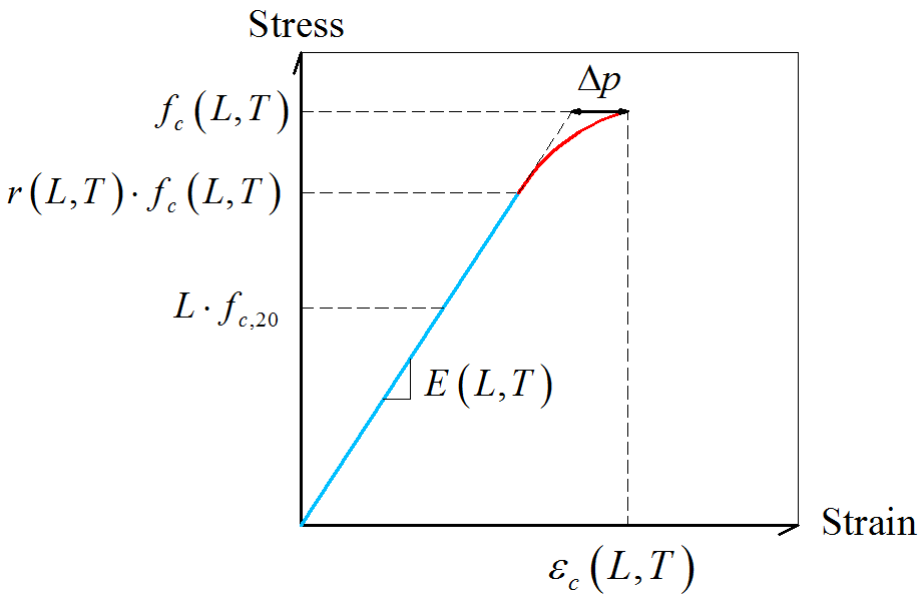

Fig.5.5 The stress-strain relationship of stressed concrete at high temperatures

Therefore, in addition to the compressive strength, peak strain, and elastic modulus, the yield ratio is also necessary to determine the stress-strain response for stressed specimens at high temperatures. The yield ratio-temperature relationship of OPC concrete under different pre-fire load levels is plotted in Fig.5.6. The results show that the yield ratios of specimens under different pre-fire load levels are very close to each other at 400 °C. Above 400 °C, yield ratio develops in a relative high rate with increasing temperature and pre-fire load levels. However, the yield ratios of specimens with different load levels will finally achieve the identical value of around 0.87 when the stressed specimens are approaching the break point, which suggests that the ultimate linearity of the stressed specimen approaching failure is the same. This phenomenon could be caused by the release of the plastic deformation energy during the transient heating process. Before 400 °C, the release of deformation energy is limited, thus the yield ratios for different load levels are similar to each other. When the temperature is above 400 °C, the plastic deformation energy is quickly released, thus the rate of yield ratio is increasing with temperature and pre-fire load level. However, the total plastic deformation energies of specimens with same mix proportion are the same, therefore, the final values of yield ratios when they are approaching to the failure point are the same.

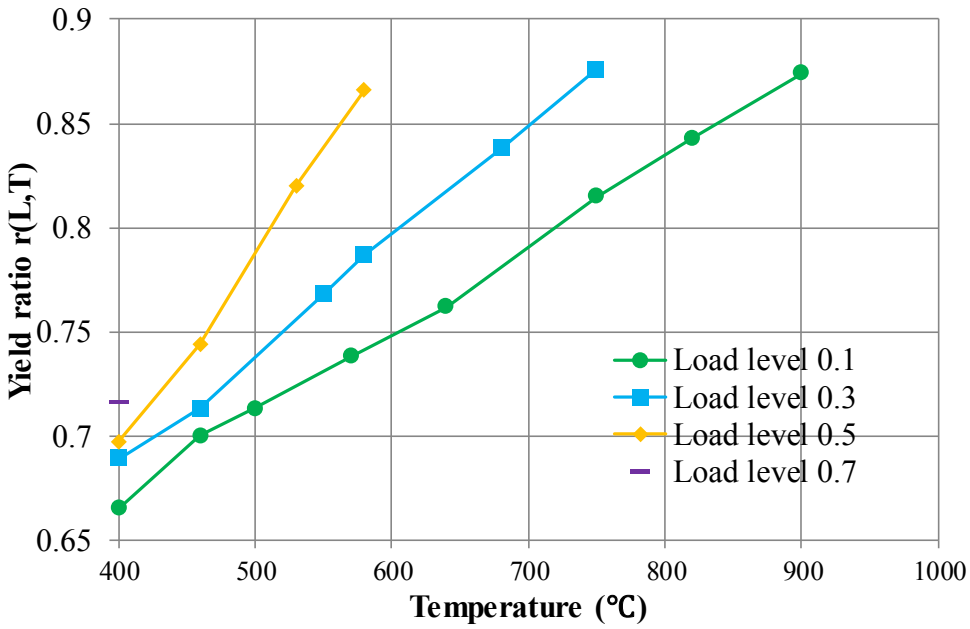

Fig.5.6 Yield ratio-temperature relationships of stressed concrete

5.3 Constitutive model for stressed concrete at high temperatures

5.3.1 Determination of the basic equation

To capture the characteristics of stress-strain relationship for stressed concrete at high temperature, the model proposed by Khennane and Baker (Khennane & Baker, 1993) was selected as the basic equation, in which the curve is initially linear to yield strength and the reminder of the curve is taken as a quarter of ellipse, expressed as:

$$\left(\frac{\sigma - f_y}{f_c - f_y}\right)^2 + \left(\frac{\Delta p + \varepsilon_p}{\Delta p}\right)^2 = 1 \qquad (5.1)$$

where $\Delta p = \varepsilon_c - \frac{f_c}{E}$, $f_y = r \times f_c$, ε_p is the plastic strain.

When a pre-fire load level L and a temperature level T are considered, the above equation can be expressed as:

$$\varepsilon = \varepsilon_e + \varepsilon_p \tag{5.2}$$

$$\varepsilon_e = \frac{\sigma}{E(L,T)} \tag{5.3}$$

$$\varepsilon_p = \left(\varepsilon_c(L,T) - \frac{f_c(L,T)}{E(L,T)} \right) \left(1 - \sqrt{1 - \left(\frac{\sigma - r(L,T) \times f_c(L,T)}{f_c(L,T) - r(L,T) \times f_c(L,T)} \right)^2} \right) \tag{5.4}$$

where $f_c(L,T)$, $\varepsilon_c(L,T)$, $E(L,T)$, $r(L,T)$ are the compressive strength, peak strain, elastic modulus and yield ratio of concrete specimen with a pre-fire load level L, at temperature T. To implement the proposed model, these four parameters need to be formulated as a function of L and T, which will be presented in Section 5.3.2.

5.3.2 Formulation of key parameters

As illustrated in Section 5.2, the effect of pre-fire load on the mechanical properties of concrete is limited from 400 °C to 460 °C, therefore, the parameters discussed in this section are for temperatures ranging from 460 °C to 900 °C.

5.3.2.1 Compressive strength

The development of compressive strength of stressed concrete specimens at high temperature can be divided into two phases.

Phase 1: 460 °C - 580 °C

Above 460 °C, CH decomposes, resulting in vapour pressure and structural damage in ITZ. When concrete is loaded during heating, the accumulated micro-cracks caused by

the pre-fire load would reduce the development of vapour pressure in micro-pores of ITZ and corresponding structural damage, which will mitigate the deterioration of compressive strength. Therefore, the compressive strength of the stressed specimens would be higher than that of the unstressed specimens in this temperature range. The compressive strength ratio of stressed concrete with different load levels to unstressed concrete is plotted in Fig.5.7. By curve fitting, the parameter $\lambda_f(L,580)$, defined as the compressive strength ratio of the stressed concrete with a pre-fire load level L to unstressed concrete at 580 °C, can be formulated as:

$$\lambda_f(L,580) = -2.60 \times L^2 + 2.46 \times L + 1.02 \tag{5.5}$$

Then the compressive strength of the stressed concrete at 580 °C is:

$$f_c(L,580) = f_c(580) \times \lambda_f(L,580) = 0.4 f_{c,20} \times \left(-2.60 \times L^2 + 2.46 \times L + 1.02\right) \tag{5.6}$$

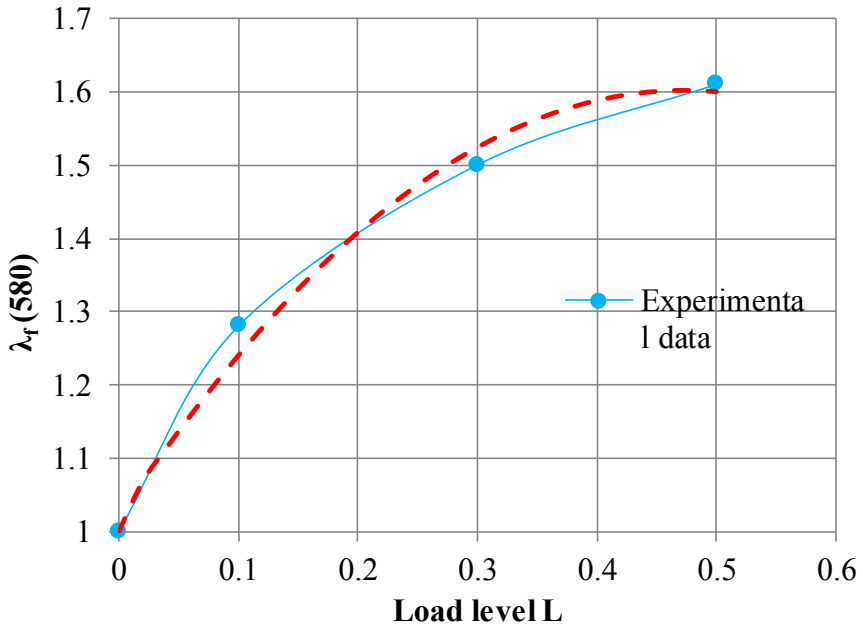

Fig.5.7. Compressive strength ratio of stressed concrete to unstressed concrete at 580 °C

According to Fig.5.1, the compressive strength-temperature relationship between 460 °C and 580 °C can be treated as linear, thus the compressive strength of the stressed concrete under load level from 0 to 0.5, at any temperature between 460 °C and 580 °C can be formulated as:

$$f_c(L,T) = f_c(L,460) + \frac{f_c(L,580) - f_c(L,460)}{120} \times (T - 460) \tag{5.7}$$

where $f_c(L,T) = 1.05 \times f_c(T)$.

Thus, parameter $\lambda_f(L,T)$ from 460 °C to 580 °C can be calculated:

$$\begin{aligned} \lambda_f(L,T) = \frac{f_c(L,T)}{f_c(T)} &= \frac{f_c(L,460) + \dfrac{f_c(L,580) - f_c(L,460)}{120} \times (T - 460)}{f_c(T)} \\ &= \frac{96 - (1.04 \times L^2 - 0.98 \times L + 0.39) \times (T - 460)}{91.2 - 0.36 \times (T - 460)} \end{aligned} \tag{5.8}$$

Phase 2: 580 °C - 900 °C

When the specimen is heated up to 580 °C, CH has completely decomposed and the pore structure in ITZ will be severely damaged. Therefore, at this stage the pre-fire load has little impact on ITZ. It can be seen in Fig.5.1 that the curves in this temperature range are almost parallel to each other, indicating the decrease rates of specimens under different load levels are similar. In conclusion, the strengthening effect caused by pre-fire load is minor, thus the increasing rate of parameter $\lambda_f(L,T)$ can be assumed to be linear. The variation rate of $\lambda_f(L,T)$ from 580 °C to 740 °C under different load levels can be calculated as:

$$\lambda_f'(L,T)=\frac{\lambda_f(L,740)-\lambda_f(L,580)}{160} \tag{5.9}$$

The results are plotted in Fig.5.8.

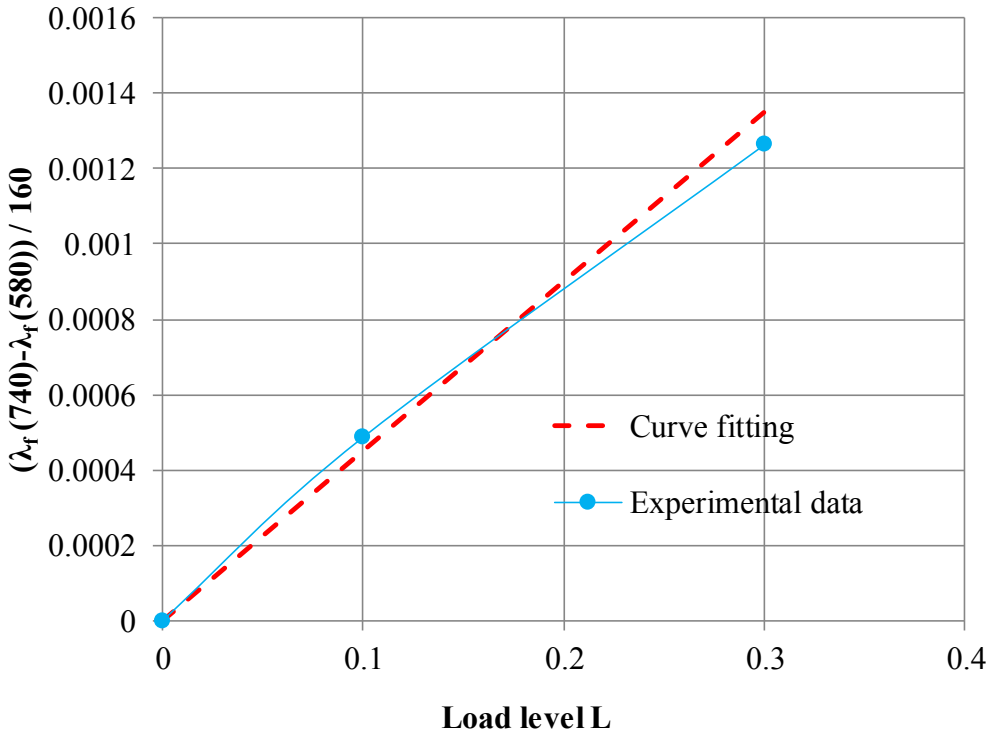

Fig.5.8. Variation rate of $\lambda_f(L,T)$ from 580 °C to 740 °C under different load levels

By curve fitting, the variation can be evaluated:

$$\lambda_f'(L,T)=0.0045L \tag{5.10}$$

Thus, parameter $\lambda_f(L,T)$ from 580 °C to 900 °C can be calculated:

$$\begin{aligned}\lambda_f(L,T)&=\lambda_f(L,580)+\lambda_f'(L,T)\times(T-580)\\&=-2.60\times L^2+2.46\times L+1.02+0.0045L\times(T-580)\end{aligned} \tag{5.11}$$

Based on above analysis, the variation of parameter $\lambda_f(L,T)$ from 460 °C to 900 °C has been formulated and the proposed model is plotted against the experimental data in Fig.5.9.

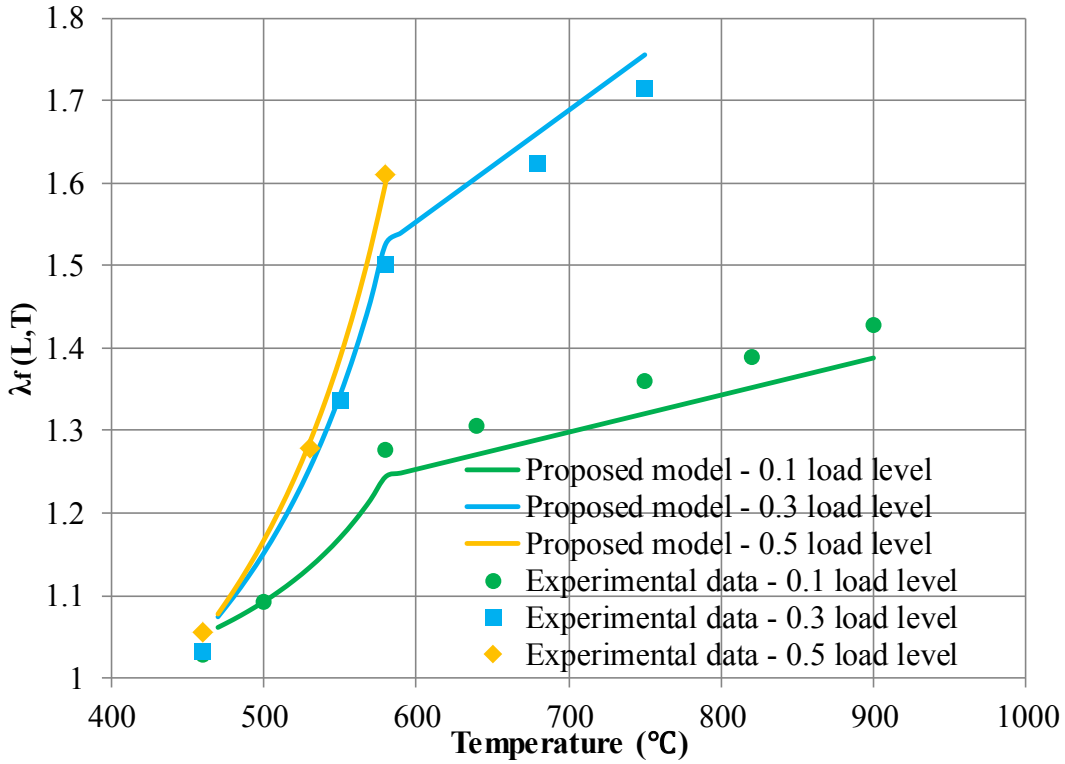

Fig.5.9. Comparison of experimental $\lambda_f(L,T)$ with the proposed model

According to Fig.5.9, the model has a good agreement with the experimental results. It shows that the strengthening effect is mainly developed from 460 °C to 580 °C, where CH decomposes. Above 580 °C, specimens with pre-fire load levels of 0.5 have broken down, while specimens with pre-fire load levels of 0.1 and 0.3 are still strengthened by the pre-fire load but at a relatively slow rate.

5.3.2.2 Peak strain

The peak strain ratios of unstressed concrete to stressed concrete with a pre-fire load level L at temperature T is represented by parameter $\lambda_\varepsilon(L,T)$. Its variation with temperature is also divided into two phases.

Phase 1: 460 °C - 680 °C

In this phase, parameter $\lambda_\varepsilon(L,T)$ increases proportionally with temperature. The $\lambda_\varepsilon(L,T)$-L relationships at 460 °C and 580 °C are plotted in Fig.5.10.

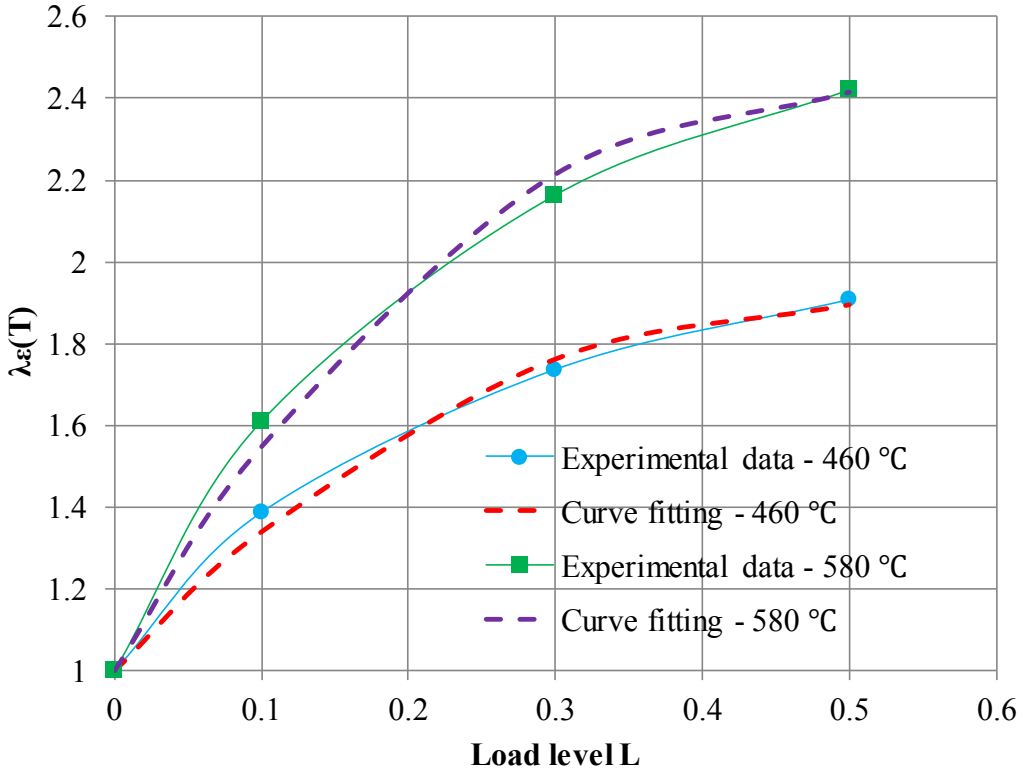

Fig.5.10. Peak strain ratio of unstressed concrete to stressed concrete

By using a curve fitting, they can be formulated as:

$$\lambda_\varepsilon(L,460) = -3.62L^2 + 3.56L + 1.02 \tag{5.12}$$

$$\lambda_\varepsilon(L,580) = -5.82L^2 + 5.66L + 1.04 \tag{5.13}$$

Then the variation rate of $\lambda_\varepsilon(L,T)$ in phase 1 can be derived:

$$\lambda'_\varepsilon(L,T) = \frac{\lambda_\varepsilon(L,580) - \lambda_\varepsilon(L,460)}{120} = \frac{-2.20L^2 + 2.10L + 0.02}{120} \tag{5.14}$$

$$\begin{aligned}\lambda_\varepsilon(L,T) &= \lambda_\varepsilon(L,460) + \lambda'_\varepsilon(L,T) \times (T-460) \\ &= -3.62L^2 + 3.56L + 1.02 + \frac{-2.20L^2 + 2.10L + 0.02}{120} \times (T-460)\end{aligned} \tag{5.15}$$

Phase 2: 680 °C - 900 °C

Above 680 °C, C-S-H decomposes and the thermal incompatibility between the cement paste and the aggregate becomes overwhelming. For unstressed specimens, the elasticity decreases while the plasticity increases, resulting in a sharp increase in the peak strain. On the contrary, for stressed specimens, their deformation energy has been released at a much higher rate in the transient heating process, thus the peak strain obtained under the thermal steady state decreased a lot. Meanwhile, since the compressive strength of concrete has decreased a lot above 680 °C, even a pre-fire load level of 0.1 is enough to release its deformation energy. Therefore, the variation rates of $\lambda_\varepsilon(0.1,T)$ and $\lambda_\varepsilon(0.3,T)$ could be taken as the following values:

$$\lambda'_\varepsilon(0.1,T)=\frac{\lambda_\varepsilon(0.1,900)-\lambda_\varepsilon(0.1,750)}{900-750}=0.011 \tag{5.16}$$

$$\lambda'_\varepsilon(0.3,T)=\frac{\lambda_\varepsilon(0.3,750)-\lambda_\varepsilon(0.1,680)}{750-680}=0.012 \tag{5.17}$$

$$\lambda'_\varepsilon(L,T)=\frac{\lambda'_\varepsilon(0.1,T)+\lambda'_\varepsilon(0.3,T)}{2}=0.012 \tag{5.18}$$

On the foundation of above analysis, $\lambda_\varepsilon(L,T)$ is formulated as:

$$\lambda_\varepsilon=\begin{cases}\lambda_\varepsilon(L,460)+\lambda'_\varepsilon(L,T)\times(T-460)\\ \lambda_\varepsilon(L,680)+\lambda'_\varepsilon(L,T)\times(T-680)\end{cases} \tag{5.19}$$

According to Eq.(5.15), $\lambda_\varepsilon(L,680)$ can be calculated:

$$\lambda_\varepsilon(L,680)=-7.65L^2+7.41L+1.06 \tag{5.20}$$

Then the variation rate of $\lambda_\varepsilon(L,T)$ in phase 2 can be derived as:

$$\lambda_\varepsilon = -7.65L^2 + 7.41L + 1.06 + 0.012 \times (T - 680) \tag{5.21}$$

The variation of parameter $\lambda_\varepsilon(L,T)$ from 460 °C to 900 °C is plotted in Fig.5.11. It shows good agreement with experimental values.

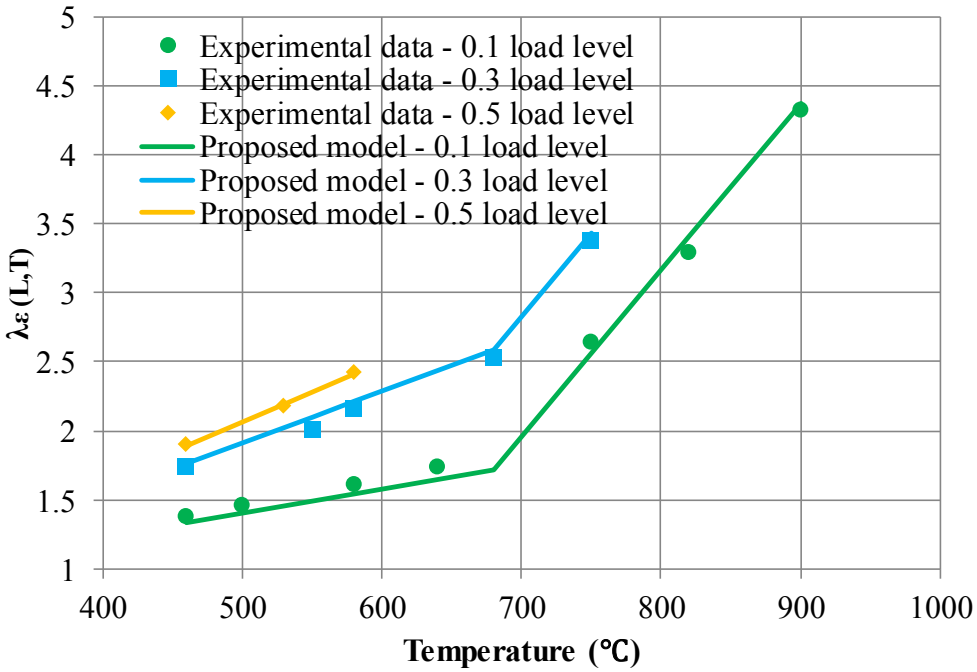

Fig.5.11. Comparison of experimental $\lambda_\varepsilon(L,T)$ with the proposed model

5.3.2.3 Elastic modulus

The mechanism of variation of elastic modulus for stressed concrete specimens at high temperature is the same as the compressive strength, thus the parameter $\lambda_e(L,T)$, defined as the elastic modulus ratio of stressed concrete with a pre-fire load level L to unstressed concrete at temperature T could be formulated in the same way.

Phase 1: 460 °C - 580 °C

The elastic modulus ratios of stressed concrete with different load levels to unstressed concrete at 460 °C and 580 °C are plotted in Fig.5.12.

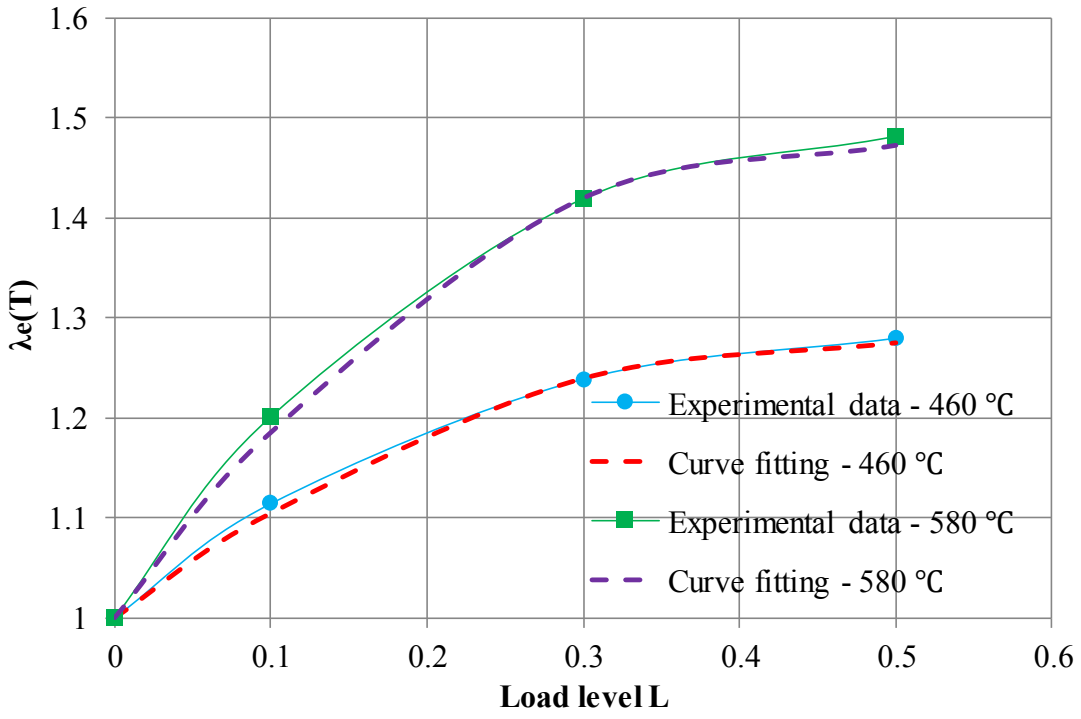

Fig.5.12. Elastic modulus ratio of stressed concrete to unstressed concrete

By using curve fitting, the parameters $\lambda_e(L,460)$ and $\lambda_e(L,580)$ can be obtained:

$$\lambda_e(L,460) = -1.24L^2 + 1.17L + 1 \tag{5.22}$$

$$\lambda_e(L,580) = -2.27L^2 + 2.08L + 1 \tag{5.23}$$

Then the variation rate can be derived:

$$\lambda_e'(L,T) = \frac{\lambda_e(L,580) - \lambda_e(L,460)}{120} = \frac{-1.03L^2 + 0.91L}{120} \tag{5.24}$$

Thus the parameter $\lambda_e(L,T)$ in this temperature range can be formulated as:

$$\lambda_e(L,T)=\lambda_e(L,460)+\lambda_e'(L,T)\times(T-460)$$
$$=-1.24L^2+1.17L+1+\frac{-1.03L^2+0.91L}{120}\times(T-460) \quad (5.25)$$

Phase 2: 580 °C - 900 °C

Above 580 °C, the strengthening effect caused by the pre-fire load is minor, thus the increasing rate of parameter $\lambda_e(L,T)$ can be assumed to be linear. The variation rate of $\lambda_e(L,T)$ from 580 °C to 750 °C under different load levels, calculated as $\frac{\lambda_e(L,750)-\lambda_e(L,580)}{170}$, is plotted in Fig.5.13. By curve fitting, the variation can be evaluated:

$$\lambda_e'(L,T)=0.0015L \quad (5.26)$$

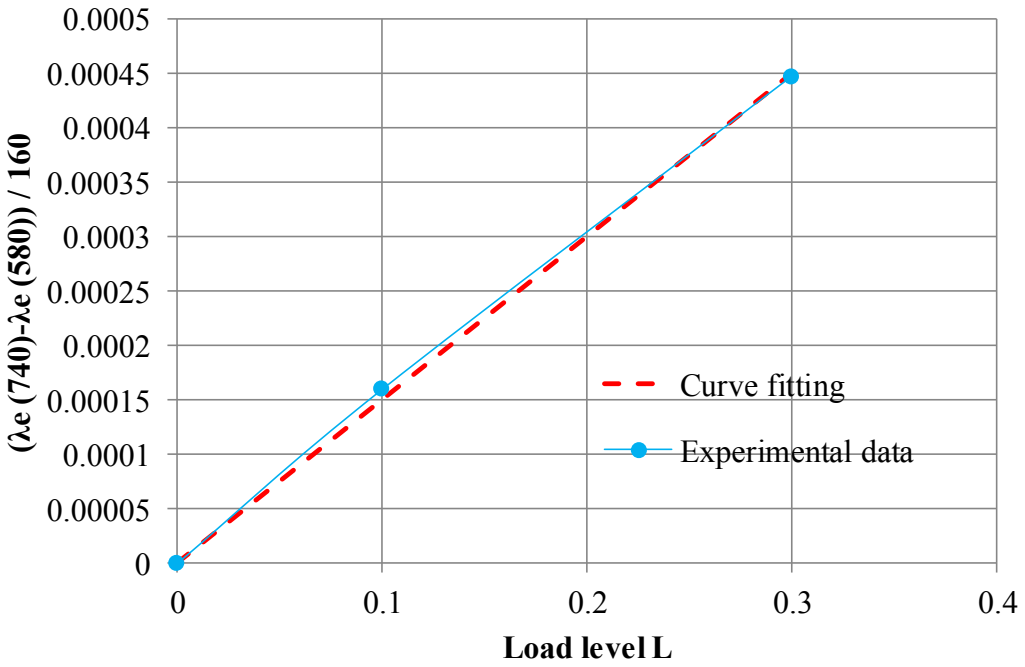

Fig.5.13. Variation rate of $\lambda_e(L,T)$ from 580 °C to 740 °C under different load levels

Thus the parameter $\lambda_e(L,T)$ in this temperature range can be formulated as:

$$\lambda_e(L,T) = \lambda_e(L,580) + \lambda_e'(L,T) \times (T - 580) \tag{5.27}$$

Then

$$\lambda_e = -2.27L^2 + 2.08L + 1 + 0.0015L \times (T - 580) \tag{5.28}$$

The variation of parameter $\lambda_e(L,T)$ from 460 °C to 900 °C is plotted in Fig.5.14. It shows good agreement with experimental values.

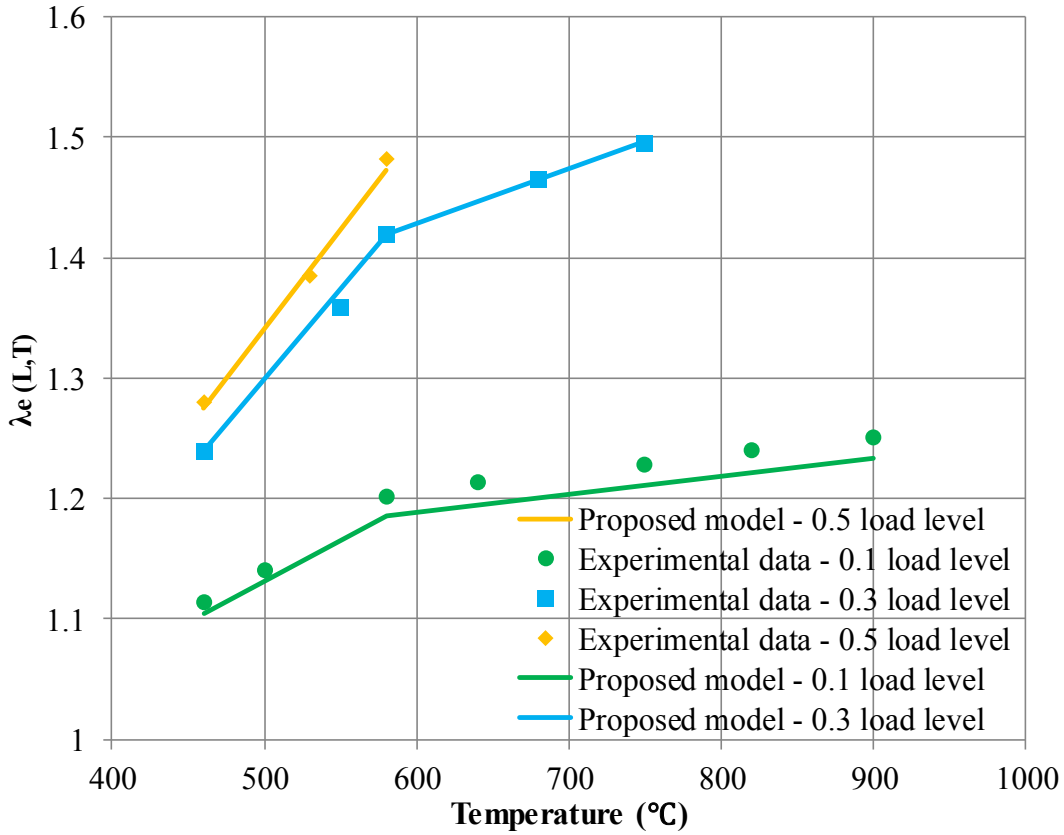

Fig.5.14. Comparison of experimental $\lambda_e(L,T)$ with the proposed model

5.3.2.4 Yield ratio

As illustrated in Fig.5.6, the yield ratio of specimens under different pre-fire load

levels are very similar at around 400 °C, thus an average value 0.68 is used to represent the yield ratio at this temperature. Above 400 °C, the yield ratio develops at a relative high rate with increasing temperature and pre-fire load levels. The yield ratios of specimens with different load levels will finally achieve the identical value of around 0.87 when the stressed specimens are approaching the break point. The failure temperature of stressed specimens is plotted in Fig.5.15 and can be formulated linearly:

$$T_{\max}(L) = 980 - 800L \tag{5.29}$$

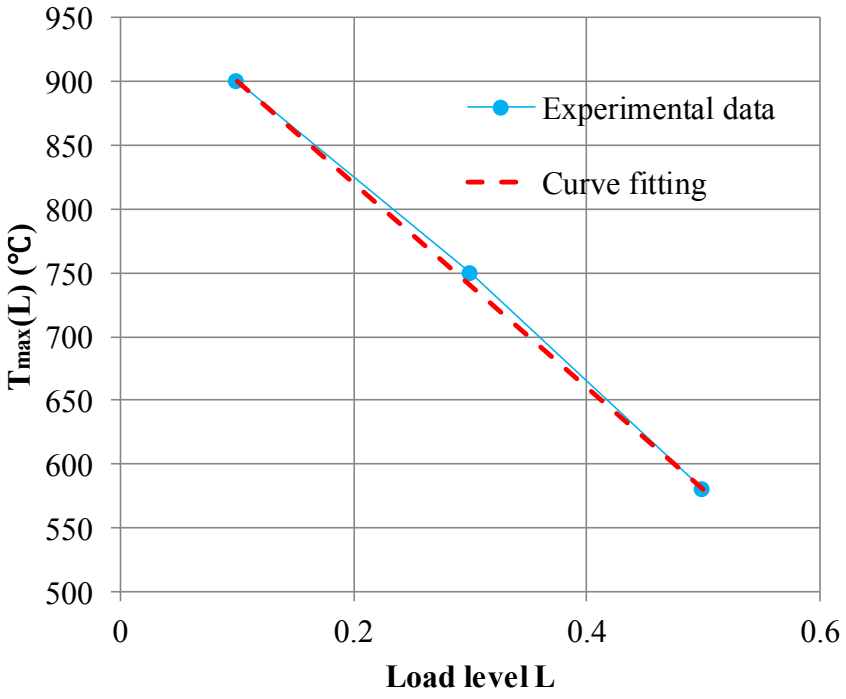

Fig.5.15. Failure temperature of stressed specimens under different load levels

The variation rate of yield ratio from 400 °C to failure temperature is treated proportionally, thus the rate can be derived:

$$r'(L) = \frac{0.87 - 0.68}{980 - 800L - 400} = \frac{0.19}{580 - 800L} \tag{5.30}$$

Then the yield ratio is formulated as:

$$r(L,T) = 0.68 + \frac{0.19(T-400)}{580-800L} \tag{5.31}$$

The variation of parameter $r(L,T)$ from 460 °C to 900 °C is plotted in Fig.5.16. It shows good agreement with experimental values.

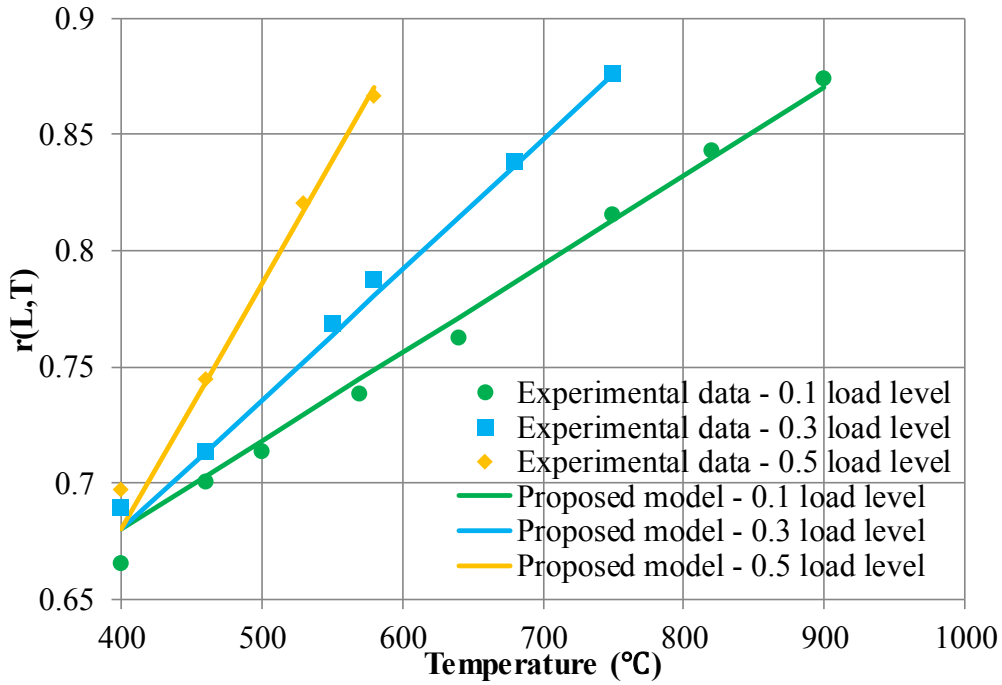

Fig.5.16. Comparison of experimental yield ratios with the proposed model

5.3.3 Verification of proposed model

On the foundation of the above analysis, constitutive model for unstressed and stressed OPC concrete have been completely formulated.

For unstressed concrete:

$$\frac{\sigma}{f_c(T)}=\frac{\varepsilon}{\varepsilon_c(T)}\frac{n(T)}{n(T)-1+\left(\frac{\varepsilon}{\varepsilon_c(T)}\right)^{n(T)}} \tag{5.32}$$

where the related parameters can be formulated according to the data in Chapter 4:

$$f_c(T)=\begin{cases} f_{c,20}\times\left(0.76-\frac{0.36}{120}\times(T-460)\right) & 460\le T\le 580 \\ f_{c,20}\times\left(0.4-\frac{0.22}{320}\times(T-580)\right) & 580<T\le 900 \end{cases} \tag{5.33}$$

$$\varepsilon_c(T)=\begin{cases} 5.77+0.0073\times(T-460) & 460\le T\le 680 \\ 7.37+0.015\times(T-680) & 680<T\le 900 \end{cases} \tag{5.34}$$

$$n(T)=6.1-0.003T \qquad 460\le T\le 900 \tag{5.35}$$

For stressed specimens:

$$\varepsilon_e(L,T,\sigma)=\frac{\sigma}{\lambda_e(L,T)\times E(T)} \tag{5.36}$$

$$\varepsilon_p(L,T,\sigma)=\left(\frac{\varepsilon_c(T)}{\lambda_\varepsilon(L,T)}-\frac{\lambda_f(L,T)\times f_c(T)}{\lambda_e(L,T)\times E(T)}\right)\times\left(1-\sqrt{1-\left(\frac{\frac{\sigma}{\lambda_f(L,T)\times f_c(T)}-r(L,T)}{1-r(L,T)}\right)^2}\right) \tag{5.37}$$

where

$$\lambda_f(L,T)=\begin{cases}\dfrac{96+\left(-1.04\times L^2+0.98\times L-0.39\right)\times\left(T-460\right)}{91.2-0.36\times\left(T-460\right)} & 460\le T\le 580\\ -2.60L^2+0.0045LT-0.15L+1.02 & 580<T\le 900\end{cases} \quad (5.38)$$

$$\lambda_\varepsilon(L,T)=\begin{cases}-3.62L^2+3.56L+1.02+\dfrac{-2.20L^2+2.10L+0.02}{120}\times\left(T-460\right) & 460\le T\le 680\\ -7.65L^2+7.41L+1.06+0.012\times\left(T-680\right) & 680<T\le 900\end{cases} \quad (5.39)$$

$$\lambda_e(L,T)=\begin{cases}-1.24L^2+1.17L+1+\dfrac{-1.03L^2+0.91L}{120}\times\left(T-460\right) & 460\le T\le 580\\ -2.27L^2+2.08L+1+0.0015L\times\left(T-580\right) & 580<T\le 900\end{cases} \quad (5.40)$$

$$r(L,T)=0.68+\frac{0.19\left(T-400\right)}{580-800L} \qquad 460\le T\le 900 \quad (5.41)$$

$$E(T)=E_{20}\times\left(1.05-1.71\times10^{-3}T+8.00\times10^{-7}\times T^2\right) \qquad 20\le T\le 900 \quad (5.42)$$

Fig.5.17 shows the comparison between the experimentally obtained stress-strain curves of OPC concrete with different pre-fire load levels, represented by dots, and those calculated from the proposed model. It is obvious from the comparisons that the proposed model excellently simulates the experimental results.

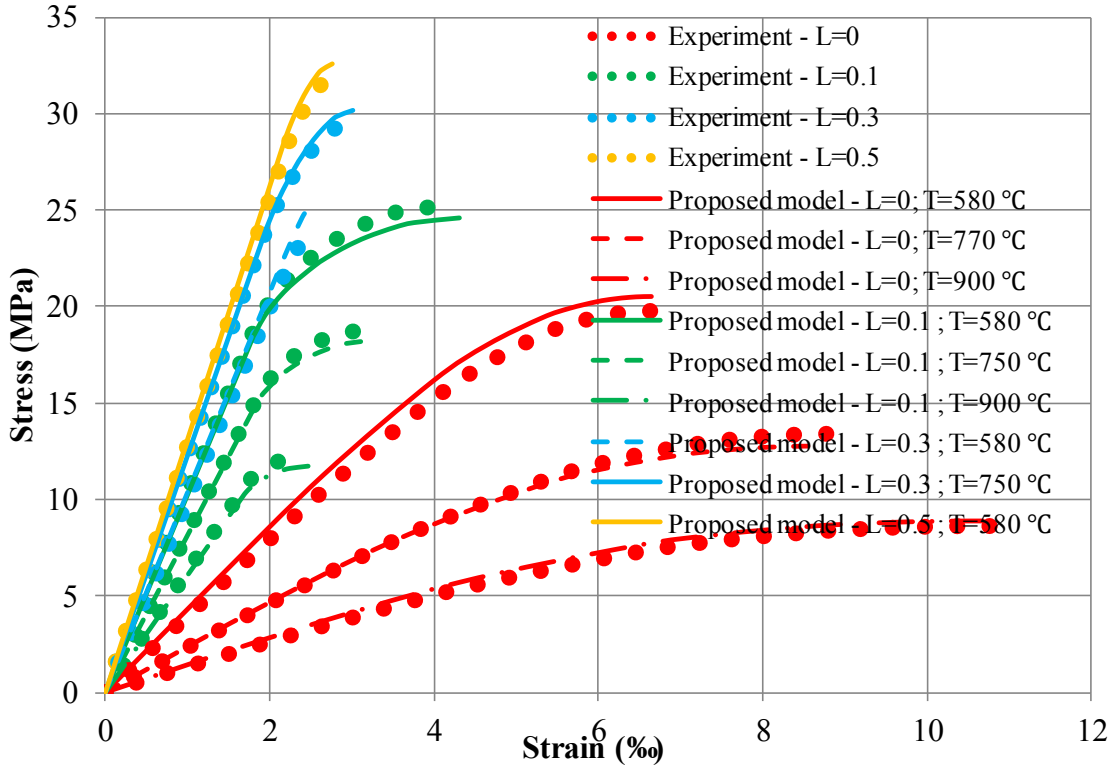

Fig.5.17. Comparison of experimental stress-strain relationships of OPC concrete with the proposed model

As discussed in Section.5.2, the effect of pre-fire load on the mechanical properties of concrete at high temperatures is more likely a physical mechanism instead of a chemical origin, thus 25% replacement of OPC with FA has no impact on the strengthening effect caused by the pre-fire load. Therefore, the proposed model for stressed OPC concrete is assumed to be also applicable to stressed FA concrete. In order to verify this assumption, several stressed FA concrete specimens were tested and the results were plotted against proposed model in Fig.5.18, in which the parameters $f_c(T)$, $\varepsilon_c(T)$, $E(T)$, $n(T)$ are taken from Chapter.4, representing the mechanical properties of unstressed FA concrete at high temperature. As illustrated in Fig.5.18, although the difference between experimental results and proposed model is

a little larger than OPC concrete, the accuracy appears to be still reasonable and acceptable, suggesting the proposed stressed model can be applied to FA concrete.

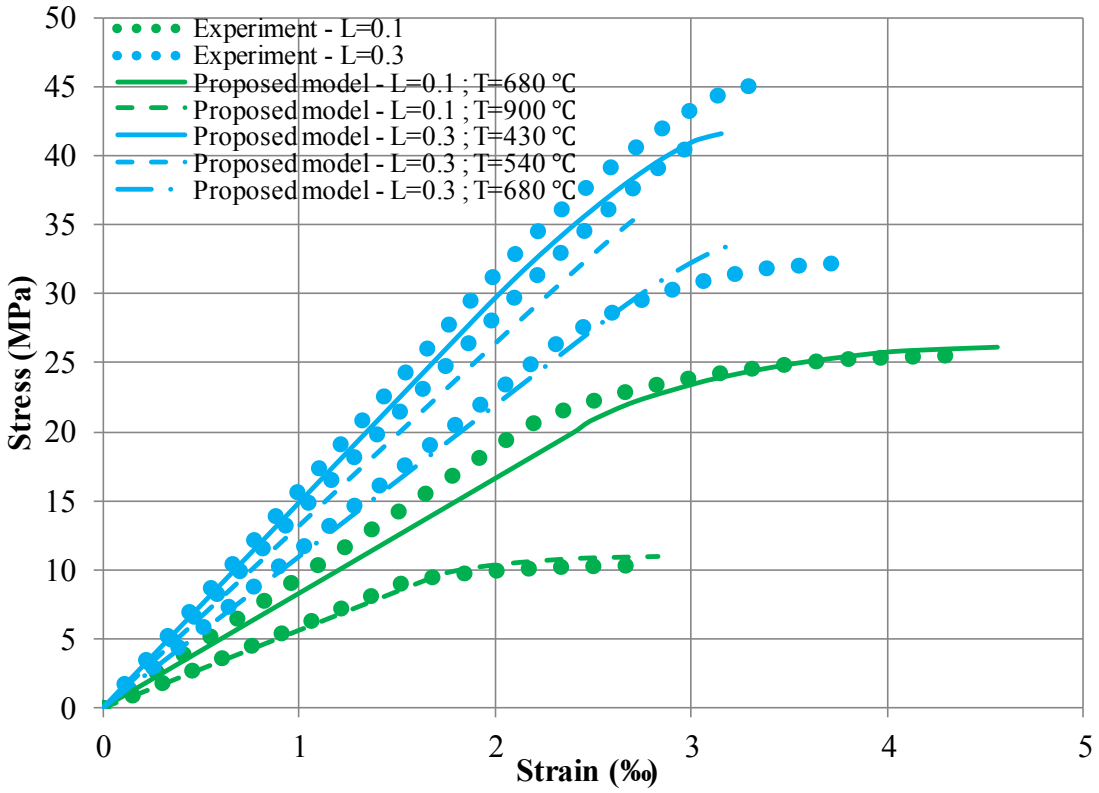

Fig.5.18. Comparison of experimental stress-strain relationships of FA concrete with the proposed model

5.4 Microstructure imaging

The microstructures of crushed powder samples of the specimens under different pre-fire load levels and temperatures were examined by using SEM techniques to understand the different heating-loading paths, on the change of the micro-structure organization of OPC concrete. As illustrated in Fig.5.19, for unstressed specimens with 0% load level at 460 °C, a series of pores developed in the cement paste, which could

be attributed to the vapour pressure caused by the decomposition of CH. In contrast, for stressed specimen with 70% load level at 460 °C, the cement paste is clearly more dense and compact because the sustained load during heating produces more micro-cracking during heating which mitigates vapour pressure and reduces the corresponding damage.

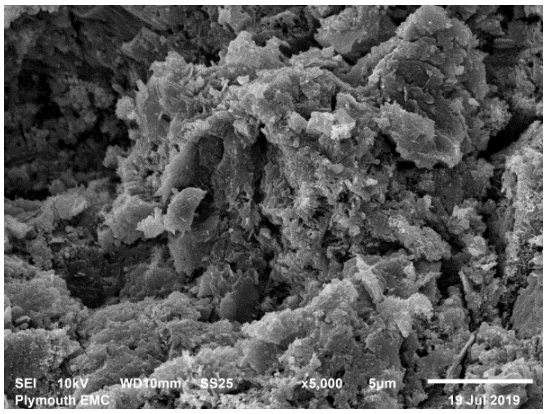

(a) 70% load level (x5000)

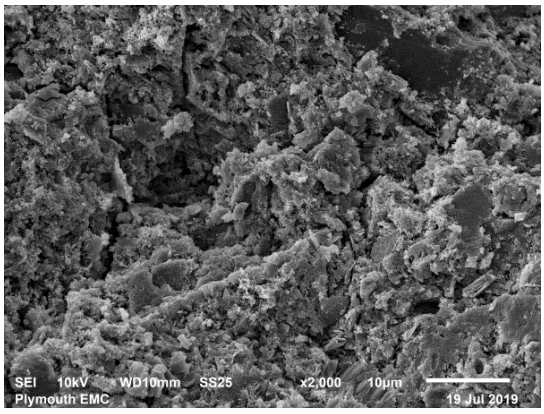

(b) 70%load level(x2000)

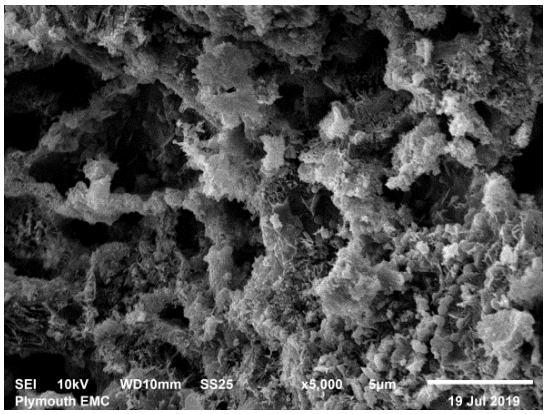

(c) 0% load level (x5000)

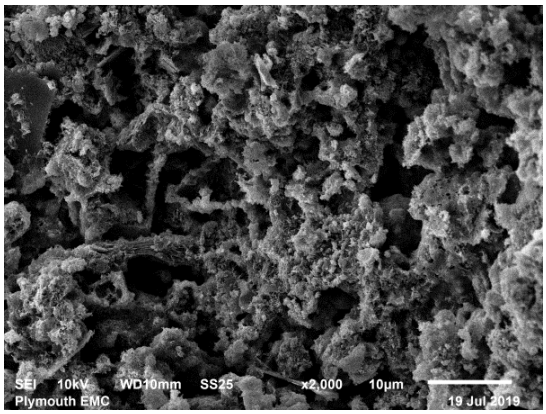

(d)0% load level (x2000)

Fig.5.19 Microstructures of crushed OPC concrete samples at 460 °C

For unstressed specimens with 0% load level at 900 °C, CSH has decomposed. The microstructure of the cement paste is very porous and weak, as shown in Fig.5.20. However, stressed specimens with 10% load level at 900 °C shows denser

microstructure of the cement paste, which could be attributed to the similar mechanism as described above.

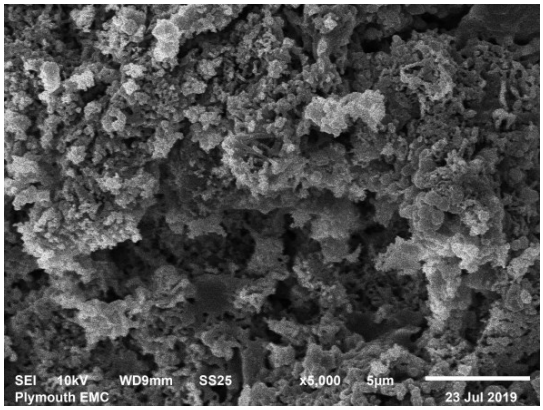

(a) 10% load level (x5000)

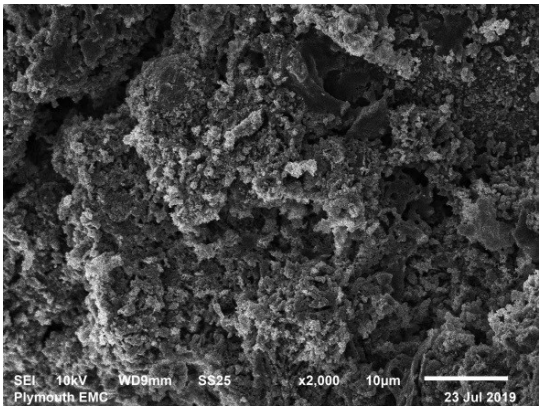

(b) 10%load level (x2000)

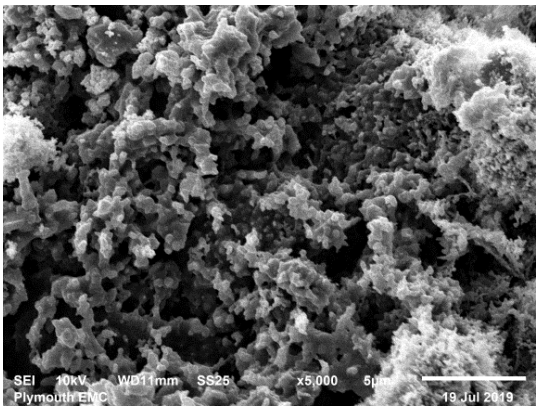

(c) 0% load level (x5000)

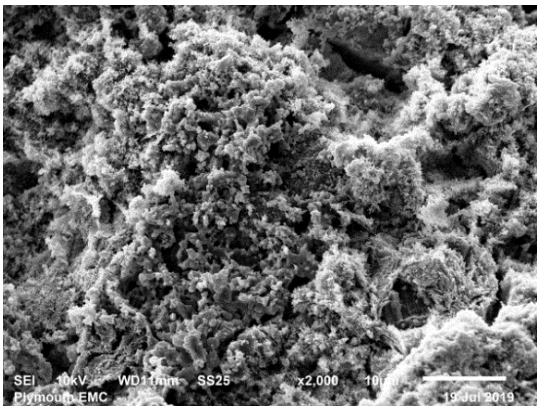

(d)0% load level (x2000)

Fig.5.20. Microstructures of crushed OPC concrete samples at 900 °C

5.5 Conclusions

Steady state tests (Series B) for stressed OPC concrete specimens are presented in this chapter. The compressive strength, peak strain, elastic modulus and stress-strain shape of stressed specimens with different pre-fire load levels from 400 °C to 900 °C have been reported to investigate the effect of load history during the heating process on the

stress-strain behaviour of concrete at high temperature. Finally, a constitutive model for stressed concrete at high temperatures as a function of pre-fire load level during the heating process was proposed and verified. Based on the results in this chapter, following conclusions can be drawn:

1) At the thermal steady state, compared with unstressed concrete, the compressive strength and elastic modulus of stressed concrete increase with the applied stress level during the heating process. The enhancement of these two parameters develops mainly from 460 °C to 580 °C, above which temperature the increasing rate caused by the pre-fire load decreases. On the contrary, the peak strain of stressed concrete decreases with the applied stress level during the heating process. The reduction develops slowly before 680 °C, above which the decreasing rate is significantly increased.

2) The enhancement in compressive strength and elastic modulus caused by pre-fire load is closely related to the decomposition of CH. As one of the main component comprising the interfacial transition zone, CH decomposes when the temperature is above 460 °C. Then the chemical bond water in CH is released and strong vapour pressure is developed in the micro-pores of ITZ, resulting in damage in the microstructure. However, for specimens heated with sustained load, load induced micro-cracks are produced and accumulate during the heating process, which could benefit the vapour diffusion process and reduce the build-up of vapour pressure, thus mitigating the explosive damage in ITZ. When the concrete is heated up to 580 °C, CH has completely decomposed and the microstructure in ITZ has been through

severe damage, thus the effect of the pre-fire load on compressive strength and elastic modulus is slight afterwards.

3) If concrete is loaded during heating, the development of thermal cracks is constrained. Part of the reduction in peak strain of stressed specimens is attributed to this mechanism. Moreover, the sustained load during heating would produce corresponding strain increments at each temperature increment continuously, resulting in the release of plastic strain during thermal exposure. This kind of deformation process is responsible for the reduction in peak strain and development of TTC. When the specimen is heated up to around 680 °C, C-S-H comprising cement paste decomposes, leading to a rapid increase in each plastic increment released during thermal exposure. Therefore, peak strain decreases in a higher rate.

4) The relationship between the variation of the mechanical properties caused by pre-fire load and the stress level itself is nonlinear. When the stress level is over 0.3, any further increase in it has little impact on the results.

5) Sustained stress during the heating process also influences the shape of the stress-strain relationships at high temperature. The yield ratio of stress-strain curve of stressed concrete at high temperature is higher than that of unstressed concrete. Then, above the yield ratio, the remainder of the stress-strain relationship behaves nonlinearly, but the peak plastic strain at compressive strength Δp is lower than that of unstressed specimens, indicating a more brittle behaviour.

Chapter 6 - A novel numerical method to calculate the effect of temperature gradient on TTC of stressed concrete during the heating process[†]

6.1 General

Ideally, the specimen in a transient state test should have a uniformly distributed temperature increase. However, this is never achieved in practice. According to the experiment of Anderberg and Thelandersson (Anderberg & Thelandersson, 1976), even for a small cylinder specimen of only 75 mm diameter and 150 mm height, under a relatively low heating rate of 5 °C/min, the largest temperature difference between its centre and exposed surface in the transient state test could be more than 100 °C. On the other hand, the specimen in a steady state test has normally had a uniformly distributed temperature before it is mechanically loaded. Therefore, except for the mechanical strain estimated by the steady state test directly, there is an extra mechanical strain component caused by the temperature gradient in the transient state test. This chapter proposes a novel numerical method to calculate the effect of temperature gradient on TTC of stressed concrete during the heating process (Fan *et al.*, 2019b).

[†] Chaper 6 is mainly based on the published work: "K. Fan, D. Li, L. Li, J. Wu, Effect of temperature gradient on transient thermal creep of heated and stressed concrete in transient state tests, Construction and Building Materials. 222 (2019) 839-851."

6.2 Development of explicit model

6.2.1 Description

The purpose of developing the numerical model is to completely decompose the strain components in the transient state test and then extract TTC from experimental data explicitly. According to the definition in Section 2.5.2.5, Eq.(2.11) can be written as:

$$\varepsilon_{ttc} = \varepsilon_{\text{tot}} - \left(\varepsilon_{fts} + \varepsilon_{\sigma,20} + \varepsilon_{ela,T} + \varepsilon_{pla,T} + \varepsilon_{pla,tg}\right) \tag{6.1}$$

where ε_{tot} is the total strain in the transient state test, which is determined experimentally, ε_{fts} is the free thermal strain, $\varepsilon_{\sigma,20}$ is the initial mechanical strain caused by the pre-fire load at ambient temperature, $\varepsilon_{ela,T}$ and $\varepsilon_{pla,T}$ are the additional elastic and plastic strains caused by the increase of temperature calculated from the steady state constitutive model, respectively, $\varepsilon_{pla,tg}$ is the mechanical strain caused by temperature gradient in the transient state test. Thus, the requirement for the simulation is to calculate the other strain components on the right hand side of Eq.(6.1). Capturing the evolution of these strain components at elevated temperatures is necessary to investigate the influence of including them in TTC. A significant difference of this model from existing models is that the effect of temperature gradient on the development of mechanical strain is considered, while it is always neglected in previous studies.

Under the action of thermal gradient in a transient state test, the expansion of concrete is always larger in the region near the exposed surface than that near the centre, which

leads to stress shifting from inside to outside (see Fig.6.1.a). The deterioration of the mechanical properties is much faster in the region near the exposed surface than in the region near the centre, which makes stress transfer in an opposite direction to balance the deformation (see Fig.6.1.b). The combination of these two actions results in a stress fluctuation, which can produce a transient mechanical stress gradient that could be much stronger than thermal stress gradient. This mechanical stress gradient can influence not only the temperature of the crush point but also the magnitude of measured strains since there will be some residual strain yielded from the unloading process of the stress fluctuation.

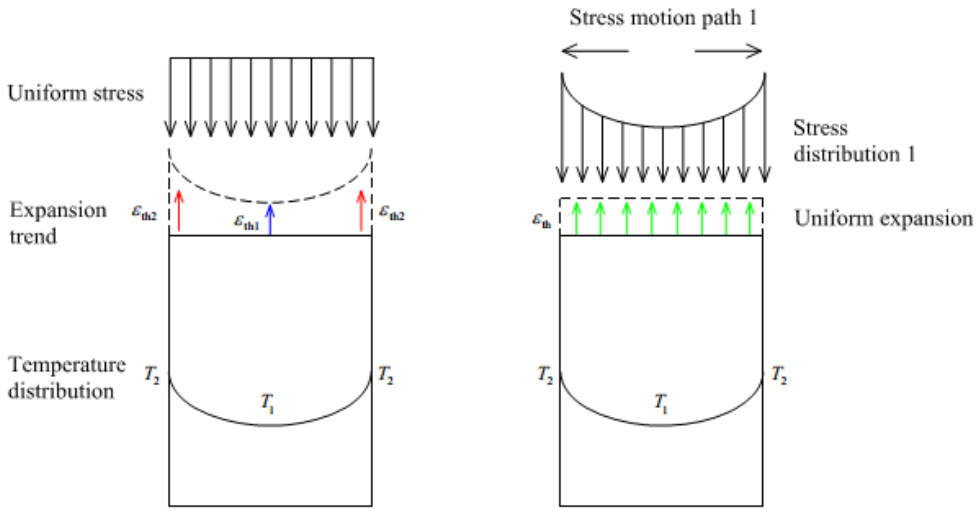

(a) Stress resulting from thermal expansion gradient

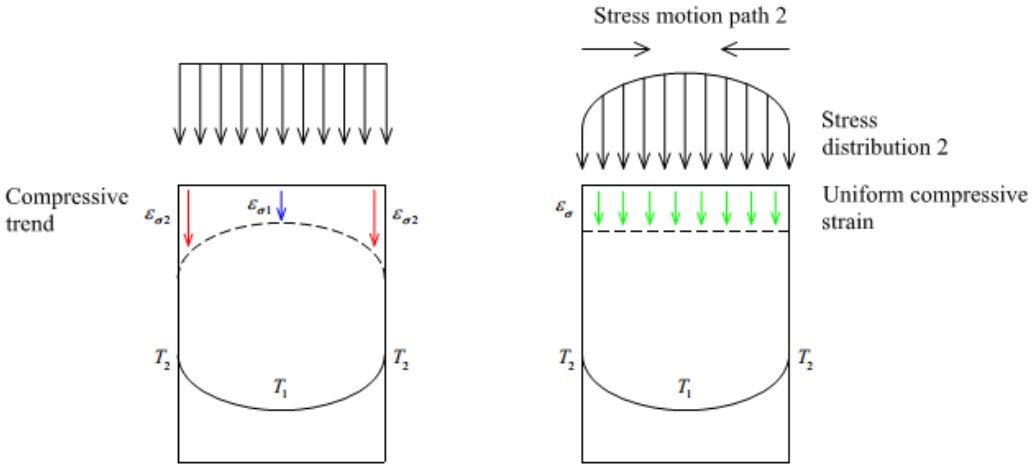

(b) Stress resulting from mechanical strain gradient

Fig.6.1 Stress redistribution under thermal gradient

In order to simulate the above process, two rigid steel plates are used to interact with the concrete cylinder specimen (see Fig.6.2). In this way, the applied stress distribution on the top surface can fluctuate with temperature instantly while the total external load remains constant.

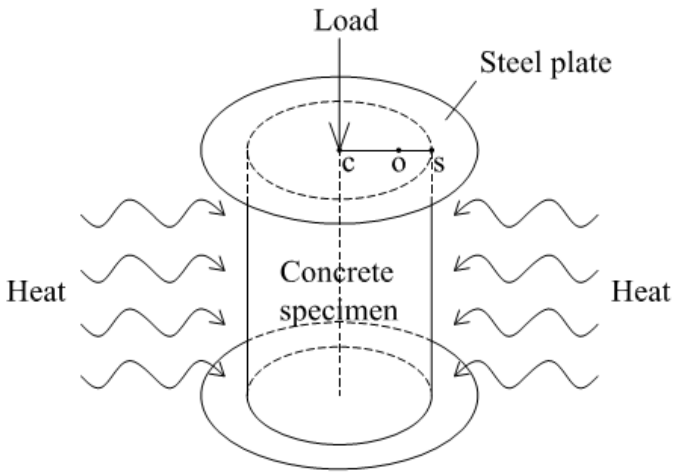

Fig.6.2 Graphical representation of the proposed numerical model

In addition, the following assumptions are used in the proposed model:

(a) The problem is treated as an axial-symmetrical problem with coupled thermal and stress fields.

(b) A free contact surface is used between the rigid steel plates and concrete cylinder specimen.

(c) The displacement boundary conditions of the concrete cylinder specimen are applied at the central axis where the horizontal displacement is zero and at the bottom surface where the vertical displacement is zero.

(d) The key parameters used to define the stress-strain relationships, like peak stress, strain at peak stress and elastic modulus are obtained from corresponding steady state tests, which exclude the effect of TTC.

(e) The nonlinearities of normalized stress-strain functions vary with temperature rather than being fixed as in previous models. This is because the nonlinearity of a normalized stress-strain function can influence the calculation of plastic strain at high temperature, which has been illustrated in Section 4.3.

(f) The selected stress-strain function must have an inverse form in order to implement the calculation.

(g) Three points, c, o, and s represent the centre point, reference point (0.7 times of radius) and surface point, which are selected to inspect the variation of thermal and mechanical responses (see Fig.6.2).

6.2.2 Calculation of temperature field

The first step of the analysis is to calculate the transient temperature field $T(x,y,z,t)$, which describes the temperature at each point in concrete at time t. In the transient state test, there is no internal heat generated in the concrete, thus, the following heat transfer equation can be used,

$$\frac{\partial T}{\partial t} = \frac{\lambda}{\rho c} \times \left(\frac{\partial^2 T}{\partial x^2} + \frac{\partial^2 T}{\partial y^2} + \frac{\partial^2 T}{\partial z^2} \right) \tag{6.2}$$

where λ is the thermal conductivity in W/(m °C), ρ is the density of the concrete in kg/m^3, c is the specific heat in J/(kg °C), x, y and z are the coordinates.

To obtain the temperature distribution, the following initial and boundary conditions are used,

$$T(x,y,z,0) = T_0 \tag{6.3}$$

$$\lambda \times \left(\frac{\partial T}{\partial x} l_x + \frac{\partial T}{\partial y} l_y + \frac{\partial T}{\partial z} l_z \right) = 0 \tag{6.4}$$

$$\lambda \times \left(\frac{\partial T}{\partial x} l_x + \frac{\partial T}{\partial y} l_y + \frac{\partial T}{\partial z} l_z \right) = h \times (T_e - T_s) + e \times S \times (T_e^4 - T_s^4) \tag{6.5}$$

where T_0 = 20 °C is the ambient temperature, l_x, l_y, and l_z are the direction cosines of the normal to the boundary surface, h is the convection coefficient in W/(m^2 °C), e is the resultant emissivity of the exposure surface, $S = 5.67 \times 10^{-8}$ W/(m^2 °C^4) is the Stefan-Boltzmann constant, T_s is the surface temperature of concrete and T_e is the environment gas temperature determined based on the heating rate. Eq.(6.4) is applied to the top, bottom, and central lines, whereas Eq.(6.5) is applied to the exposed line.

Eqs.(6.3)-(6.5) are solved using the commercial software ABAQUS. For heat transfer analysis in ABAQUS, the concrete cylinder is discretized into a set of 4-node linear axisymmetric heat transfer quadrilateral elements with linear geometric order in axial-symmetrical space and the elements are meshed as 2.5 mm "squares". The type of the elements is DCAX4 and has only one active degree of freedom, i.e., temperature, at each node. Transfer of heat to the concrete from fire zone occurs through convection and radiation, and this is simulated through surface film condition and surface radiation. Heat transfer analysis is performed at incremental time steps and the interval is fixed as 1 min. The identification of the related thermal properties is discussed in Section.6.3.2.

6.2.3 Thermal-mechanical analysis

The key of the thermal-mechanical analysis is to quantify the effect of the temperature gradient and the related stress fluctuation on the development of the mechanical strain in the transient state test. Fig.6.3 illustrates the concept of the analysis. Under thermal gradient, the initially uniform stress σ_0 will fluctuate as the direction of blue arrows to eliminate the mechanical strain gradient caused by the change of constitutive relationships. Thus, the balanced strain will be ε_1, which is between $\varepsilon_{0,c}$ (strain evaluated according to the temperature at centre) and $\varepsilon_{0,s}$ (strain evaluated according to the temperature at surface) as shown in Fig.6.3. In addition, if there is an unloading at a stress higher than the yield stress, irrecoverable residual strain $\varepsilon_{r,T}$ is produced. In this way, the fluctuation will be amplified further as indicated by the red arrows in

Fig.6.3 and the balanced strain will have a higher value ε_2. Meanwhile, the opposite stress fluctuation caused by thermal strain gradient can produce plastic strain, which will influence the balance point. This indicates that to estimate the variation of mechanical strain only based on the temperature of a single point, disregarding its location, is inappropriate since there is an extra mechanical strain component $\varepsilon_{pla,tg}$ yielded by the temperature gradient in the transient state test. The way to implement the above-mentioned idea into the numerical analysis is described as follows.

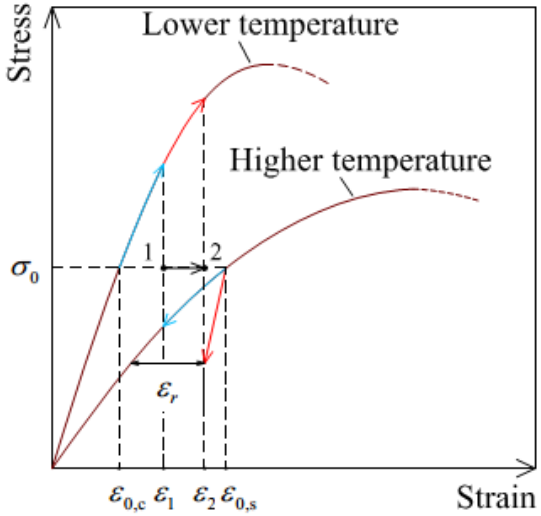

Fig.6.3 Rebalance of mechanical strain under thermal gradient

The aim of the numerical model developed here is to calculate the strain:

$$\varepsilon_{s,\exp} = \varepsilon_{fts} + \varepsilon_{\sigma,T} \tag{6.6}$$

where $\varepsilon_{\sigma,T}$ is defined by Eq.(2.10). To implement the numerical calculation, $\varepsilon_{\sigma,T}$ is rewritten as:

$$\varepsilon_{\sigma,T} = \varepsilon_{e,T} + \varepsilon_{p,T} + \varepsilon_{r,T} \tag{6.7}$$

where $\varepsilon_{e,T}$ and $\varepsilon_{p,T}$ are the elastic and plastic strains at temperature T, respectively. According to the constitutive model proposed in Chapter 5, for one point at any location on the top surface of the concrete cylinder specimen, their value at the increment time step i can be expressed as follows,

$$\varepsilon_{e,T}^{i} = \frac{\sigma_i}{E(L,T_i)} \tag{6.8}$$

$$\varepsilon_{p,T}^{i} = \left(\varepsilon_c(L,T_i) - \frac{f_c(L,T_i)}{E(L,T_i)}\right)\left(1 - \sqrt{1 - \left(\frac{\sigma_i - r(L,T_i)\times f_{c,T}(L,T_i)}{f_{c,T}(L,T_i) - r(L,T_i)\times f_{c,T}(L,T_i)}\right)^2}\right) \tag{6.9}$$

where σ_i , T_i are the stress and temperature at that point at time increment i. The accumulated residual strain $\varepsilon_{r,T}$ caused by unloading due to stress fluctuation can be calculated using an incremental method as follows,

$$\Delta\varepsilon_{r,T}^{i} = \left(\varepsilon_c(L,T_i) - \frac{f_c(L,T_i)}{E(L,T_i)}\right)\left(1 - \sqrt{1 - \left(\frac{f_r(\sigma_i,\sigma_{i\text{-}1})}{f_c(L,T_i) - r(L,T_i)\times f_c(L,T_i)}\right)^2}\right) \tag{6.10}$$

where $f_r(\sigma_i,\sigma_{i-1})$ is the corresponding increment of unloading stress:

$$f_r(\sigma_i,\sigma_{i-1}) = \begin{cases} 0 & \text{if } \sigma_{i-1} < \sigma_i \\ \sigma_{i-1} - \sigma_i & \text{if } \sigma_i \le \sigma_{i-1} \end{cases} \tag{6.11}$$

The gradient of free thermal strain induces stress fluctuation but its value only depends on temperature:

$$\varepsilon_{fts}^{i} = \alpha(T_i)\times T_i \tag{6.12}$$

where $\alpha(T_i)$ is the coefficient of thermal expansion in $℃^{-1}$. According to Eqs.(6.9)-(6.13), all strain components can be calculated. At a time increment i, $\varepsilon_{s,\exp}$ at node j can be calculated as follows,

$$\begin{aligned}\varepsilon_{s,\exp}^{i,j} &= \varepsilon_{fts}^{i,j} + \varepsilon_{e,T}^{i,j} + \varepsilon_{p,T}^{i,j} + \sum_{i=1}^{i}\Delta\varepsilon_{r,T}^{i,j} \\ &= \alpha\left(T_{i,j}\right)T_{i,j} + \frac{\sigma_{i,j}}{E\left(L,T_{i,j}\right)} \\ &+ \left(\varepsilon_c\left(L,T_{i,j}\right) - \frac{f_c\left(L,T_{i,j}\right)}{E\left(L,T_{i,j}\right)}\right)\times\left(1-\sqrt{1-\left(\frac{\sigma_{i,j}-r\left(L,T_{i,j}\right)\times f_c\left(L,T_{i,j}\right)}{f_c\left(L,T_{i,j}\right)-r\left(L,T_{i,j}\right)\times f_c\left(L,T_{i,j}\right)}\right)^2}\right) \\ &+ \sum_{i=1}^{i}\left(\left(\varepsilon_c\left(L,T_{i,j}\right) - \frac{f_c\left(L,T_{i,j}\right)}{E\left(L,T_{i,j}\right)}\right)\left(1-\sqrt{1-\left(\frac{f_r\left(\sigma_{i,j},\sigma_{i-1,j}\right)}{f_{c,T}\left(L,T_{i,j}\right)-r\left(L,T_{i,j}\right)\times f_{c,T}\left(L,T_{i,j}\right)}\right)^2}\right)\right)\end{aligned} \tag{6.13}$$

Due to the restraint provided by the rigid plates, at time increment i, all nodes on the top line should have an identical strain, that is

$$\varepsilon_{s,\exp}^{i,1}\left(\sigma_{i,1},T_{i,1}\right) = \varepsilon_{s,\exp}^{i,2}\left(\sigma_{i,2},T_{i,2}\right) = \cdots = \varepsilon_{s,\exp}^{i,m-1}\left(\sigma_{i,m-1},T_{i,m-1}\right) = \varepsilon_{s,\exp}^{i,m}\left(\sigma_{i,m},T_{i,m}\right) \tag{6.14}$$

In addition, the force balance requires the following equation:

$$\sum_{j=1}^{m}\left(\sigma_{i,j}\pi\left(\left(\frac{j\times R}{m}\right)^2 - \left(\frac{\left(j-1\right)\times R}{m}\right)^2\right)\right) = L\times f_{c,20} \tag{6.15}$$

where R is the radius of concrete cylinder.

In each time step, the transient temperature field is calculated first according to the thermal analysis described in Section 6.2.2 to obtain the nodal temperatures. Then the stress analysis is carried out using Eqs.(6.15) and (6.16) to obtain an equilibrium state from which both the stress and strain are obtained for each node. In this way, the relationship between $\varepsilon_{s,\exp}$ and temperature T can be obtained. For a given heating-loading condition and with the knowledge of specific material properties from the steady state test, TTC can be extracted accurately and explicitly from the total strain measured in the transient state test:

$$\varepsilon_{ttc}\left(L,T\right) = \varepsilon_{tot}\left(L,T\right) - \varepsilon_{s,\exp}\left(L,T\right) \tag{6.16}$$

6.3 Case Study

6.3.1 Description

A total of 10 different cases are analysed according to the experiment of Anderberg and Thelandersson (Anderberg & Thelandersson, 1976). The details for each case are listed in Tab.6.1.

Tab.6.1 Case study details

<table>
<tr><th>Category</th><th>Loading regime</th><th>Case</th><th>Temperature</th><th>Load</th></tr>
<tr><td rowspan="2">Steady</td><td rowspan="2"> 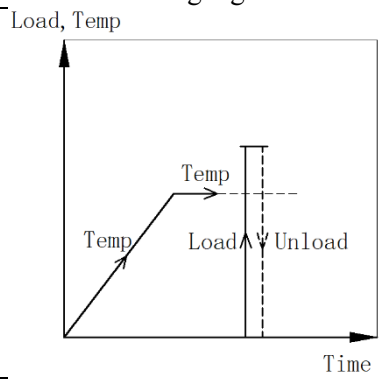
</td><td>1</td><td>20 °C</td><td>191 kN</td></tr>
<tr><td>2</td><td>500 °C</td><td>109 kN</td></tr>
<tr><td rowspan="10">Transient</td><td rowspan="10"> 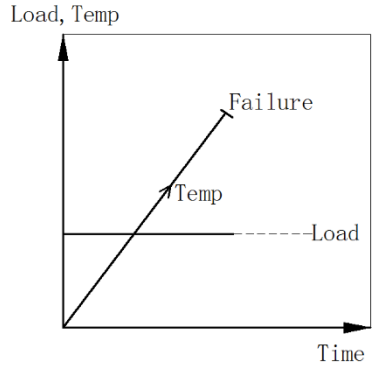
</td><td>Case</td><td>Heating Rate</td><td>Load level</td></tr>
<tr><td>3</td><td rowspan="5">5 °C/min</td><td>0%</td></tr>
<tr><td>4</td><td>22.5%</td></tr>
<tr><td>5</td><td>35%</td></tr>
<tr><td>6</td><td>45%</td></tr>
<tr><td>7</td><td>67.5%</td></tr>
<tr><td>8</td><td>1 °C/min</td><td rowspan="3">45%</td></tr>
<tr><td>9</td><td>10 °C/min</td></tr>
<tr><td>10</td><td>20 °C/min</td></tr>
</table>

Cases 1-3 are designed to validate the numerical model, whereas cases 4-7 are designed to investigate the effect of the temperature gradient and different methods used for calculating TTC from the total strain measured in the transient state test. Cases 6, 8-10 are the parametric study of the heating rate used in transient tests to

explore the sensitivity of the results to thermal gradient. All the specimens discussed here are the axially unrestrained cylinders of 75 mm diameter and 150 mm height.

6.3.2 Identification of material properties

The numerical analysis requires the input of two sets of parameters, namely thermal properties and mechanical properties. In the heat transfer analysis, a time–dependent temperature curve is used for the environment gas temperature which is applied to the exposed surface. The thermal properties required include the thermal conductivity, specific heat, and thermal expansion; all are assumed to be temperature-dependent and taken from the experimental study of Anderberg and Thelandersson (Anderberg & Thelandersson, 1976). In addition, a convection heat transfer coefficient of 25 W/(m^2 °C) and a resultant emissivity factor of 0.7 are used for the surface film condition and radiative heat transfer.

In the thermal-mechanical analysis, the mechanical properties required include the density, elastic modulus, Poisson's ratio, peak stress, strain at peak stress and crush strain. There are very few experimental results on the effect of temperature on Poisson's ratio and crush strain. Therefore, in the present numerical examples the Poisson's ratio is assumed to be 0.15 and the crush strain is assumed to be a function of temperature and increases linearly from the value of 0.005 at ambient temperature to 0.013 at 800 °C. The values of the peak stress, strain at peak stress and elastic modulus are taken from Anderberg's study as follows,

$$f_c(T)=\begin{cases} f_{c,20}\times(1-0.0001T) & \text{if } 20<T\le 400 \\ f_{c,20}\times(0.96-0.0023(T-400)) & \text{if } 400<T\le 600 \\ f_{c,20}\times(0.5-0.00135(T-600)) & \text{if } 600<T\le 800 \end{cases} \tag{6.17}$$

$$\varepsilon_c(T)=\begin{cases} 3 & \text{if } 20<T\le 200 \\ \dfrac{T-200}{90}+3 & \text{if } 200<T\le 600 \\ 8 & \text{if } 600<T\le 800 \end{cases} \tag{6.18}$$

$$E(T)=E_{20}\times(-0.0012T+1.0244) \quad \text{if } 20<T\le 800 \tag{6.19}$$

where $f_{c,20}=43.8$ MPa and E_{20} =28 GPa are the compressive strength and elastic modulus of concrete at 20 °C.

6.3.3 Model Validation

6.3.3.1 Validation of thermal analysis

In Anderberg's experiment, the specimen was first heated to 800 °C at a rate of 5 °C/min, and then the temperature was maintained for 1.5h. Three thermocouples were installed at three points as shown in Fig.6.2 to monitor the variation of temperatures in those locations. As demonstrated in Fig.6.4, the results given by the present numerical model and experiment are very close at the central and reference points. However, at the surface the temperature computed from the present numerical model is slightly lower than the experimental value until the temperature almost reaches its maximum value. The reason for this is because the experimentally measured temperature is the gas temperature at the exposed surface, whereas the numerically predicted temperature is the surface temperature of concrete. The

difference between them represents the interface effect of the heat transfer between different phases. It is observed from Fig.6.4 that the experimentally measured surface temperature is very close to the heating rate, i.e. the temperature of the furnace rather than the surface temperature of concrete. Nevertheless, the difference between them is small and its effect is insignificant particularly for the temperatures greater than 400 °C when concrete deteriorates sharply and the corresponding material nonlinearity becomes important.

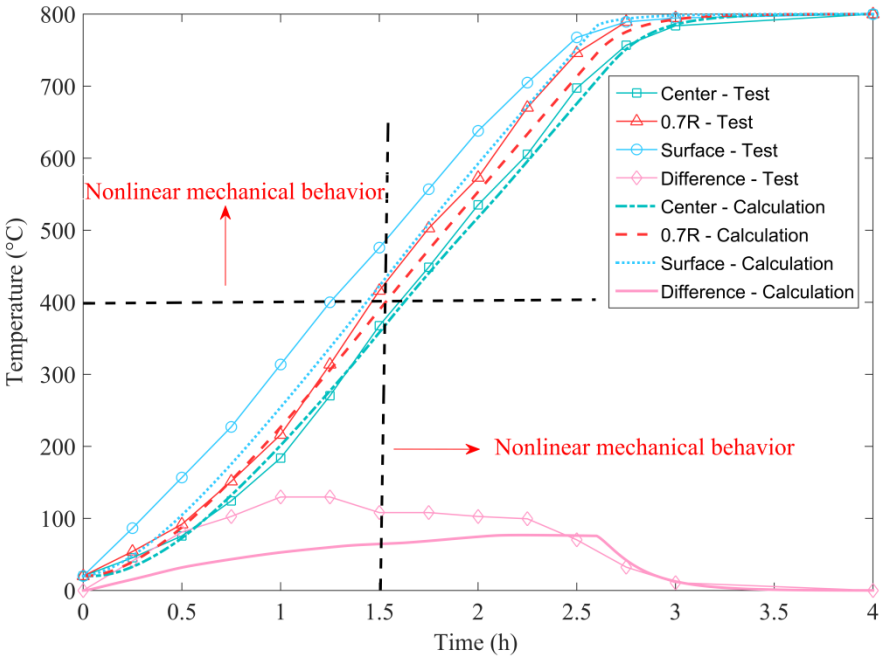

Fig.6.4 Validation of thermal response in the transient state test

6.3.3.2 Validation of free thermal strain

Case 3 with 0% pre-fire load level is designed to simulate the free thermal strain in the transient state test. The corresponding experimental data and predicted value are plotted in Fig.6.5. The free thermal strain of concrete is a sum of expansion of the

aggregate and shrinkage of the cement paste. Above 700 °C, most of the siliceous aggregate indicate little or reduced expansion, therefore, the free thermal strain of concrete develop with temperature gradually before it is heated to 700 °C but decline afterwards. It can be seen that there is excellent agreement between the numerical and experimental results. This demonstrates the capability of the present model in capturing the response of thermal expansion in the transient state test.

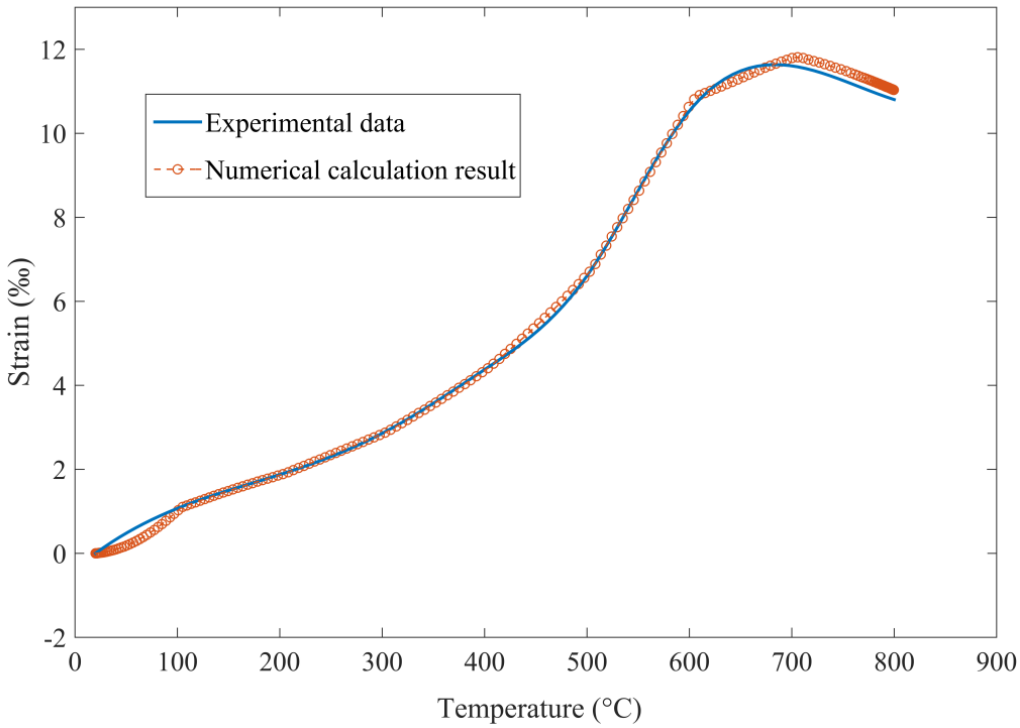

Fig.6.5 Validation of free thermal strain in the transient state test (case 3)

6.3.3.3 Validation of thermal-mechanical analysis

Cases 1 and 2 are designed to validate the accuracy of the numerical model in thermal-mechanical analysis. For the ambient temperature and a high temperature (500 °C), the numerical model is run for both loading and unloading. The corresponding results are shown in Fig.6.6. It can be seen from the figure that the numerical results match

perfectly with the theoretical predictions for both the loading and unloading situations.

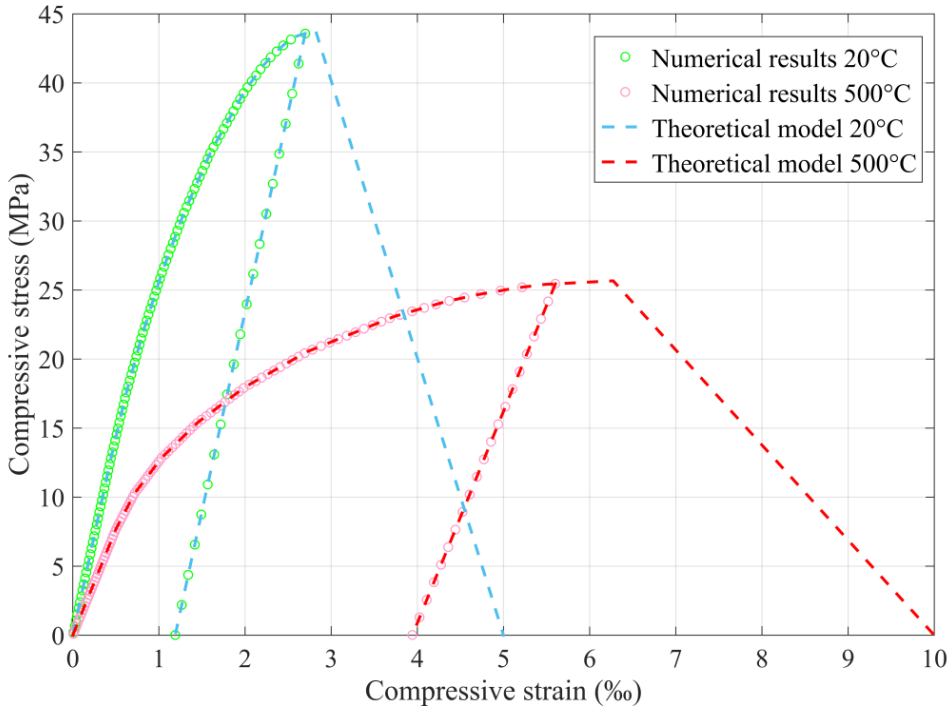

Fig.6.6 Validation of thermal-mechanical analysis (cases 1 and 2)

6.3.4 Results and discussions

6.3.4.1. Effect of thermal gradient on applied stress fluctuation in the transient state test

To illustrate the effect of temperature gradient on stress fluctuation, the variations of axial compressive stresses on the top of the concrete cylinder with time obtained in cases 4 and 7 are plotted in Fig.6.7.b as a function of time for each of the 21 analysis points shown in Fig.6.7.a.

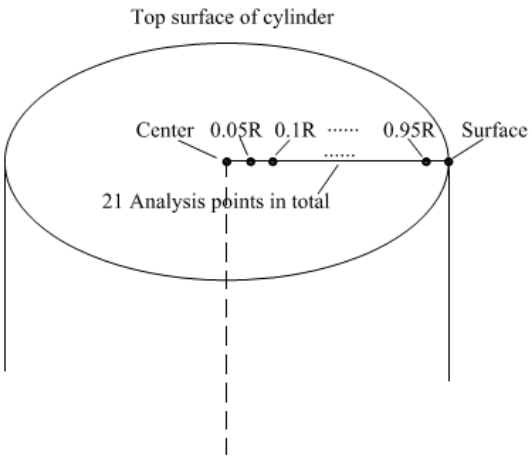

(a) Analysis points

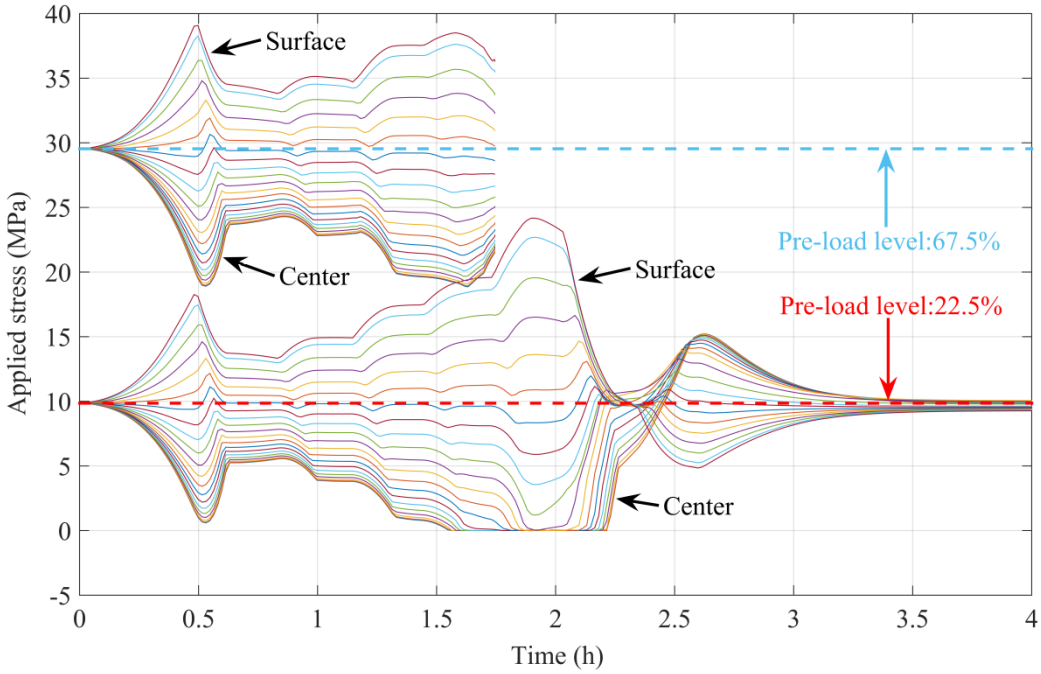

(b) Stress fluctuations with time (case 4 and case 7)

Fig.6.7 Stress fluctuations resulting from thermal gradient in transient test

For case 4 (load level 22.5%, heating rate 5 °C/min), when compared with the dash line representing constant pre-stress, the predicted stresses using the present model (solid lines) show a strong fluctuation from the beginning until the final stage of fire

exposure where the temperature gradient decreases to 0. The compressive stress on the surface increases sharply at the beginning because of the emergent temperature gradient. With the increase of temperature and stress gradient, the mechanical strain gradient develops in the opposite direction, which confines the further development of the stress fluctuation from the centre to the exposed surface and thus leads to a slight reverse trend at around 0.5 h. However, due to the mild deterioration of mechanical properties at an early stage, the overall trend before 500 °C is the relocation of stress from the centre to the surface. After 500 °C (around 2 h of fire exposure), the mechanical properties of concrete begin to deteriorate rapidly. Thus the fluctuation trend turns in an opposite direction. Until around 2.5 h, and after the temperature approaches 700 °C, the stress distribution is totally opposite. In the last 1.4 h (2.6-4 h), the heating rate becomes zero and there is no temperature difference. In this case the stress gradient caused by the thermal gradient becomes minimal. Finally, it ends up with an almost even stress distribution as at the start. The slight difference is caused by the evolution of different residual strains accumulated at different points. Although the specimen has no damage during the whole process due to a relatively low pre-fire load level, strong stress fluctuation is clearly observed, where the highest stress could be more than twice the initial value, while the lowest stress could be zero.

For case 7 (load level 67.5%), the basic trend in the early stage (0-1.5 h) is very similar to that shown in case 4 (22.5% load level). This demonstrates that before 400 °C, the stress fluctuation is controlled mainly by the thermal expansion. After 1.5

h, when the temperature hits to 400 °C, the reverse convergence happens much earlier than that happened in the case 4. This is probably attributed to the large mechanical strain due to the application of high pre-fire load. The sharp deterioration of the mechanical properties and the accumulated irrecoverable plastic strain are amplified by the high pre-fire load. At around 1.75 h, the distribution trend turns around and the curves terminate. This is because the specimen is crushed due to the stress at one point being in excess of its compressive strength. This indicates that the stress fluctuation may also influence the temperature of the crush point. In conclusion, the stress fluctuation caused by temperature gradient in the transient state test is complicated and it is too large to be ignored. The predicted mechanical strain, without considering the effect of temperature gradient, is significantly underestimated particularly when the temperature is high.

6.3.4.2 Effect of thermal gradient on calculating TTC in transient test

To quantify the effect of the temperature gradient on the TTC obtained from a transient state test, the development of different strain components at the reference point in cases 4-7 is plotted in Fig.6.8 as a function of temperature, in which the free thermal strain ε_{fts} and the total strain ε_{tot} are taken from the experimental results of Anderberg and Thelandersson. The difference between them is the sum of the mechanical strain and TTC. The four dash lines shown in Fig.6.8 represent the strains when the free thermal strain is added with different parts of mechanical strain, which are calculated by using the semi-implicit models 1-3 as discussed in Section.2.5.2.5 and our proposed

explicit numerical method, respectively. The difference between the total measured strain and any of the calculated curves is regarded as LITS or TTC according to different authors (see Fig.6.8.b), as discussed in Section.2.5.2.5. Fig.6.8.c illustrates the various parts of mechanical strain. The strain definitions used in Fig.6.8.b and Fig.6.8.c can be applied to other cases.

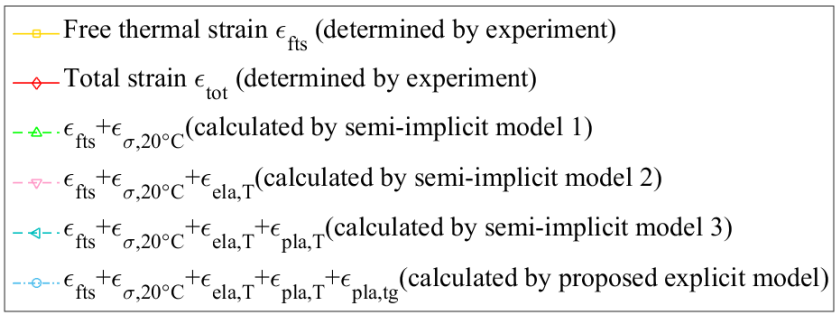

(a) Legend

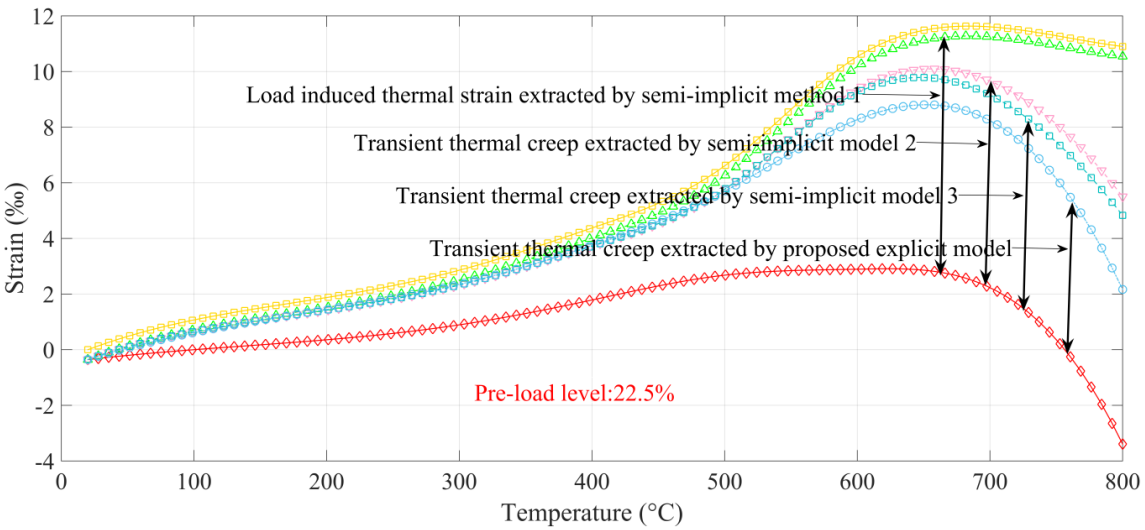

(b) Loadlevel-22.5% (case 4)

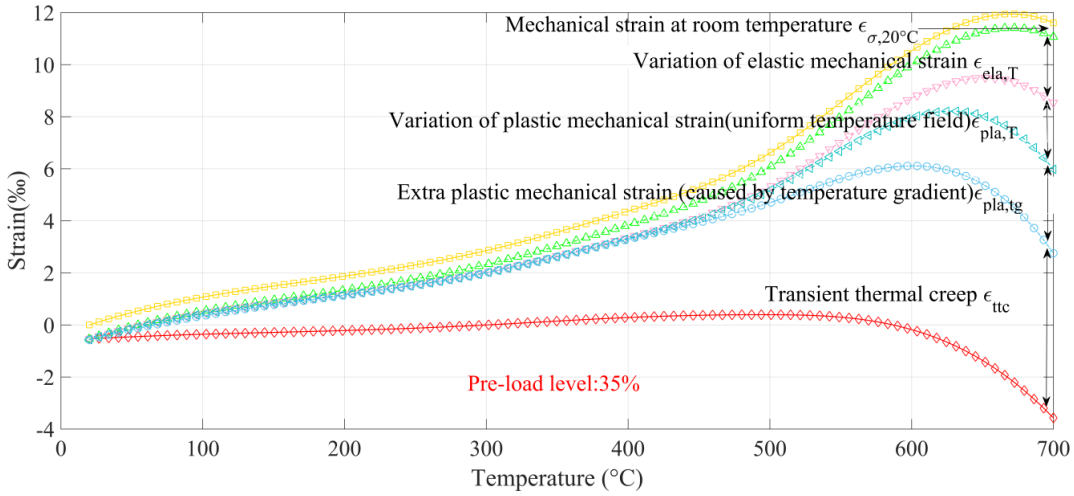

(c) Loadlevel-35% (case 5)

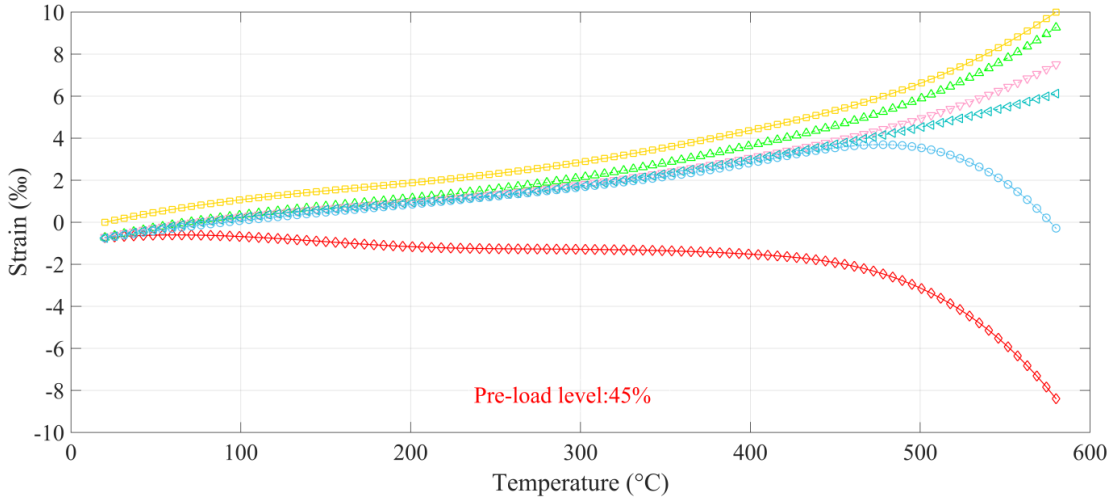

(d) Loadlevel-45% (case 6)

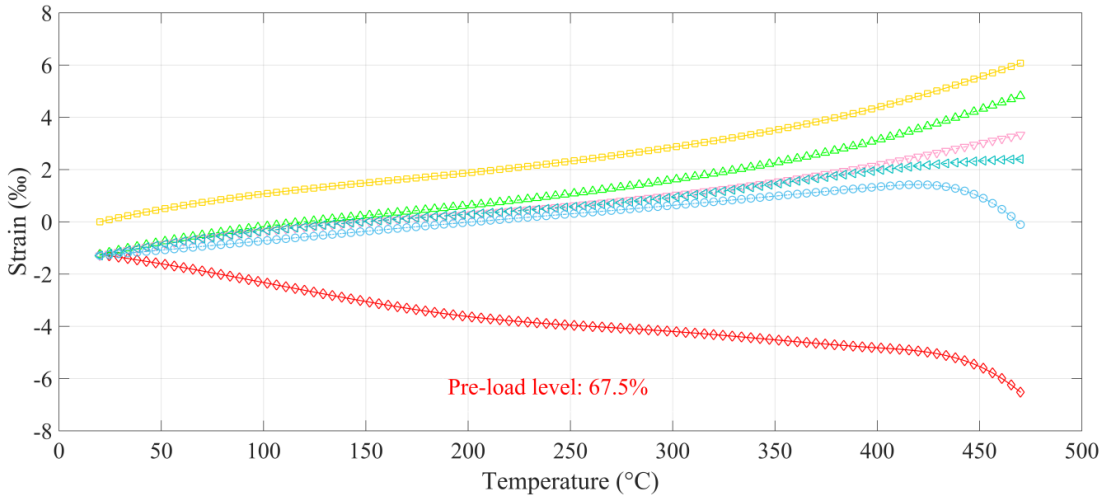

(e) Loadlevel-67.5% (case 7)

Fig.6.8 Strain decomposition and model comparison in transient test (cases 4-7)

According to Fig.6.8.b-Fig.6.8.e, before 400 °C, the mechanical strain parts ($\varepsilon_{ela,T}$, $\varepsilon_{pla,T}$ and $\varepsilon_{pla,tg}$) are very small when compared to the TTC at the same temperature. Hence, the results calculated by using different models are similar. However, after the temperature exceeds 450 °C, the mechanical properties of concrete deteriorate sharply, which leads to the rapid increase of various mechanical strain components and results in remarkable differences between different models, particularly when the temperature approaches the crush point. It is noted from Fig.6.8 that the descending slope of the numerical curve present is almost parallel to the experimental curve, indicating that the sudden descending part of the total strain in the transient state test is likely to be attributed to the growth of the mechanical strain. It is evident from Fig.6.8 that the plastic strain caused by the temperature gradient is the dominant one among the mechanical strain components. For example, at the end of case 6 (Fig.6.8.d), the value of $\varepsilon_{pla,tg}$ is larger than the sum of all other mechanical strain components and is almost the same as the magnitude of TTC. This implies that the TTC defined in many existing models actually includes some of mechanical strains, while the nature of the mechanical strain is completely different from that of TTC.

6.3.4.3 Refinement of TTC model

According to above numerical results, TTC can be refined in a completely explicit way. When plotting ε_{TTC} / L, the ratio of TTC to the corresponding pre-fire load level L, against temperature, a set of data less scattered is obtained, as the red dots shown in Fig.6.9. By regression analysis, a refined formula of TTC is proposed:

$$\varepsilon_{ttc} = L\left(a(T-T_0)^3 + b(T-T_0)^2 + c(T-T_0)\right) \tag{6.20}$$

where $a = 1.076\times10^{-10}$ °C^{-3}, $b = -5.846\times10^{-7}$ °C^{-2}, $c = 3.11\times10^{-5}$ °C^{-1}.

The above proposed model (red solid line) is plotted with Anderberg's model (Eq.(2.18) represented by blue solid line) in Fig.6.9. They both fit corresponding data quite well and are very close to each other at early stages. As the analysis in Tab.2.2 and Section 2.5.2.5, the TTC formulated by Anderberg has semi-implicitly included the plastic strain caused by the temperature gradient in the transient state test. This is the reason why the value predicted by it is greater than the explicit model at high temperature. At the same time, two LITS models are plotted for the purpose of comparison. The nonlinear LITS model of Diederichs (Eq.(2.13)) has the same form as the proposed TTC model, however, its parameters are calibrated by the semi-implicit method 1 rather than the explicit method. The value predicted by it has a good agreement with the two TTC models at relatively low temperature, but its overestimation at high temperature is even more severe than Anderberg's model, which is caused by the inclusion of $\varepsilon_{ela,T}$ and $\varepsilon_{pla,T}$. The master LITS curve proposed by Khoury (Eq.(2.14)) gives a basically similar trend as Diederichs's model but with higher magnitude. In conclusion, the mechanical strain semi-implicitly included in existing TTC and LITS models, especially the part caused by temperature gradient, would be amplified and become more and more dominant with elevated temperature, resulting in obvious overestimation of TTC.

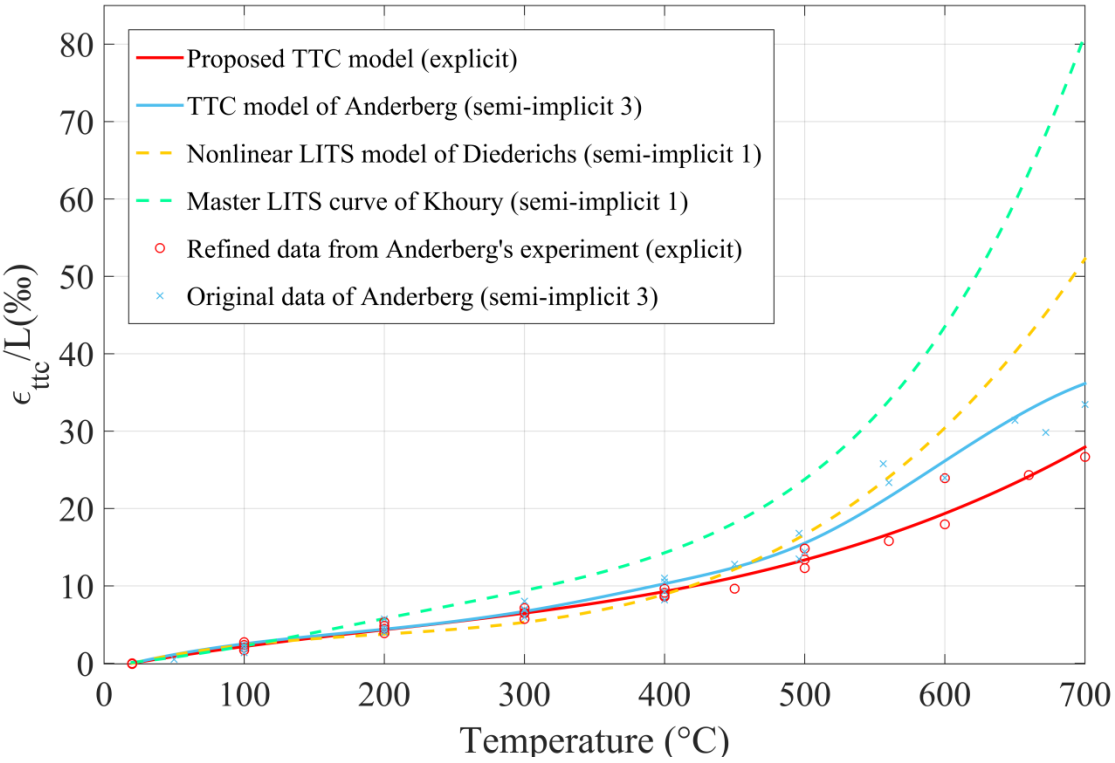

Fig.6.9 Comparison of different LITS / TTC models

6.4. Parametric study of heating rate and related temperature gradient in the transient state test

As discussed above, the temperature gradient in a transient state test not only results in stress fluctuation but also yields extra mechanical strain, which can influence the evaluation of TTC. Since the temperature gradient in concrete is heavily dependent on the heating rate of transient state tests, it is of interest to examine the sensitivity of the results to the heating rate. Cases 6, 8, 9, 10 are designed with the same pre-fire load level (45%) but with different heating rates. The corresponding results are shown in Fig.6.10. As is demonstrated in the previous analysis, the reference point (0.7 times of radius) has the smallest stress fluctuation because it is on the bisectrix of the area and

thus the reference point is selected here as the place where the variation of results with temperature is examined.

It is shown in Figs.6.10.a and 6.10.b that both the temperature gradient and stress fluctuation are very slight under the heating rate of 1 °C/min and the corresponding strain calculated shown in Fig.6.10.c is almost the same as that under homogeneous temperature field, indicating that the temperature gradient effect is negligible. With the increase of the heating rate, however, both the temperature gradient and stress fluctuation become large, and at the same time, the temperature of the crush point becomes low. This leads to a large mechanical strain, as illustrated in Fig.6.10.c, and thus has great influence on TTC.

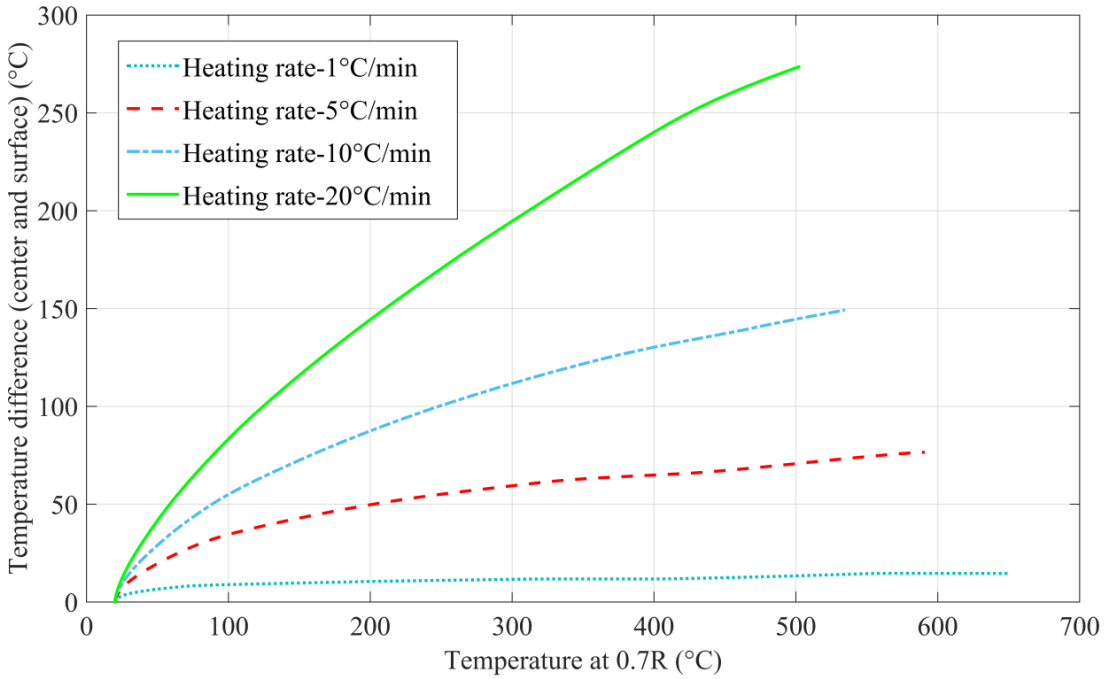

(a) Temperature difference

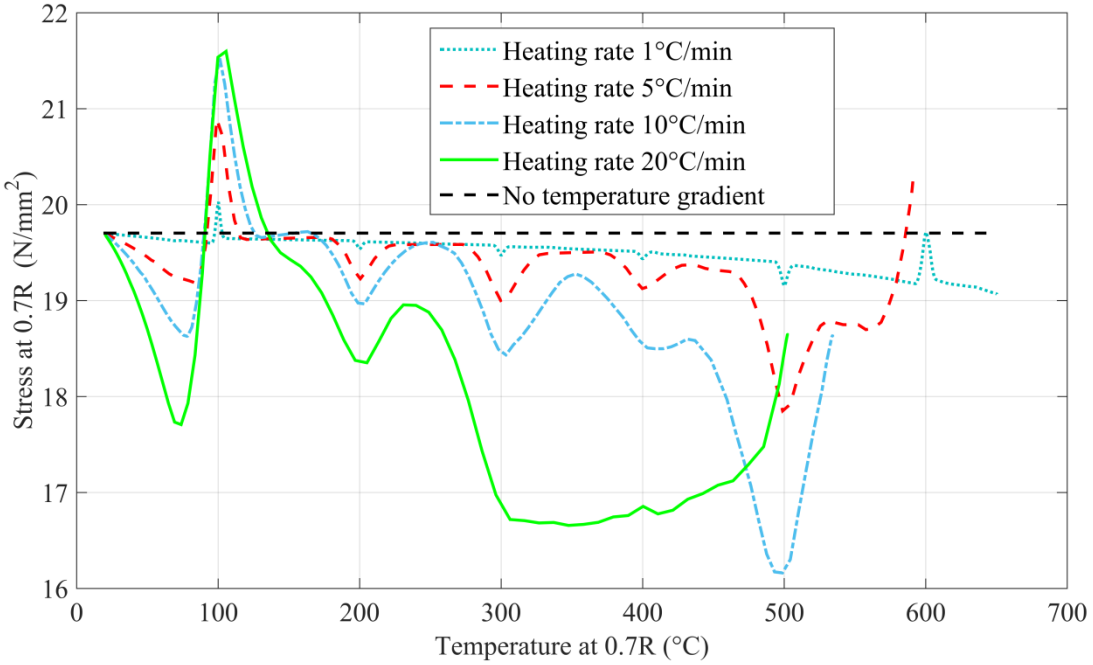

(b) Stress fluctuation of the reference point

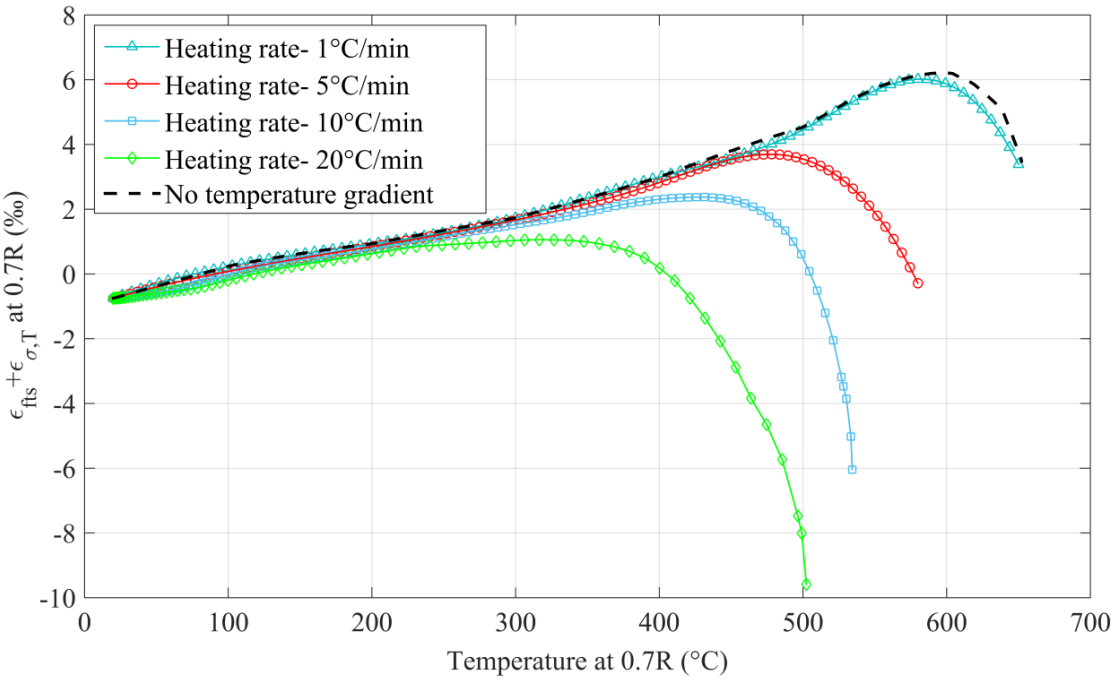

(c) Development of strain with time

Fig.6.10 Parametric study of heating rate and related temperature gradient (cases 6,8,9,10)

6.5 Conclusions

In this chapter, a numerical method has been developed to analyse the stress fluctuation and corresponding plastic strain caused by the combination of pre-fire load and temperature gradient. The results obtained have been compared with those calculated from existing models, from which the following conclusions can be drawn:

1) The drawback of existing TTC and LITS models is the incomplete separation between TTC and mechanical strain, which makes it difficult to identify and understand the mechanism of how TTC is developed and what factors affect the evolution of TTC.

2) Stress fluctuation is found in two opposite directions simultaneously due to the thermal gradient produced in the transient state test. At the early stage of exposure, the stress fluctuation is mainly controlled by the variation of thermal expansion. But at high temperature the deterioration of the mechanical properties can have a great influence on the stress fluctuation. The stress fluctuation can affect not only the evaluation of TTC but also the temperature of the crush point.

3) Extra mechanical strain can be produced by the thermal gradient in the transient state test, which has not been considered in previous models. At relatively high temperatures this extra mechanical strain becomes very remarkable. The implicit inclusion of the extra mechanical strain in existing models is the reason for the observation of the sharp increase of TTC beyond 500 °C in many previous works.

4) The explicit numerical model proposed in this study can accurately evaluate TTC on the basis of experimental results and can calculate the different parts of mechanical strain, especially the one caused by the thermal gradient.

5) As an example, a recalibration is accomplished by applying the present explicit model to Anderberg's experimental study. The results demonstrated that ignoring the effect of the temperature gradient leads an overestimation of TTC, particularly when the temperature is high.

6) The effect of temperature gradient on the evolution of mechanical strain can be neglected in the transient state test if the maximum temperature does not exceed 400 °C or if the heating rate is very low.

Chapter 7 - Explicit TTC model for concrete containing FA

7.1 General

In Chapter 6, the effect of the temperature gradient on TTC in the transient state test has been investigated and a numerical method has been established to exclude this effect. This chapter reports on tests of Series C, in which specimens are heated with sustained load (10%，30%，50%，70% of reference strength) until failure. Results including the temperature distribution of concrete specimens and deformation-temperature relationships are presented. And the results are calculated via the numerical method proposed in Chapter 6. Explicit TTC of OPC concrete and FA concrete are formulated and compared to investigate the effect of using FA as SCM in concrete on the development of TTC. Relative average deviations of load induced thermal strain investigated in tests of series C are presented in Appendix.

7.2 Temperature distribution during the transient heating process

As an example, Fig.7.1 shows the experimental results from thermocouple readings for specimens heating at 5 °C/min to 800 °C. The location of the thermocouples on the surface is illustrated in Chapter 3. It can be seen that the temperature difference between the surface of specimen and furnace is significant. This is because a steel sleeve exists between the specimen and the heating elements in the furnace, which is designed to protect furnace from potential violent spalling of heated and stressed concrete specimens. In this way, the heat would firstly flow from the heating element

to the steel sleeve, then conduct to the specimen, resulting in a nonlinear heating rate in the specimens. Therefore, the increasing rate of temperature in the specimens is relatively slow at an early stage. When the temperature of furnace achieves 800 °C, the temperature is held for 60 minutes, during which the temperature difference between surface and centre decreases. However, it should be noted that the temperature of the specimen is obviously lower than the furnace temperature at the end of the heating process, which could also be attributed to the heat loss caused by the steel sleeve. Although there is a significant temperature difference between the furnace and specimen, the temperature difference between concrete surface and its centre is much smaller, as shown in Fig.7.1.

As the introduction in Section.2.2.2, the variation of the specific heat and density of concrete with elevated temperature is relatively small, and thus the estimation of these two parameters can be taken directly from Eurocode. With the knowledge of specific heat, density and temperature difference between surface and centre, the value of thermal conductivity can also be calculated. In this way, all the thermal properties of the specimens can be evaluated and by applying the heat transfer analysis proposed in Section.6.2.2, in which the temperature at the surface is defined as the experimental results, the temperature distribution through the cross section of specimen at any time can, therefore, be derived.

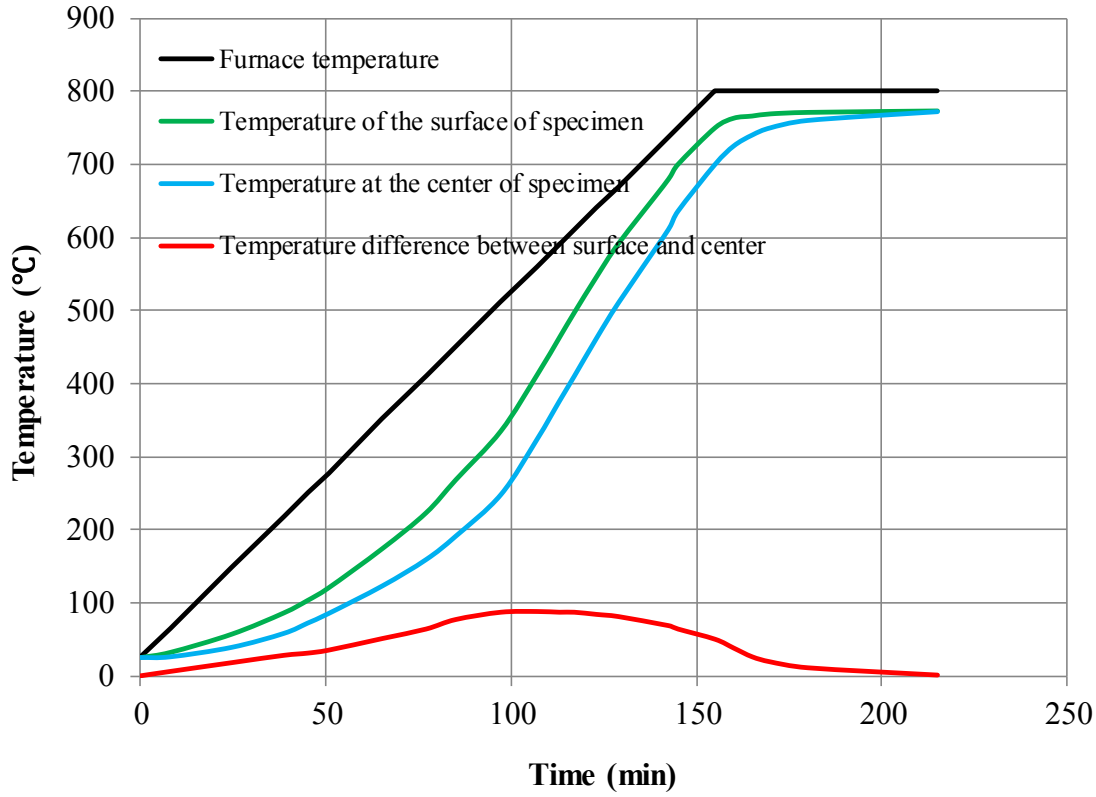

Fig.7.1 Temperature distribution in specimens in the transient heating process

7.3 Deformation in the transient heating process

7.3.1 Free thermal strain

The free thermal strain of FA concrete and OPC concrete specimens, tested under 0% load level and including thermal shrinkage and expansion during the transient heating process, is plotted in Fig.7.2. Because the temperature over the cross-section of specimens varies during the transient heating process, as illustrated in Fig.7.1, a representative temperature should be adopted. For the results presented in Fig.7.2, the representative temperature of the specimen is defined as the temperature at a distance 0.7R (17.5mm) from the centre since this distance corresponds to the location of the centroid of a uniform stress distribution as presented in Fig.6.7.

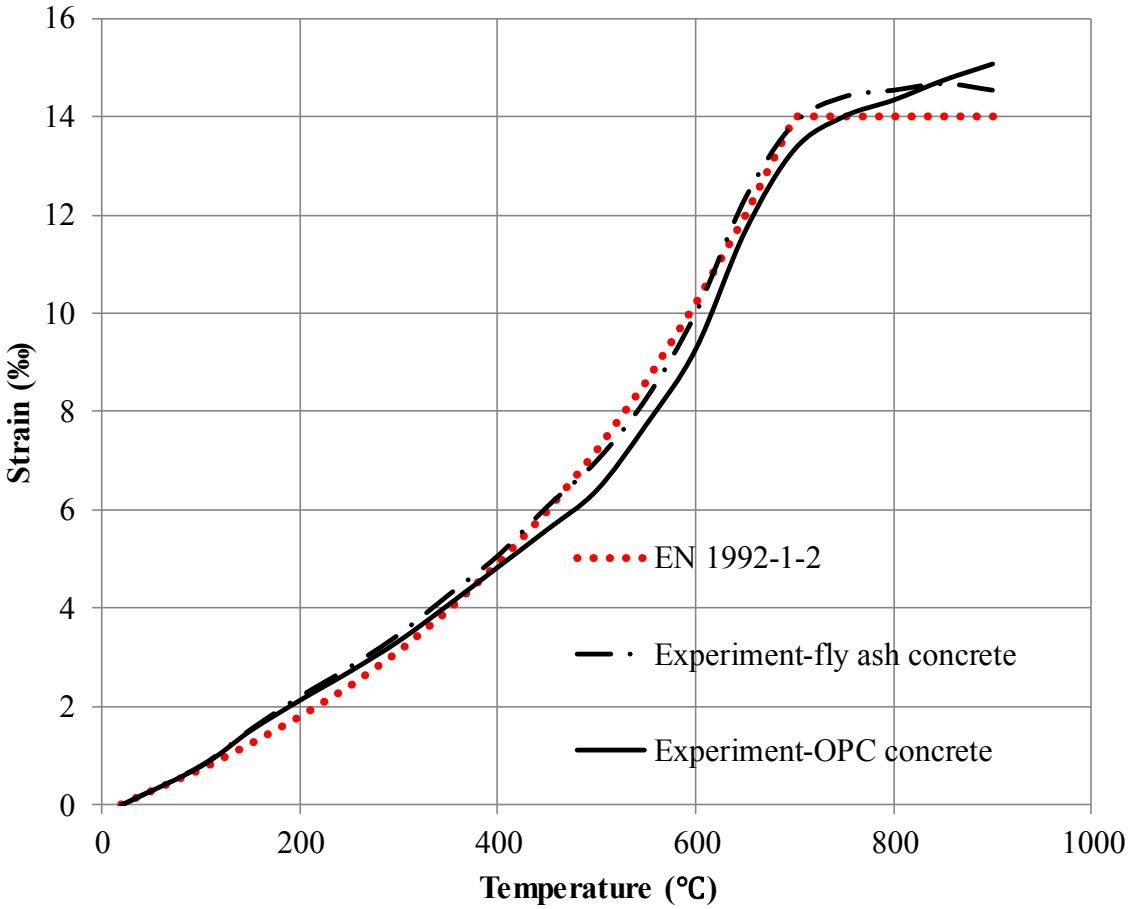

Fig.7.2 Development of free thermal strain with temperature

According to Fig.7.2, the values of free thermal strain of two mix proportions are very close to each other and both fit the free thermal strain curve of siliceous aggregate concrete recommended in EN1992-1-2 very well. This is because the main factor affecting the free thermal strain is the aggregate. The type of coarse aggregate plays a dominant role in heat transfer and thermal expansion. And partly replacing OPC with FA in manufacturing concrete would not influence its free thermal expansion, thus the value can be estimated by using the equation given in Eurocode. In addition, it is evident that free thermal strain is a non-linear function of temperature. It increases quickly with temperature from room temperature to around 700 °C. The maximum

rate happens at around 400 °C – 600 °C, where a significant decrease in compressive strength develops. Above 700 °C, the free thermal strain varies little with the rise of temperature.

7.3.2 LITS

Fig.7.3 presents the strain-temperature relationships obtained from test Series C, in which FA concrete and OPC concrete specimens were heated at 5 °C/min under different pre-fire load levels until failure. For the results presented in Fig.7.3, the representative temperature of the specimen is also defined as the temperature at a distance 0.7R (17.5mm) from the centre. The deformations shown in Fig.7.3 have already excluded the mechanical strain obtained upon initial loading so that the comparison of LITS is more direct. It can be seen that the thermal expansion is strongly reduced under stress and for stress level of 0.7 the thermal expansion is fully compensated by LITS. As the temperature approaches a critical value the compressive strain increases rapidly and ultimately failure occurs. The influence of partly replacing OPC with FA in concrete on the development of LITS is also presented in Fig.7.3. For FA concrete, its thermal strain under sustained stress is considerably greater than thermal strain of OPC concrete under the same thermal-mechanical condition and the difference increases with load level and temperature. The results suggest that using FA as SCM in concrete results in less LITS, compared with OPC based concrete.

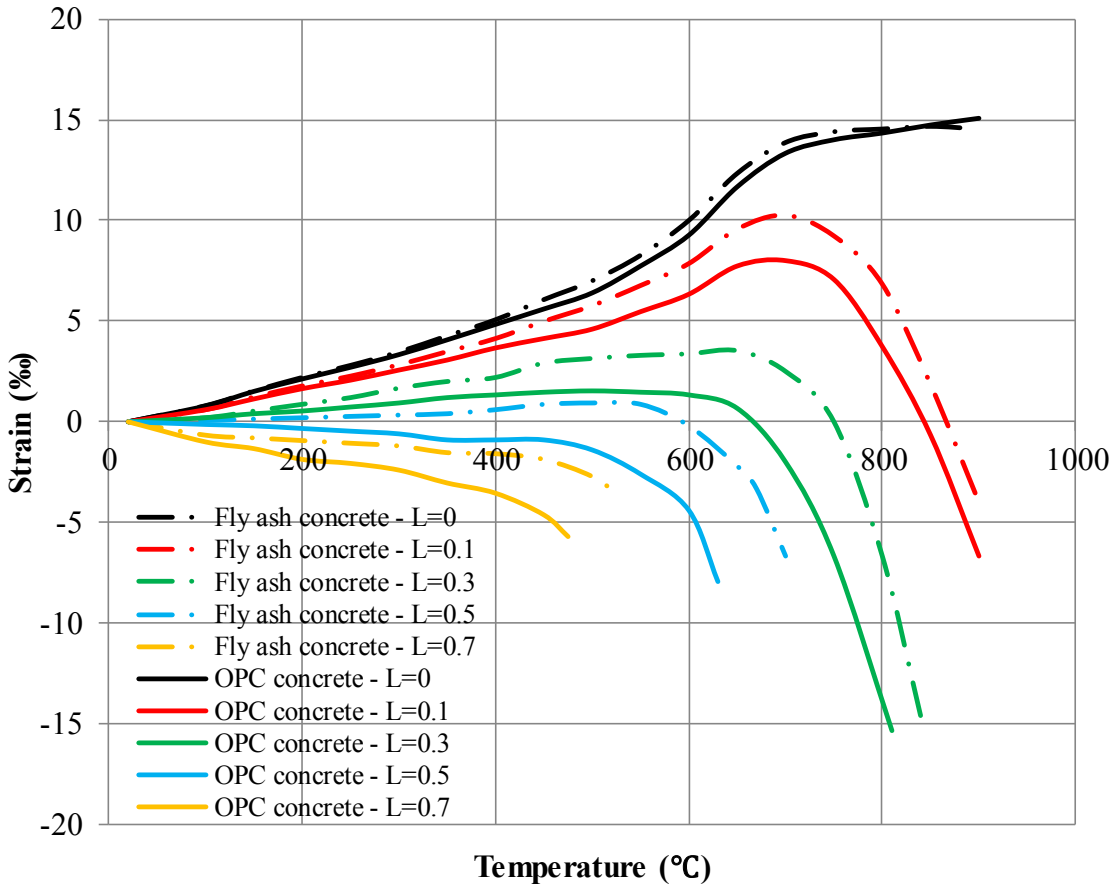

Fig.7.3 Strain-temperature relationships of speicmens under different load levels

To quantify the difference, LITS is calculated according to Tab.2.2 and the results are plotted in Fig.7.4 as the form of ε_{LITS} / L, that is the ratio of LITS to corresponding pre-fire load level L. It should be noted that the sharp decrease of the strain-temperature relationship for stressed concrete specimens when it is approaching to the crush point is caused by the increase in mechanical strain, as demonstrated in Chapter 6. The specimen at this stage is approaching failure, and thus becomes very unstable. Its corresponding mechanical strain is hard to evaluate precisely. Therefore, the sharp descending branches have been excluded in the following analysis for LITS and the highest temperature is up to 750 °C.

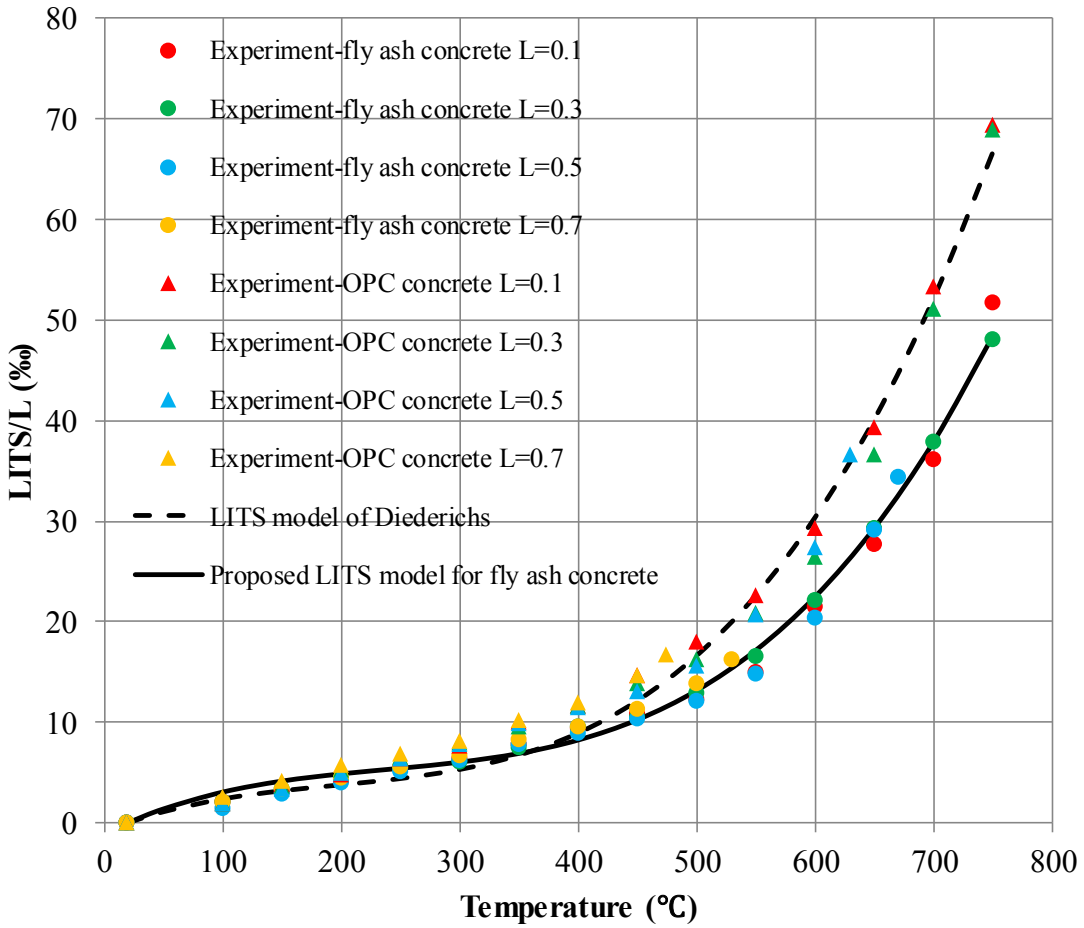

Fig.7.4 LITS – temperature relationship of OPC concrete and FA concrete

In Fig.7.4, the LITS model proposed by Diederichs (Eq.(2.13)) is also plotted for the purpose of comparison. As can be seen, the value predicted by the model fits well the experimental data of OPC concrete, which suggests that the results provided in this study have a good agreement with previous research. The experimental results of LITS obtained from FA concrete specimens presents a similar trend, but with lower magnitude. One possible explanation for this phenomenon is that further hydration of FA at elevated temperatures has reduced the deterioration in compressive strength with the increasing temperature, as discussed in Chapter 4. Higher compressive strength means less plasticity under the same thermomechanical condition. Thus less plastic

deformation energy could be released by the sustained load in the transient heating process, which might be the physical origin of less LITS observed in FA concrete. More details about this mechanism is discussed in Section 7.3.4. By regression analysis, a refined LITS model for FA concrete is proposed:

$$\varepsilon_{ttc} = L\left(a(T-T_0)^3 + b(T-T_0)^2 + c(T-T_0)\right) \tag{7.1}$$

where $a = 2.81\times10^{-10}$ °C^{-3}, $b = -1.84\times10^{-7}$ °C^{-2}, $c = 5.10\times10^{-5}$ °C^{-1}.

7.3.3 Explicit TTC model

As the analyses given in Chapter 6, LITS has semi-implicitly included the increase in mechanical strain caused by increasing temperature and temperature gradient. By applying the numerical method proposed in Chapter 6, explicit TTC excluding these irrelevant components, can be obtained from the results of LITS presented in 7.3.2. The constitutive model to implement the numerical process is adopted from the model formulated in Chapters 4 and 5. The explicit values of TTC are plotted in Fig.7.5, in which the LITS curves of OPC concrete and FA concrete are also plotted for the purpose of comparison. The difference between LITS and TTC is the variation in mechanical strain. Meanwhile, it can be seen that the refined explicit TTC model proposed in Section.6.3.4, on the foundation of Anderberg's experimental data, fits the experimental value very well. Nevertheless, both LITS and explicit TTC values of FA concrete are less than that of OPC concrete, which is probably due to the contribution of FA used as SCM. By regression analysis, the refined explicit model of TTC for FA

concrete is formulated as follows:

$$\varepsilon_{ttc} = L\left(a(T-T_0)^3 + b(T-T_0)^2 + c(T-T_0)\right) \tag{7.2}$$

where $a = 1.08\times10^{-10}$ °C^{-3}, $b = -8.16\times10^{-7}$ °C^{-2}, $c = 3.5\times10^{-5}$ °C^{-1}.

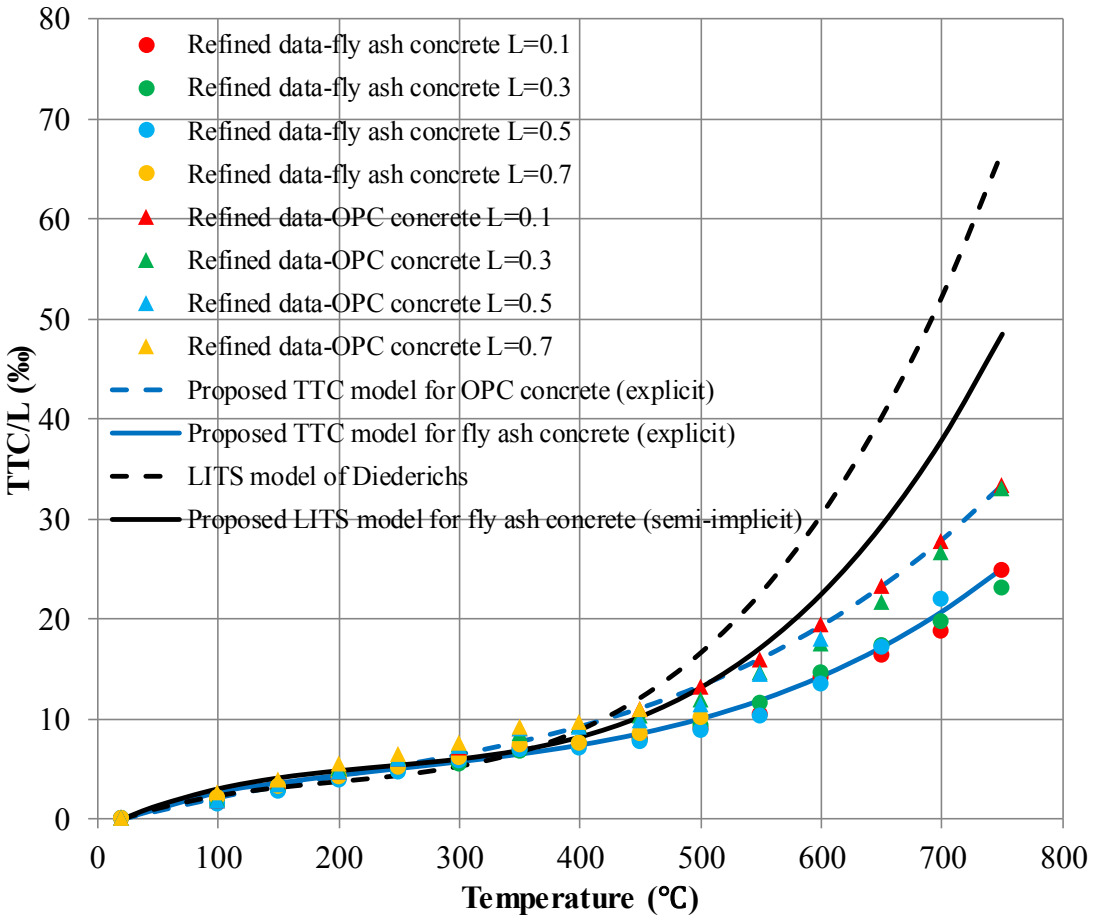

Fig.7.5 Explicit TTC models excluding the effect of temperature gradient

7.4 Physical mechanism of TTC

As introduced in Chapter 2, the physical/chemical mechanism of TTC is still not clearly understood. Firstly, the thermal incompatibility between aggregates (which tend to expand) and cement paste (which tends to shrink) is unlikely to be the cause of TTC, since it has been experimentally proved that the development of TTC in pure

cement paste is greater than that in concrete (Pan, Sanjayan & Collins, 2014; Torelli *et al.*, 2016). Then, according to the analysis in Chapter 6, the mechanical strain caused by the temperature gradient during the transient heating process is obviously lower than the value of TTC, indicating that the variation in mechanical strain caused by temperature gradient is not the dominant one. Moreover, the development of cracks due to the temperature gradient also cannot be the main mechanism since it has been demonstrated that TTC develops even for specimens heated at very slow rates, i.e. in case of negligible thermal gradients (Anderberg & Thelandersson, 1976; Illston & Sanders, 1974; Khoury, 1983).

In the author's opinion, the mechanism of TTC should be physical instead of chemical because there is no evidence to support that the chemical reactions in cement paste could be significantly influenced by mechanical loading sequences. One possible explanation for this physical mechanism is the accumulation of plastic strain during the transient heating process. When concrete is heated, its stress-strain response will gradually deteriorate with increasing temperature. If there is a sustained stress applied during the heating process, the deformation will rebalance at each temperature increment continuously and the irrecoverable plastic strain is accumulated. In contrast, if concrete is heated without any mechanical load to a thermal steady state and then loaded to the same load as the stressed specimen, the deformation only develops at the constant temperature in a very short period.

As shown in Fig.7.6, for specimens loaded at the thermal steady state, the strain only

depends on the temperature and stress level. However, for a specimen stressed during heating, from the same batch and under the same stress level, the strain at the same temperature level depends on the previous accumulation process. The plastic strain increment of stressed concrete is less than the plastic strain of unstressed specimen at the same temperature and stress level, because the part of the potential plastic deformation energy at that temperature instant has been consumed in previous stages, which is also the reason why the peak strain of the stressed specimen is lower than that of the unstressed specimen. However, with the accumulated process, the final accumulated plastic strain of stressed concrete is much greater than the instantaneous plastic strain of unstressed concrete at the corresponding thermal steady state, indicating a more thorough release of plastic deformation energy.

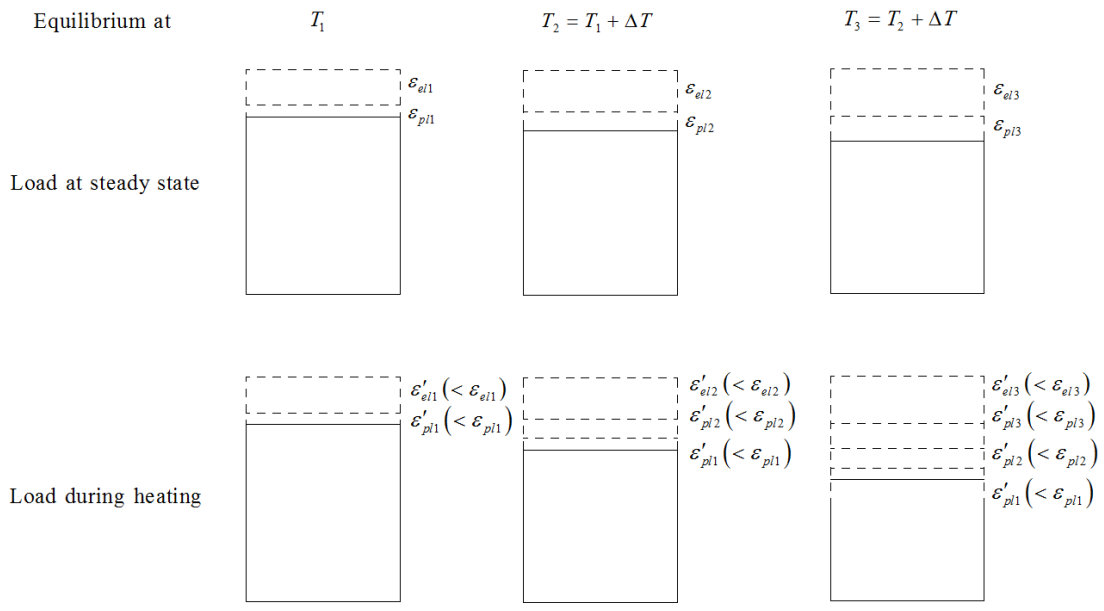

Fig.7.6 Diagrammatic representation of the physical origin of TTC

In conclusion, for stressed specimens, the applied mechanical load keeps releasing the plastic deformation energy during the whole process, resulting in more

thermomechanical damage than unstressed specimens. The plastic strain accumulated in the transient heating process is the main source of the development of TTC. As the nature of plastic strain, TTC is irrecoverable on cooling or unloading, and also increases with applied stress and temperature. Under relatively low temperature or stress level, the variation of plastic strain at each temperature increment is limited, and thus the magnitude of TTC of specimens at the early stage of the heating process is also not that obvious, especially for low load levels. For a specific heating process and constant loading level, the amount of TTC depends on the plastic increment at each temperature increment. For FA concrete, its compressive strength deterioration is generally slower than the OPC concrete due to the further hydration of FA with elevated temperature. Therefore, in the same thermomechanical condition, the plastic deformation increment of FA concrete at each temperature increment is lower than that of the OPC concrete, which is the reason why the TTC of FA concrete is lower than that of corresponding OPC concrete.

7.5 Conclusions

Transient state tests (Series C) for OPC concrete and FA concrete specimens are presented in this Chapter. The results of temperature gradient, free thermal strain, and LITS during the heating process have been reported. By applying the numerical model proposed in Chapter 6 to the experimental data, the effect of the temperature gradient on the development of mechanical strain has been excluded. On the basis of the present experimental investigation, the following conclusions can be drawn:

1) 25% replacement of OPC with FA in manufacturing concrete has little impact on its free thermal strain at high temperatures. The free thermal strain model of Eurocode EN1992-1-2 is applicable to FA concrete.

2) The development of LITS and TTC in FA concrete is slower than those in OPC concrete, which could be attributed to the reduction in deterioration of compressive strength, resulting from the further hydration of FA at high temperature. The parameters used in the LITS model and the proposed explicit TTC model have been calibrated for FA concrete.

3) One assumption for the physical source for the development of TTC has been made according to the results. With the increase of temperature, the mechanical properties of concrete will deteriorate. When the concrete is heated with a sustained load, at each temperature increment, there will be a corresponding strain increment. In this way, the applied load keeps producing deformation energy during the heating process and the corresponding plastic strain increments are accumulated during the process. Finally, the released plastic deformation energy behaves as the sum of the plastic strain increments macroscopically, thus forming an additional strain component, named as TTC.

Chapter 8 - Conclusions and future work

8.1 Conclusions

One main aim of this thesis is to investigate the mechanical behaviour of concrete under different thermomechanical conditions and obtain a better understanding of the mechanism of how pre-fire load affects the fire performance of concrete. Through the experimental research and numerical analysis presented in this thesis, an advanced constitutive model for concrete at high temperature has been proposed and verified. Different from previous models, the model proposed in this thesis has included the effect of loading history during thermal exposure on stress-strain response at the thermal steady state and excluded the mechanical strain caused by the thermal gradient during the heating process from TTC. In addition, the influence caused by using FA as SCM on the fire performance of concrete has been examined.

8.1.1 Effect of using FA as SCM on fire performance of concrete

1) Adding FA in concrete hardly influence its deformation characteristics at high temperature, but the compressive strength is enhanced due to the further hydration of FA under hydrothermal conditions.

2) The shape of stress-strain curve, represented by nonlinearity, varies with temperature. Adding FA into concrete makes it behave more linearly and reduce its plasticity.

3) Eurocode is safe to be applied to NSC with 25% replacement of FA ash as SCM. However, the peak strain recommended has implicitly included the TTC, which should be explicitly calculated in advanced analysis.

4) The development of LITS and TTC in FA concrete is slower than those in OPC concrete, which could be attributed to the reduction in deterioration of compressive strength resulting from the further hydration of FA at high temperature. The parameters used in the LITS model and the proposed explicit TTC model have been calibrated for FA concrete.

8.1.2 Effect of temperature gradient on TTC in transient tests

1) The drawback of the existing TTC and LITS models is the incomplete separation between TTC and mechanical strain, which makes it difficult to identify and understand the mechanism of how TTC is developed and what factors affect the evolution of TTC.

2) Stress fluctuation is found in two opposite directions simultaneously due to the thermal gradient produced in the transient state test. At the early stage of exposure, the stress fluctuation is mainly controlled by the variation of thermal expansion. But at high temperature the deterioration of the mechanical properties can have great influence on the stress fluctuation. The stress fluctuation can affect not only the evaluation of TTC but also the temperature of the crush point.

3) Extra mechanical strain can be produced by the thermal gradient in the transient state test, which has not been considered in previous models. At relatively high temperatures this extra mechanical strain becomes very remarkable. The implicit inclusion of the extra mechanical strain in existing models is the reason for the observation of the sharp increase of TTC beyond 500 °C in many previous works.

4) The explicit numerical model proposed in this study can accurately evaluate the TTC on the basis of experimental results and can calculate the different parts of the mechanical strain, especially the one caused by the thermal gradient.

5) As an example, a recalibration is accomplished by applying the present explicit model to Anderberg's experimental study. The results demonstrated that ignoring the effect of temperature gradient leads to an overestimation of TTC, particularly when the temperature is high.

6) The effect of temperature gradient on the evolution of mechanical strain can be ignored in the transient state test if the maximum temperature does not exceed 400 °C or if the heating rate is very low.

8.1.3 Effect of load history during thermal exposure on fire performance of concrete

1) At the thermal steady state, compared with unstressed concrete, the compressive strength and the elastic modulus of stressed concrete increase with the applied stress

level during the heating process. On the contrary, the peak strain of stressed concrete decrease with the applied stress level during the heating process.

2) The enhancement of compressive strength and elastic modulus caused by the pre-fire load is closely related to the decomposition of CH in ITZ. Above 460 °C, for specimens heated with a sustained load, load induced micro-cracks are produced and accumulated during the heating process, which benefits the vapour diffusion process and reduces the build-up of vapour pressure caused by the decomposition of CH, thus mitigating the explosive damage in ITZ.

3) If concrete is loaded during heating, the development of thermal cracks is constrained. Moreover, the sustained load during heating would produce a corresponding strain increment at each temperature increment continuously. In this way, the applied load keeps producing deformation energy during the heating process and the corresponding plastic strain increments are accumulated in the process, which might be the physical origin of TTC and responsible for the reduction in peak strain.

4) The relationship between the variation of the mechanical properties caused by pre-fire load and the stress level itself is nonlinear. When the stress level is over 0.3, its further increase has little impact on the results.

5) Sustained stress during the heating process also influences the shape of the stress-strain relationships at high temperature. Different from unstressed concrete, the stress-strain curve of stressed concrete at high temperature is initially linear to a yield ratio

which is much higher than 0.3 $f_c(L,T)$ and pre-fire load level L. Meanwhile, the peak plastic strain at compressive strength is lower than that of unstressed specimens.

8.2 Future works

The main conclusions presented above have identified several aspects that need for further research, which can be summarized as follows:

1) The replacement percentage of FA in this thesis is limited to a common but moderate value 25%. The higher replacement percentages of FA in cement should be further verified.

2) The constitutive model for the stressed condition at high temperatures, proposed in this thesis, is formulated based on experiments of normal strength concrete. The mechanical properties of stressed high strength concrete at high temperatures should be further studied.

3) The applicability of this model to different types of concrete, like geopolymer concrete, concrete with lithium slag as SCM, and concrete incorporating graphene oxide, should be further examined.

4) The fire performance of concrete subjected to multiaxial loadings during the heating process should be assessed in future.

5) The effect of the pre-fire load on the spalling of concrete, especially for high

strength concrete, during thermal exposure, should be investigated in future.

6) For stressed conditions tested in this thesis, the applied load keeps constant during the thermal exposure. However, the external load on concrete structures varies with time in practical fire scenarios. Therefore, the effect of the varying stress during thermal exposure on stress-strain response at the thermal steady state and TTC should be explored in future.

References

Abdulkareem, O. A., Al Bakri, A. M., Kamarudin, H., Nizar, I. K. & Ala'eddin, A. S. (2014) 'Effects of elevated temperatures on the thermal behavior and mechanical performance of fly ash geopolymer paste, mortar and lightweight concrete'. *Construction and Building Materials*, 50 pp. 377-387.

Abe, T., Furumura, F., Tomatsuri, K., Kuroha, K. & Kokubo, I. (1999) 'Mechanical properties of high strength concrete at high temperatures'. *AIJ The Journal of Asian Architecture and Building Engineering*, 515 pp. 163-168.

Abrams, M. S. (1971) 'Compressive strength of concrete at temperatures to 1600F'. *Journal of American Concrete Institute*, SP-25 (2), pp. 33-58.

Alogla, S. & Kodur, V. K. R. (2018) 'Quantifying transient creep effects on fire response of reinforced concrete columns'. *Engineering Structures*, 174 pp. 885-895.

Anderberg, Y. & Thelandersson, S. (1976) *Stress and deformation characteristics of concrete at high temperatures.* Bulletin of Division of Structural Mechanics and Concrete Construction. vol. 54. Lund: Lund Institute of Technology.

Anderberg, Y. & Thelandersson, S. (1978) 'A constitutive law for concrete at transient high temperature conditions'. *Journal of American Concrete Institute*, SP-55 pp. 187-205.

Arioz, O. (2007) 'Effects of elevated temperatures on properties of concrete'. *Fire Safety Journal*, 42 (8), pp. 516-522.

Arthanari, S. & Yu, C. (1967) 'Creep of concrete under uniaxial and biaxial stresses at elevated temperatures'. *Magazine of Concrete Research*, 19 (60), pp. 149-156.

Bažant, Z. (1972) 'Thermodynamics of interacting continua with surfaces and creep analysis of concrete structures'. *Nuclear Engineering and Design*, 20 (2), pp. 477-505.

Bazant, Z. P. (1983) 'Mathematical-model for creep and thermal shrinkage of concrete at high-temperature'. *Nuclear Engineering and Design*, 76 (2), pp. 183-191.

Bažant, Z. P. & Chern, J.-C. (1987) 'Stress-induced thermal and shrinkage strains in concrete'. *Journal of engineering mechanics*, 113 (10), pp. 1493-1511.

Bažant, Z. P., Cusatis, G. & Cedolin, L. (2004) 'Temperature effect on concrete creep modeled by microprestress-solidification theory'. *Journal of engineering mechanics*, 130 (6), pp. 691-699.

Bažant, Z. P. & Yunping, X. (1994) 'Drying creep of concrete: constitutive model and new experiments separating its mechanisms'. *Materials and Structures*, 27 (1), pp. 3-14.

Castillo, C. (1987) *Effect of transient high temperature on high-strength concrete*. Rice University.

Cheng, F.-P., Kodur, V. & Wang, T.-C. (2004) 'Stress-strain curves for high strength concrete at elevated temperatures'. *Journal of Materials in Civil Engineering*, 16 (1), pp. 84-90.

Colina, H., Moreau, G. & Cintra, D. (2004) 'Experimental study of transient thermal creep and other phenomena of concrete at high temperature'. *Journal of Civil Engineering and Management*, 10 (4), pp. 255-260.

Colina, H. & Sercombe, J. (2004) 'Transient thermal creep of concrete in service conditions at temperatures up to 300°C'. *Magazine of Concrete Research*, 56 (10), pp. 559-574.

Cruz, C. R. (1962) 'Elastic properties of concrete at high temperatures'. *Journal of the PCA Research and Development Laboratories*, 8 (1), pp. 37-45.

Diederichs, U. (1987) 'Modelle zur beschreibung der betonverformung bei instantionaren temperaturen'. *Abschlubkolloquium Bauwerke Unter Brandeinwirkung*, pp. 25-34.

Diederichs, U., Jumppanen, U.-M. & Penttala, V. (1988) 'Material properties of high strength concrete at elevated temperatures'. *13th Congress of International Association for Bridge and Structural Engineering*. Helsinki, pp 489-494.

Elahi, A., Basheer, P., Nanukuttan, S. & Khan, Q. (2010) 'Mechanical and durability properties of high performance concretes containing supplementary cementitious

materials'. *Construction and Building Materials*, 24 (3), pp. 292-299.

EN1992-1-2 (2004) *Eurocode2: Design of concrete structures-Part 1-2: General rules-Structural fire design.* Brussels: European Committee for Standardization.

ENV1992-1-2 (1995) *Eurocode2: Design of concrete structures-Part 1-2: General rules-Structural fire design.* Brussels: European Prestandard.

Fan, K., Li, D., Damrongwiriyanupap, N. & Li, L.-y. (2019a) 'Compressive stress-strain relationship for fly ash concrete under thermal steady state'. *Cement and Concrete Composites*, 104 pp. 103371.

Fan, K., Li, D., Li, L.-y. & Wu, J. (2019b) 'Effect of temperature gradient on transient thermal creep of heated and stressed concrete in transient state tests'. *Construction and Building Materials*, 222 pp. 839-851.

Furumura, F., Abe, T. & Shinohara, Y. (1995) 'Mechanical properties of high strength concrete at high temperatures'. *Proceedings of the Fourth Weimar Workshop on High Performance Concrete: Material Properties and Design*, pp. 237-254.

Gao, W. Y., Dai, J.-G., Teng, J. G. & Chen, G. M. (2013) 'Finite element modeling of reinforced concrete beams exposed to fire'. *Engineering Structures*, 52 pp. 488-501.

Gernay, T. (2012) 'Effect of transient creep strain model on the behavior of concrete columns subjected to heating and cooling'. *Fire technology*, 48 (2), pp. 313-329.

Gernay, T. & Franssen, J. M. (2012) 'A formulation of the Eurocode 2 concrete model at elevated temperature that includes an explicit term for transient creep'. *Fire Safety Journal*, 51 pp. 1-9.

Gernay, T., Millard, A. & Franssen, J.-M. (2013) 'A multiaxial constitutive model for concrete in the fire situation: Theoretical formulation'. *International Journal of Solids and Structures*, 50 (22-23), pp. 3659-3673.

Gross, H. (1975) 'High-temperature creep of concrete'. *Nuclear Engineering and Design*, 32 (1), pp. 129-147.

Hager, I. (2013) 'Behaviour of cement concrete at high temperature'. *Bulletin of the Polish Academy of Sciences: Technical Sciences*, 61 (1), pp. 145-154.

Hansen, T. C. & Eriksson, L. (1966) 'Temperature change effect on the behavior of cement paste, mortar, and concrete under load'. *Journal of American Concrete Institute*, 63 (4), pp. 489-504.

Harada, T., Takeda, J., Yamane, S. & Furumura, F. (1972) 'Strength, elasticity and thermal properties of concrete subjected to elevated temperatures'. *Concrete for Nuclear Reactors*, (34), pp. 377-406.

Harmathy, T. Z. & Allen, L. W. (1973) 'Thermal properties of selected masonry unit concretes'. *Journal of American Concrete Institute*, 70 (2), pp. 132-142.

Hassen, S. & Colina, H. (2006) 'Transient thermal creep of concrete in accidental conditions at temperatures up to 400 °C'. *Magazine of Concrete Research*, 58 (4), pp. 201-208.

Hertz, K. D. (2005) 'Concrete strength for fire safety design'. *Magazine of Concrete Research*, 57 (8), pp. 445-453.

Hossain, K. M. A. (2006) 'High strength blended cement concrete incorporating volcanic ash: Performance at high temperatures'. *Cement and Concrete Composites*, 28 (6), pp. 535-545.

Huismann, S., Weise, F., Meng, B. & Schneider, U. (2011) 'Transient strain of high strength concrete at elevated temperatures and the impact of polypropylene fibers'. *Materials and Structures*, 45 (5), pp. 793-801.

Illston, J. & Sanders, P. (1973) 'The effect of temperature change upon the creep of mortar under torsional loading'. *Magazine of Concrete Research*, 25 (84), pp. 136-144.

Illston, J. & Sanders, P. (1974) 'Characteristics and prediction of creep of a saturated mortar under variable temperature'. *Magazine of Concrete Research*, 26 (88), pp. 169-179.

Juenger, M. C. & Siddique, R. (2015) 'Recent advances in understanding the role of supplementary cementitious materials in concrete'. *Cement and Concrete Research*, 78 pp. 71-80.

Kalifa, P., Chéné, G. & Gallé, C. (2001) 'High-temperature behaviour of HPC with polypropylene fibres - From spalling to microstructure'. *Cement and Concrete Research*, 31 (10), pp. 1487-1499.

Kalifa, P., Menneteau, F. D. & Quenard, D. (2000) 'Spalling and pore pressure in HPC at high temperatures'. *Cement and Concrete Research*, 30 (12), pp. 1915-1927.

Kallel, H., Carré, H., La Borderie, C., Masson, B. & Tran, N. C. (2017) 'Effect of temperature and moisture on the instantaneous behaviour of concrete'. *Cement and Concrete Composites*, 80 pp. 326-332.

Kallel, H., Carré, H., Laborderie, C., Masson, B. & Cuong Tran, N. (2018) 'Evolution of mechanical properties of concrete with temperature and humidity at high temperatures'. *Cement and Concrete Composites*, 91 pp. 59-66.

Karakurt, C. & Topçu, İ. B. (2012) 'Effect of blended cements with natural zeolite and industrial by-products on rebar corrosion and high temperature resistance of concrete'. *Construction and Building Materials*, 35 pp. 906-911.

Khaliq, W. & Kodur, V. (2011) 'Thermal and mechanical properties of fiber reinforced high performance self-consolidating concrete at elevated temperatures'. *Cement and Concrete Research*, 41 (11), pp. 1112-1122.

Khatri, R., Sirivivatnanon, V. & Gross, W. (1995) 'Effect of different supplementary cementitious materials on mechanical properties of high performance concrete'.

Cement and Concrete Research, 25 (1), pp. 209-220.

Khennane, A. & Baker, G. (1993) 'Uniaxial model for concrete under variable temperature and stress'. *Journal of engineering mechanics*, 119 (8), pp. 1507-1525.

Khoury, G. (2006) 'Strain of heated concrete during two thermal cycles. Part 1: strain over two cycles, during first heating and at subsequent constant temperature'. *Magazine of Concrete Research*, 58 (6), pp. 367-385.

Khoury, G., Majorana, C., Pesavento, F. & Schrefler, B. (2002) 'Modelling of heated concrete'. *Magazine of Concrete Research*, 54 (2), pp. 77-101.

Khoury, G. A. (1983) *Transient thermal creep of nuclear reactor pressure vessel type concretes*. Imperial College, University of London.

Khoury, G. A. (1995) 'Strain components of nuclear-reactor-type concretes during first heat cycle'. *Nuclear Engineering and Design*, 156 (1-2), pp. 313-321.

Khoury, G. A. (2000) 'Effect of fire on concrete and concrete structures'. *Progress in Structural Engineering and Materials*, 2 (4), pp. 429-447.

Khoury GA, A. S. (1998) 'Advanced mechanical characterisation of HPC and UHPC concretes at high temperatures', *Proceedings of the International Workshop on Durable Concrete Structures*. Weimar.

Khoury, G. A., Grainger, B. N. & Sullivan, P. J. (1985a) 'Transient thermal strain of

concrete: literature review, conditions within specimen and behaviour of individual constituents'. *Magazine of Concrete Research*, 37 (132), pp. 131-144.

Khoury, G. A., Grainger, B. N. & Sullivan, P. J. (1985b) 'Strain of concrete during first heating to 600 C under load'. *Magazine of Concrete Research*, 37 (133), pp. 195-215.

Khoury, G. A., Grainger, B. N. & Sullivan, P. J. E. (1986) 'Strain of Concrete during First Cooling from 600 °C under Load'. *Magazine of Concrete Research*, 38 (134), pp. 3-12.

Kodur, V. (2014) 'Properties of concrete at elevated temperatures'. *ISRN Civil Engineering*, 2014 pp. 1-15.

Kodur, V. & Alogla, S. (2017) 'Effect of high-temperature transient creep on response of reinforced concrete columns in fire'. *Materials and Structures*, 50 (1), pp. 27.

Kodur, V. R. & Harmathy, T. Z. (2008) 'Properties of building materials', in DiNenno, P.J. (ed.) *SFPE Handbook of Fire Protection Engineering*. Quincy: National Fire Protection Association, pp. 277-324.

Kordina, K., Ehm, C. & Schneider, U. (1986) 'Effects of biaxial loading on the high temperature behaviour of concrete', *1st International Symposium on Fire Safety Science*. Washington, D.C., pp. 281-291.

Lea, F. C. & Stradling, R. E. (1922) 'The resistance to fire of concrete and reinforced

concrete'. *Journal of the Society of Chemical Industry*, 41 (18), pp. 395-396.

Lie, T. T. (1992) *Structural fire protection.* Reston: American Society of Civil Engineers.

Lie, T. T. & Kodur, V. K. R. (1996) 'Thermal and mechanical properties of steel-fibre-reinforced concrete at elevated temperatures'. *Canadian Journal of Civil Engineering*, 23 (2), pp. 511-517.

Lothenbach, B., Scrivener, K. & Hooton, R. (2011) 'Supplementary cementitious materials'. *Cement and Concrete Research*, 41 (12), pp. 1244-1256.

Lu, L., Yuan, Y., Caspeele, R. & Taerwe, L. (2015) 'Influencing factors for fire performance of simply supported RC beams with implicit and explicit transient creep strain material models'. *Fire Safety Journal*, 73 pp. 29-36.

Ma, Q., Guo, R., Zhao, Z., Lin, Z. & He, K. (2015) 'Mechanical properties of concrete at high temperature—a review'. *Construction and Building Materials*, 93 pp. 371-383.

Malhotra, H. L. (1956) 'The effect of temperature on the compressive strength of concrete'. *Magazine of Concrete Research*, 8 (23), pp. 85-94.

Malhotra, V. (1993) 'Fly ash, slag, silica fume, and rice husk ash in concrete: A review'. *Concrete International*, 15 (4), pp. 23-28.

Maréchal, J. C. (1970) 'Influence des températures sur la résistance, sur le fluage, sur

la déformation plastique du béton'. *Annales de L'Institute Technique du Bâtiment et des Travaux Publics*, 23 pp. 123-146.

Mindeguia, J.-C., Hager, I., Pimienta, P., Carré, H. & La Borderie, C. (2013) 'Parametrical study of transient thermal strain of ordinary and high performance concrete'. *Cement and Concrete Research*, 48 pp. 40-52.

Mindess, S., Young, J. F. & Darwin, D. (2003) *Concrete.* Upper Saddle River: Prentice Hall.

Monteiro, P. (2006) *Concrete: Microstructure, Properties, and Materials*. New York: McGraw-Hill.

Nadeem, A., Memon, S. A. & Lo, T. Y. (2014) 'The performance of Fly ash and Metakaolin concrete at elevated temperatures'. *Construction and Building Materials*, 62 pp. 67-76.

Naus, D. J. (2006) *The effect of elevated temperature on concrete materials and structures-a literature review.* Oak Ridge: Oak Ridge National Laboratory.

Nielsen, C. V., Pearce, C. J. & Bićanić, N. (2004) 'Improved phenomenological modelling of transient thermal strains for concrete at high temperatures'. *Computers & concrete*, 1 pp. 189-209.

Noumowe, A., Clastres, P., Debicki, G. & Costaz, J.-L. (1996) 'Transient heating effect

on high strength concrete'. *Nuclear Engineering and Design*, 166 (1), pp. 99-108.

Ožbolt, J., Bošnjak, J., Periškić, G. & Sharma, A. (2014) '3D numerical analysis of reinforced concrete beams exposed to elevated temperature'. *Engineering Structures*, 58 pp. 166-174.

Pan, Z., He, L., Qiu, L., Korayem, A. H., Li, G., Zhu, J. W., Collins, F., Li, D., Duan, W. H. & Wang, M. C. (2015) 'Mechanical properties and microstructure of a graphene oxide–cement composite'. *Cement and Concrete Composites*, 58 pp. 140-147.

Pan, Z., Sanjayan, J. G. & Collins, F. (2014) 'Effect of transient creep on compressive strength of geopolymer concrete for elevated temperature exposure'. *Cement and Concrete Research*, 56 pp. 182-189.

Peng, G.-F. & Huang, Z.-S. (2008) 'Change in microstructure of hardened cement paste subjected to elevated temperatures'. *Construction and Building Materials*, 22 (4), pp. 593-599.

Petkovski, M. (2010) 'Effects of stress during heating on strength and stiffness of concrete at elevated temperature'. *Cement and Concrete Research*, 40 (12), pp. 1744-1755.

Petkovski, M. & Crouch, R. (2008) 'Strains under transient hygro-thermal states in concrete loaded in multiaxial compression and heated to 250 °C'. *Cement and Concrete Research*, 38 (4), pp. 586-596.

Phan, L. T. (1996) *Fire performance of high-strength concrete: A report of the state-of-the-art*. Gaithersburg: National Institute of Standards and Technology.

Phan, L. T. & Carino, N. J. (2002) 'Effects of test conditions and mixture proportions on behavior of high-strength concrete exposed to high temperatures'. *ACI Materials Journal*, 99 (1), pp. 54-66.

Philleo, R. (1958) 'Some physical properties of concrete at high temperatures'. *Proceedings of the American Concrete Institute*, (54), pp. 857-864.

Pimienta, P., McNamee, R. J. & Mindeguia, J. C. (2018) *Physical properties and behavior of high-performance concrete at high temperatures*. New York: Springer.

Popovics, S. (1973) 'A numerical approach to the complete stress-strain curve of concrete'. *Cement and Concrete Research*, 3 (5), pp. 583-599.

Purkiss, J. A. & Li, L.-Y. (2013) *Fire safety engineering design of structures*. Boca Raton: CRC Press.

Rickard, W. D. A., Gluth, G. J. G. & Pistol, K. (2016) 'In-situ thermo-mechanical testing of fly ash geopolymer concretes made with quartz and expanded clay aggregates'. *Cement and Concrete Research*, 80 pp. 33-43.

RILEM (2007) 'Recommendation of RILEM TC 200-HTC: mechanical concrete properties at high temperatures—modelling and applications'. *Materials and*

Structures, 40 (9), pp. 841-853.

Ryu, G. S., Lee, Y. B., Koh, K. T. & Chung, Y. S. (2013) 'The mechanical properties of fly ash-based geopolymer concrete with alkaline activators'. *Construction and Building Materials*, 47 pp. 409-418.

Sabeur, H. & Colina, H. (2014) 'Effect of heating–cooling cycles on transient creep strain of high performance, high strength and ordinary concrete under service and accidental conditions'. *Materials and Structures*, 48 (5), pp. 1561-1579.

Sadaoui, A. & Khennane, A. (2009) 'Effect of transient creep on the behaviour of reinforced concrete columns in fire'. *Engineering Structures*, 31 (9), pp. 2203-2208.

Schneider, U. (1976) 'Behaviour of concrete under thermal steady state and non - steady state conditions'. *Fire and Materials*, 1 (3), pp. 103-115.

Schneider, U. (1988) 'Concrete at high temperatures - A general review'. *Fire Safety Journal*, 13 (1), pp. 55-68.

Schneider, U., Diederichs, U. & Ehm, C. (1982) 'Effect of temperature on steel and concrete for PCRV's'. *Nuclear Engineering and Design*, 67 (2), pp. 245-258.

Schneider, U. & Schneider, M. (2009) 'An advanced transient concrete model for the determination of restraint in concrete structures subjected to fire'. *Journal of advanced concrete technology*, 7 (3), pp. 403-413.

Schneider, U., Schneider, M. & Franssen, J.-M. (2008) 'Consideration of nonlinear creep strain of siliceous concrete on calculation of mechanical strain under transient temperatures as a function of load history'. *Proceedings of the Fifth International Conference Structures in Fire*. Singapore, pp 463-476.

Sivakumaran, K. & Dilger, W. H. (1984) 'Analysis of concrete structures subjected to sustained temperature gradients'. *Canadian Journal of Civil Engineering*, 11 (3), pp. 404-410.

Sullivan, P. J. E. & Sharshar, R. (1992) 'The performance of concrete at elevated temperatures (as measured by the reduction in compressive strength)'. *Fire technology*, 28 (3), pp. 240-250.

Taylor, H. F. (1997) *Cement chemistry*. London: Thomas Telford.

Terro, M. J. (1998) 'Numerical modeling of the behavior of concrete structures in fire'. *ACI Structural Journal*, 95 (2), pp. 183-193.

Thelandersson, S. (1983) 'On the multiaxial behaviour of concrete exposed to high temperature'. *Nuclear Engineering and Design*, 75 (2), pp. 271-282.

Thelandersson, S. (1987) 'Modeling of combined thermal and mechanical action in concrete'. *Journal of engineering mechanics*, 113 (6), pp. 893-906.

Thienel, K. C. & Rostásy, F. S. (1996) 'Transient creep of concrete under biaxial stress

and high temperature'. *Cement and Concrete Research*, 26 (9), pp. 1409-1422.

Torelli, G., Gillie, M., Mandal, P. & Tran, V.-X. (2017) 'A multiaxial load-induced thermal strain constitutive model for concrete'. *International Journal of Solids and Structures*, 108 pp. 115-125.

Torelli, G., Mandal, P., Gillie, M. & Tran, V.-X. (2016) 'Concrete strains under transient thermal conditions: A state-of-the-art review'. *Engineering Structures*, 127 pp. 172-188.

Torelli, G., Mandal, P., Gillie, M. & Tran, V.-X. (2018) 'A confinement-dependent load-induced thermal strain constitutive model for concrete subjected to temperatures up to 500 °C'. *International Journal of Mechanical Sciences*, 144 pp. 887-896.

Vlahinić, I., Thomas, J. J., Jennings, H. M. & Andrade, J. E. (2012) 'Transient creep effects and the lubricating power of water in materials ranging from paper to concrete and Kevlar'. *Journal of the Mechanics and Physics of Solids*, 60 (7), pp. 1350-1362.

Wang, Y., Bisby, L. A., Wang, T.-y., Yuan, G. & Baharudin, E. (2018a) 'Fire behaviour of reinforced concrete slabs under combined biaxial in-plane and out-of-plane loads'. *Fire Safety Journal*, 96 pp. 27-45.

Wang, Y., Burgess, I., Wald, F. & Gillie, M. (2012) *Performance-based fire engineering of structures*. Boca Raton: CRC Press.

Wang, Y., Guo, W., Huang, Z., Long, B., Yuan, G., Shi, W. & Zhang, Y. (2018b) 'Analytical model for predicting the load–deflection curve of post-fire reinforced-concrete slab'. *Fire Safety Journal*, 101 pp. 63-83.

Wei, Y., Au, F. T., Li, J. & Tsang, N. C. (2017) 'Effects of transient creep strain on post-tensioned concrete slabs in fire'. *Magazine of Concrete Research*, 69 (7), pp. 337-346.

Xu, Y., Wong, Y., Poon, C. & Anson, M. (2001) 'Impact of high temperature on PFA concrete'. *Cement and Concrete Research*, 31 (7), pp. 1065-1073.

Yin, J., Zha, X.-x. & Li, L.-y. (2006) 'Fire resistance of axially loaded concrete filled steel tube columns'. *Journal of Constructional Steel Research*, 62 (7), pp. 723-729.

Youssef, M. & Moftah, M. (2007) 'General stress–strain relationship for concrete at elevated temperatures'. *Engineering Structures*, 29 (10), pp. 2618-2634.

Zhang, Q. & Ye, G. (2012) 'Dehydration kinetics of Portland cement paste at high temperature'. *Journal of Thermal Analysis and Calorimetry*, 110 (1), pp. 153-158.

Zhang, Q. & Ye, G. (2013) 'Quantitative analysis of phase transition of heated Portland cement paste'. *Journal of Thermal Analysis and Calorimetry*, 112 (2), pp. 629-636.

Zhang, Q., Ye, G. & Koenders, E. (2013) 'Investigation of the structure of heated Portland cement paste by using various techniques'. *Construction and Building*

Materials, 38 pp. 1040-1050.

Publications

Kunjie Fan*, Dawang Li, Nattapong Damrongwiriyanupap, Long-yuan Li. (2019) 'Compressive stress-strain relationship for fly ash concrete under thermal steady state'. Cement and Concrete Composites, 104, 103371.

DOI: http://dx.doi.org/10.1016/j.cemconcomp.2019.103371

PEARL (OA): http://hdl.handle.net/10026.1/14667

Kunjie Fan*, Dawang Li, Long-yuan Li, Jiayu Wu. (2019) 'Effect of temperature gradient on transient thermal creep of heated and stressed concrete in transient state tests'. Construction and Building Materials, 222, 839-851.

DOI: https://doi.org/10.1016/j.conbuildmat.2019.06.197

PEARL (OA): https://pearl.plymouth.ac.uk/handle/10026.1/14605

Appendix

A. Relative average deviation of parameters (tests of series A)

Type of concrete	Temperature	Relative average deviation of parameters			
	T	$f_c(T)$	$\varepsilon_c(T)$	$E(T)$	$n(T)$
	°C	%			
NSC	20	3.51	4.25	3.66	2.13
	200	4.12	5.13	4.51	5.79
	300	3.99	2.87	3.78	4.23
	400	5.16	6.02	6.11	3.55
	460	6.68	5.37	4.39	3.93
	520	4.95	3.98	3.97	4.91
	580	5.86	4.79	4.99	5.28
	680	3.58	4.31	4.03	6.01
	770	2.99	4.66	3.45	4.93
	900	4.87	5.28	5.92	3.81
NSFC	20	4.36	5.96	3.51	3.04
	200	5.21	6.89	4.97	4.55
	300	4.33	5.66	4.32	3.72
	450	4.16	4.98	3.92	4.89
	550	5.66	5.86	5.12	5.19
	600	3.89	3.63	4.56	4.78
	700	6.06	2.79	2.94	2.76
	800	4.65	3.54	3.49	3.79
	900	5.86	4.99	4.31	4.23

B. Relative average deviation of parameters (tests of series B)

Temperature	Pre-fire load level	Relative average deviation of parameters			
T	L	$f_c(L,T)$	$\varepsilon_c(L,T)$	$E(L,T)$	$r(L,T)$
°C	%	%			
400	10	4.18	5.77	4.54	4.66
460		5.28	4.73	5.87	3.85
500		3.89	5.31	3.56	4.38
580		4.38	3.97	4.37	4.29
640		5.99	5.11	4.49	5.81
750		3.72	2.65	5.92	4.23
820		4.78	3.06	3.60	5.00
900		2.31	4.31	4.57	4.22
400	30	3.85	4.00	3.98	3.28
460		4.04	3.05	5.20	4.77
550		5.29	7.01	4.21	3.19
580		3.07	3.74	3.93	4.58
680		2.95	4.43	4.40	5.02
750		4.87	3.82	3.99	2.89
400	50	3.95	4.31	5.10	3.08
460		4.29	3.33	3.29	3.44
530		6.04	5.69	4.73	4.10
580		5.30	6.00	6.06	5.16
400	70	5.09	4.04	4.88	4.73

C. Relative average deviation of load induced thermal strain (tests of series C)

Type of concrete	Temperature	Pre-fire load level				
		0%	10%	30%	50%	70%
	T	Relative average deviation of load induced thermal strain				
	°C	%				
NSC	100	3.20	3.57	5.82	1.04	4.92
	200	2.35	1.39	6.63	2.48	3.58
	300	2.81	3.25	4.95	5.77	7.51
	400	4.51	4.27	5.42	4.39	3.34
	500	3.77	2.74	5.23	5.21	4.91
	600	1.03	4.56	2.34	3.99	5.37
	700	2.70	7.10	4.73	5.38	4.38
	800	4.59	4.57	3.81	4.91	2.94
	900	3.29	4.26	3.50	3.73	2.34
NSFC	100	4.19	3.24	3.53	3.92	3.44
	200	2.37	2.81	2.39	5.08	3.49
	300	2.80	3.93	4.64	3.29	4.32
	400	6.34	2.86	2.97	3.33	5.94
	500	3.76	5.08	4.42	4.49	4.02
	600	2.11	4.10	5.59	2.10	5.49
	700	5.89	4.72	3.42	1.97	2.83
	800	3.45	3.97	5.01	3.94	3.29
	900	2.44	5.90	3.90	5.63	3.32